Monthly Scientific-Technical and Production Journal

The Paton WELDING JOURNAL

September 2002 # 9

English translation of the monthly «Avtomaticheskaya Svarka» journal published in Russian since 1948

Founders: *The National Academy of Sciences of Ukraine, The E.O. Paton Electric Welding Institute of the NAS of Ukraine, International Association «Welding»*

Publisher: *International Association «Welding»*

Editorial and advertising offices:
E.O. Paton Electric Welding Institute,
International Association «Welding»,
11, Bozhenko str., 03680, Kyiv, Ukraine
Tel.: (38044) 227 67 57
Fax: (38044) 268 04 86
E-mail: journal@paton.kiev.ua
http://www.nas.gov.ua/pwj

State Registration Certificate
KV 4790 of 09.01.2001

Subscriptions:
$460, 12 issues per year,
postage and packaging included.
Back issues available

CONTENTS

ELECTRON BEAM WELDING OF 60 mm THICK STEELS USING LONGITUDINAL OSCILLATIONS OF BEAM

K.S. AKOPIANTS, V.M. NESTERENKOV and **O.K. NAZARENKO**
The E.O. Paton Electric Welding Institute, NASU, Kyiv, Ukraine

Frequency of natural oscillations of molten metal of the weld pool (tens–hundreds of hertz) has been estimated. The pulsed effect on the pool providing oscillation of the beam from a tail part of the pool to its leading part has been attained experimentally. Narrow through-penetration welds were made with a penetration depth up to 60 mm, width of about 1 mm and weld shape factor of 40.

Key words: *electron beam welding, pulsed effect, scanning with saw-shaped oscillations, narrow welds*

EBW is peculiar by producing narrow welds of «key-hole» shape (depth of penetration exceeds weld width more than 10 times). To increase still further the penetrability of the beam, different technical procedures are used, including those based on a pulsed dynamic effect on weld pool. The pulsed modulation of beam current is made and the frequency and shape of beam scanning in weld pool is selected [1–3]. It is informed in [3] that due to pulsed modulation of current at frequency 100 Hz and longitudinal oscillations of beam the more narrow and deeper welds are produced as compared with conventional welds (though the welding was performed in flat position, the weld shape is similar to that made by a horizontal beam). However, it is not indicated in the publication what kind of longitudinal beam scanning was used and how the more narrow welds are produced.

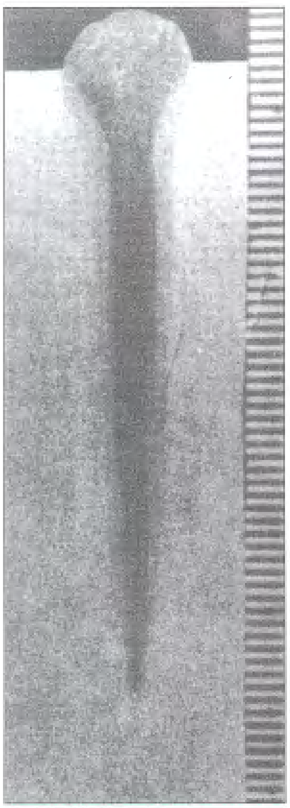

Figure 1. Transverse macrosection of typical penetration of steel 10Kh18N9T (AISI 304) in single-pass EBW with stationary electron beam (without pulsed action on the pool) at U_{acc} = 60 kV, I_b = 170 mA, v_w = 10 m/h and h/B_m = 16

The aim of this work was to study the effect of a pulsed effect on weld pool in EBW of steel using longitudinal saw-like oscillations of the electron beam. Let us consider some estimates to define the frequency of effect on weld pool. Evidently, the highest effect will be attained if the frequency of pulsed effect of beam corresponds to a natural frequency of oscillations of the molten metal in pool. To make estimations, let us consider the case given in Figure 1. It is the typical «key-hole» penetration in a single-pass EBW with a stationary electron beam without any pulsed effect on the pool. Two regions can be distinguished in the penetration: upper widened part of pool and lower extended part, in which a vapour-gas channel is known to be formed during welding.

Let us estimate first the frequency of oscillations of the upper part of pool without allowance for the presence of a vapour-gas channel in the lower part. Let us consider for simplification that the upper part of the weld pool has a cylindrical shape: depth H, radius $R = B/2$ (B – pool width). It is shown in [4] that the first (main) frequency of oscillations of liquid in a cylindrical vessel (under the action of surface tension forces) is determined by expression

$$\omega^2 = \frac{\sigma}{\rho R^3} k^3 \mathrm{th}\,(kh),$$

where ω is the cyclic frequency, equal to $2\pi f$; f is the pool oscillations frequency; σ is the surface tension; ρ is the density; k is the natural number of edge problem about surface oscillations (k = 1.841); h is the dimensionless depth of pool ($h = H/R$). In EBW the depth usually exceeds greatly the width, i.e. $h >> 1$; hyperbolic tangent $\mathrm{th}(kh) \approx 1$.

As a result we obtain expression for frequency of oscillations of the weld pool upper part f_1 depending on its width B:

$$f_1 \approx 1.1\left(\frac{\sigma}{\rho B^3}\right)^{0.5}.$$

For example, for steel (ρ = 7800 kg/m^3, σ = = 1.5 N/m) at pool width B = 5–10 mm the frequency of the pool oscillations is f_1 = 44–16 Hz.

Oscillations of the weld pool upper part are manifested in the formation of «flakes» at the weld surface. The estimation of frequency is in a good correlation with the measured values [1].

Then, it should be taken into account that a vapour-gas channel is formed in a weld pool through the entire its depth. As was shown in [5], the oscillations of the channel surface relative to equilibrium position occur at frequency

$$f_2 \approx 2.3\left(\frac{\sigma}{\rho d_{ch}^3}\right)^{0.5},$$

where d_{ch} is the channel diameter. For example, at d_{ch} = 1.5–2.5 mm the frequency of channel surface oscillations is f_2 = 550–250 Hz.

The estimation makes it possible to establish that the range of frequencies of molten metal oscillation in a weld pool in EBW lies within the ranges from tens to hundreds of hertz. Pulsed effect of beam on the pool should correspond to this range.

Experiments were carried out using EBW equipment of ELA-60/60 type (accelerating voltage U_{acc} = = 60 kV, beam current I_b = 1 A) in vacuum chamber UL-209 (2.5×2.5×3.8 m, working vacuum is not worse than $5\cdot10^{-2}$ Pa) with a gun moving inside the chamber (gun has a differential pumping to provide vacuum in gun of not worse than $1\cdot10^{-3}$ Pa). High-strength medium-alloyed steel of thickness δ = 57 mm was selected. Welding was performed at v_w = 5 mm/s (18 m/h), beam current — up to 250 mA.

Pulsed dynamic effect on weld pool was made by a beam scanning.

Taking into account the data of [3] and made estimates of frequency of natural oscillations of metal in pool (tens–hundreds of hertz) the frequency of beam scanning was selected equal to 130 Hz that corresponds approximately to the middle of frequency range of natural oscillations; the absence of beats with mains frequency was provided.

Beam scanning had a shape of longitudinal oscillations along the welding direction. The deflecting coil was supplied with a saw-shaped current from a special generator (Figure 2). In scanning with longitudinal oscillations the narrow welds [1] are produced, unlike, for example, welding with transverse oscillations or with a circular scanning.

Size of scanning (double amplitude) was 3 mm, that approximately 2 times exceeds the diameter of a vapour-gas channel existing in welding with a static beam. The effect of beam scanning in this case should be noticeable.

A remarkable feature of welding was a selection of beam movement direction in scanning: in the direction of welding or opposite to it.

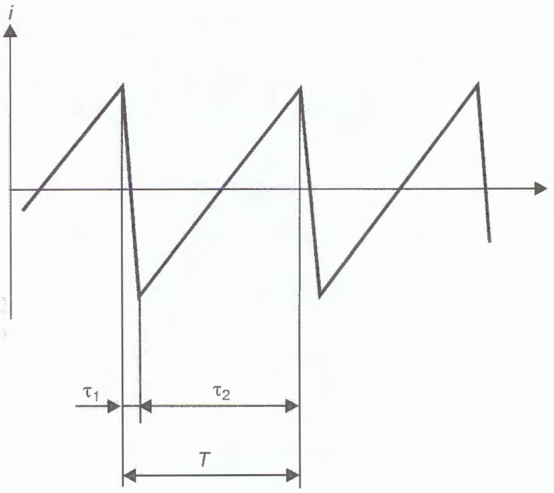

Figure 2. Saw-shaped current $i(t)$ in a defecting coil: T — period of scanning; τ_1 — time of beam overthrow to a pool tail part; τ_2 — time of beam movement in the direction from a tail pool part to the front part; t — current time

In case when the beam has a pulsed deviation into the direction of a tail part of welding pool, and then during the whole period of scanning it is moved to the front part, the welds are produced more narrow and deeper. Scheme of beam movement in this case is presented in Figure 2, and formed penetrations are shown in Figure 3.

In parallel with producing narrow through welds (width of molten zone is ≈ 1 mm) (Figure 3, *a*) the formation of a rounding in a root on non-through welds (Figure 3, *b*) should be also noted, thus preventing the root defects.

Shape of welds can be estimated numerically as follows. Let us divide the penetration image (for example, in Figure 3, *a*) into ten regions in depth and measure the weld width at different depth: $B_1(0.1h)$, $B_2(0.2h)$, ..., $B_9(0.9h)$.

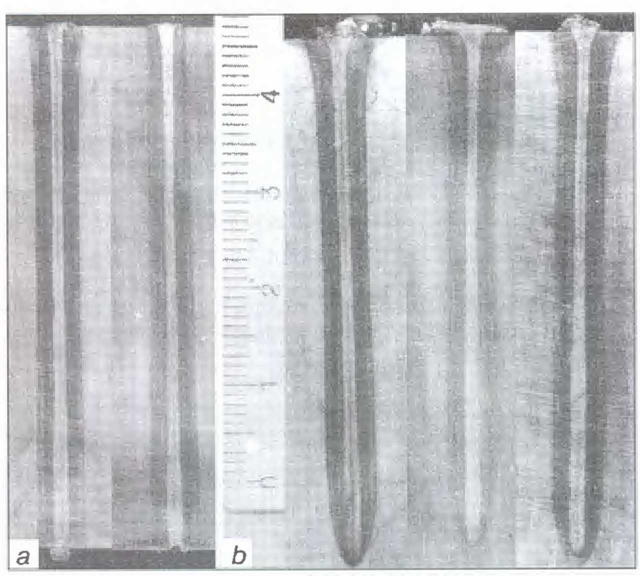

Figure 3. Through penetration of high-strength medium-alloyed steel 12Kh2N4MD (*a*) (δ = 57 mm, U_{acc} = 60 kV, I_b = 235 mA, v_w = 18 m/h, longitudinal oscillations of beam of a special shape, f = 130 Hz, size of scanning 3 mm, $h/B_m \approx 42$); non-through penetration (*b*) (I_b = 215 mA, h/B_m = 38, the rest parameters are the same as in Figure 3, *a*)

Let us determine the mean value of the weld width

$$B_m = \frac{1}{9}\sum_{i=1}^{9} B_i,$$

root-mean-square deviation of weld width

$$\Delta B_m = \frac{1}{9}\sqrt{\sum_{i=1}^{9} (B_i - B_m)^2},$$

difference between values B_{max} and B_{min}

$$\Delta B_{max} = B_{max} - B_{min},$$

and coefficient of weld shape $k = h/B_m$.

For a through penetration (Figure 3, *a*, *on the left*) we shall obtain the mean width of weld (penetration) B_m = 1.35 mm, root-mean-square deviation of weld width ΔB_m = 0.16 mm, difference between the maximum and minimum values of width ΔB_{max} = = 0.4 mm and coefficient of weld shape k = 42. For a non-through penetration (Figure 3, *b*, *on the left*) B_m = 1.42 mm, ΔB_m = 0.13 mm, ΔB_{max} = 0.35 mm, h = 54 mm and k = 38.

For comparison, we shall give the values of the same indices for penetration, presented in Figure 1: B_m = 3.1 mm, ΔB_m = 0.8 mm, ΔB_{max} = 2.2 mm, h = = 49 mm, k = 16.

As is seen from estimates the penetration, presented in Figure 3, as compared with those obtained in EBW with a static beam (see Figure 1), are more narrow, uniform in depth and having a higher shape factor. The producing of these narrow welds is explained by a pulsed dynamic effect on the molten metal in a weld pool tail part that results in its forcing out. Thus, the access to the weld pool bottom is given for the electron beam and its penetration for a larger depth is occurred. As a result, the depth of a vapour-gas channel through which the beam is passed, is increased. Depth of weld pool is increased and its width is decreased, respectively, but the pool metal volume remains the same.

Thus, it is possible to produce narrow and deep welds using the above-described technological procedure.

1. Nazarenko, O.K., Kajdalov, A.A., Kovbasenko, S.N. (1987) *Electron beam welding*. Kyiv: Naukova Dumka.
2. Ohmine, M., Hiramoto, S., Jamane, J. (1983) Fundamental study on the pulsed electron beam welding. *IIW Doc. IV-348–83*.
3. Schulze, K.-R., Fritz, D., Reindl, G. (1996) Je dicker, je lieber — Elektronenstrahlschweissen im Vakuum. *Praktiker*, **6**, 250–254.
4. (1976) *Hydromechanics of weightlessness*. Moscow: Nauka.
5. Akopiants, K.S., Yemchenko-Rybko, A.V. (1981) Control of penetration depth and electron beam focusing by frequency of ion current ripples during welding. *Avtomatich. Svarka*, **9**, 28–32.

INVESTIGATION OF BIOCERAMIC COATINGS PRODUCED BY MICROPLASMA SPRAYING

Yu.S. BORISOV[1], **S.G. VOJNAROVICH**[1], **N.V. ULIANCHICH**[2], **J. JENSEN**[3] and **J. WOLKE**[3]
[1]The E.O. Paton Electric Welding Institute, NASU, Kyiv, Ukraine
[2]Research and Production Company «KERGAP», Kyiv, Ukraine
[3]Nijmegen University, The Netherlands

Adhesion strength and biocompatibility of bioceramic coatings produced by microplasma spraying was studied. It was established that with the use of a sub-layer the adhesion strength of the hydroxyapatite coatings increased, compared with that of coatings deposited without sub-layer. It is shown that increase in thickness of the coating to 130–160 μm leads to decrease in its adhesion strength down to 4.59 MPa (without sub-layer). High biocompatibility of the microplasma coatings was proved.

Key words: *microplasma spraying, hydroxyapatite, tricalcium phosphate, parameters, adhesion strength, biological compatibility, investigations*

Metals and alloys are the materials which have received the widest acceptance for the manufacture of implants. However, their application involves some problems, including those associated with corrosion resistance and compatibility with live tissues. Insufficient corrosion resistance leads not only to failure and decay of the implant proper, but also exerts the negative effect both on the surrounding tissues and on the organism as a whole. Therefore, an increasingly wide application has been gaining by metallic implants with coatings of bioceramic materials, where mechanical strength of the metal base combines with biological peculiarities of the coating. Such bioceramic coatings are characterised by a triple positive effect, i.e. increased rate of formation of osteine, possibility of bonding with a bone (osteointegration) and decreased formation of metal corrosion products.

A series of studies has been conducted lately on deposition of bioceramic coatings by different methods of thermal spraying: plasma (traditional process in atmosphere [1–9] and in dynamic vacuum [9, 10]), high-frequency [11], HVOF [6, 9, 12] and microplasma [13] spraying. The object of this study was to investigate biocompatibility and strength of adhesion of the microplasma bioceramic coatings with a substrate.

Microplasma spraying system MPS-004. This system includes power supply with a control panel, plasmatron and special powder feeding device [14, 15]. Design and parameters of the plasmatron provide formation of a laminar plasma jet (Reynolds number is 0.10–0.55). This factor results in a number of peculiarities of the microplasma spraying process, allowing losses of a spray material in treatment of small-size parts (dental implants) to be reduced and overheating of the substrate to be avoided [13, 16].

The system has the following specifications:

Gas	
working	argon
transporting	argon, air
shielding	argon
Power, kW	up to 3.0
Current, A	10–50
Voltage, V	up to 60
Gas flow rate, l/min	
working	0.1–1.5
shielding	1.0–4.0
Productivity, kg/h	0.25–2.50
Material utilisation factor	0.6–0.8
Dimensions, mm	540×255×470
Weight, kg	15

Spray materials. Hydroxyapatite (HAP) and tricalcium phosphate (TCP) powders with particle sizes below 63 μm were provided for microplasma spraying by the Closed Joint-Stock Research and Production Company «KERGAP», which is the developer of the technology for synthesis of these powders and their manufacturer [13]. Appearance of the HAP powder particles is shown in Figure 1.

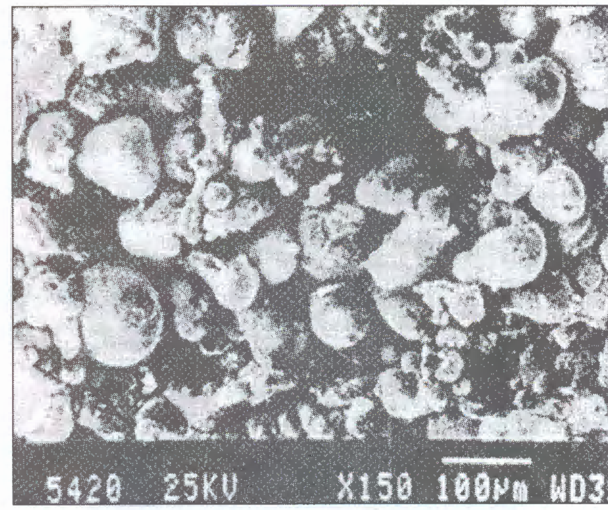

Figure 1. Appearance of the HAP powder particles produced by the Company «KERGAP»

The E.O. Paton Electric Welding Institute of the NAS of Ukraine, in collaboration with the «KERGAP» and the Nijmegen University (The Netherlands), conducted a package of investigations into biological activity of the HAP and TCP micrplasma coatings. X-ray phase analysis and scanning electron microscopy were employed to study phase composition of the coatings and behaviour of the cell cultures on their surface. Strength of adhesion of the coatings with the substrate was studied according to the ASTM C 633–79 standard by the gluing method using the film glue VK-47.

Investigation results. Adhesion strength of the bioceramic coatings was studied by microplasma spraying the HAP coatings on the end surfaces of cylindrical titanium alloy samples with a diameter of 25 mm. The spraying parameters were as follows: plasma gas flow rate 0.7 l/min, shielding gas flow rate 4.3 l/min, current 40 A, voltage 30 V and spraying distance 100 mm.

Investigated was the effect on adhesion strength by such factors as coating thickness, presence and material of a sub-layer. Ti and TiO_2 powders were used for the latter. It was established that adhesion strength of the HAP coatings increased, compared with that of coatings deposited without a sub-layer, which is in agreement with the conclusions made by other investigators [17]. For example, in spraying the HAP coating 80–100 μm thick on the titanium sub-layer the adhesion strength amounted to 8.29 MPa, and that on the TiO_2 sub-layer was 11.32 MPa, whereas without a sub-layer the adhesion strength was no more than 7.39 MPa. The use of the sub-layer provides the following advantages: ensuring favourable microroughness of the surface for deposition of a coating, and decrease in stresses at the interface between the coating and the substrate, which are formed as a result of differences in their thermal expansion coefficients. In addition, a decreased thermal conductivity of the sub-layer (especially in the case

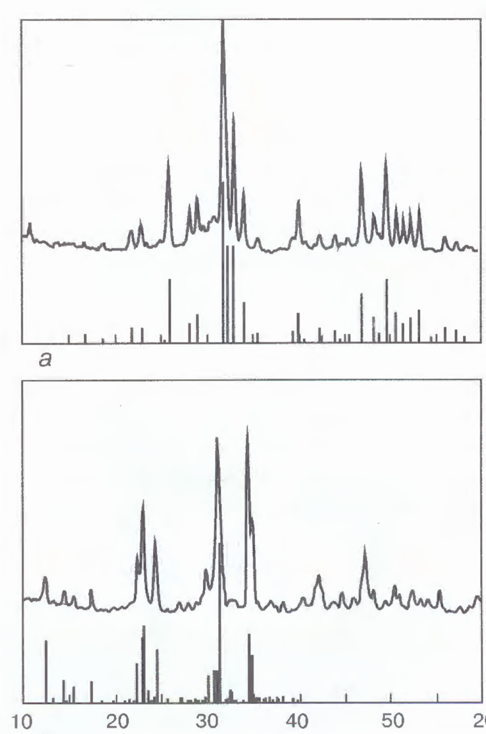

Figure 2. Diffraction patterns of the HAP (*a*) and TCP (*b*) microplasma coatings

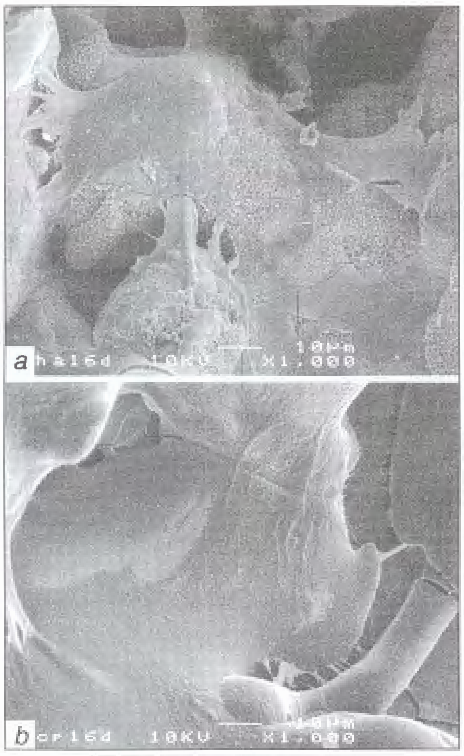

Figure 3. Appearance of the HAP (*a*) and TCP (*b*) bioceramic coatings with cell cultures

of using TiO_2 as the sub-layer) leads to decrease in the rate of cooling of the spray material particles and, therefore, to reduction of the probability of formation of the amorphous phase.

Thickness of a coating also has a considerable effect on its adhesion strength. For example, increase in thickness to 130–160 μm led to decrease in the adhesion strength down to 4.59 MPa (without a sub-layer).

Results of X-ray phase analysis of the HAP and TCP coatings are shown in Figure 2. Main peaks on the diffraction pattern of the HAP coating (Figure 2, *a*) correspond, according to the ASTM (No.9-432) file, to HAP with a small addition of TCP, resulting from spraying. All the lines on the diffraction pattern of the TCP coating (Figure 2, *b*) correspond, according to the ASTM (No.9-359) file, to TCP. Small width of the peaks is indicative of a high degree of crystallinity of the coating and absence of the amorphous phase.

To study biocompatibility of the coatings, the HAP and TCP coatings 200 μm thick were deposited on samples of titanium alloy VT6 by the microplasma spraying method. Marrow cells were taken from the femur of a young rat and grown at a temperature of 37 °C in the atmosphere of air with an addition of 5 % CO_2. Then the cells were inoculated on the surface of the coatings. Figure 3 shows surfaces of the HAP and TCP coatings, respectively, with the cell cultures. The cells were revealed to actively grow on the coatings to form a continuous film, especially in a case of the TCP coating, which is indicative of a high biological compatibility of the produced coatings and their highly promising application on the surfaces of endoprostheses.

CONCLUSIONS

1. Microplasma bioceramic coatings of HAP and TCP feature a high degree of crystallinity and contain almost no amorphous phase.

2. The use of a sub-layer of Ti and TiO_2 allows adhesion strength of the coatings to be increased and the probability of formation of the amorphous phase in spraying to be reduced.

3. Active growth of cells on the coatings to form a continuous film is indicative of a high biological compatibility of the produced coatings and their highly promising application as coatings on endoprostheses.

1. de Groot, K., Geesink, R.T.G., Klein, C.P.A.T. et al. (1987) Plasma sprayed coatings of hydroxyapatite. *J. Biomed. Mater. Res.*, **21**, 1375–1381.
2. Kay, J.F. (1993) Plasma sprayed hydroxyapatite coatings for enhanced biocompatibility. *Mater. Technology*, **1/2**, 26–29.
3. Cheang, P., Khor, K.A. (1995) Bioceramic powder and coatings by thermal spray techniques. In: *Proc. of 14th Int. Thermal Spray Conf.*, Kobe, Japan, 1995.
4. Yang, C.Y., Wang, B.C., Chang, E. et al. (1995) The influences of plasma spraying parameters on the characteristics of hydroxyapatite coatings: a quantitative study. *J. Mater. Sci. in Medicine*, **6**, 249–257.
5. McPherson, R., Gane, N., Bastow, T.J. (1995) Structural characterisation of plasma-sprayed hydroxyapatite coatings. *Ibid.*, 327–334.
6. Khor, K.A., Cheang, P., Wang, Y. (1997) The thermal spray processing of HA powders and coatings. *JOM*, Febr., 51–57.
7. Khor, K.A., Cheang, P., Wang, Y. (1998) Plasma spraying of combustion flame spheroidized hydroxyapatite (HA) powders. *J. Thermal Spray Technology*, **2**, 254–260.
8. Wang, Y., Khor, K.A., Cheang, P. (1998) Thermal spraying of functionally graded calcium phosphate coatings for biomedical implants. *Ibid.*, **1**, 50–57.
9. Brown, S.R., Turner, I.G. (1998) Acoustic emission analysis of thermal sprayed hydroxyapatite coatings examined under four point bend loading. *Surface Eng.*, **4**, 309–313.
10. Heimann, R.B., Vu, T.A. (1997) Low-pressure plasma-sprayed (LPPS) bioceramic coatings with improved adhesion strength and resorption resistance. *J. Thermal Spray Technology*, **2**, 145–149.
11. Bouyer, E., Gitzhofer, F., Boulos, M.I. (1997) The suspension plasma spraying of bioceramics by induction plasma. *JOM*, Febr., 58–62.
12. Wolke, J.G., de Groot, K., Kraak, T.G. et al. (1991) The characterization of hydroxyapatite coatings sprayed with VPS, APS and DY systems. In: *Proc. of Int. Thermal Spray Conf.*, Pittsburgh, 1991.
13. Borisov, Yu.S., Vojnarovich, S.G., Bobrik, V.G. et al. (2000) Microplasma spraying of bioceramic coatings. *The Paton Welding J.*, **12**, 62–66.
14. Yushchenko, K., Borisov, Yu., Pereverzev, Y. et al. (1998) Microplasma spraying. In: *Proc. of 15th Int. Thermal Spray Conf.*, Nice, France, 1998.
15. Yushchenko, K., Borisov, Yu., Pereverzev, Y. et al. (1995) Microplasma spraying. In: *Proc. of 14th Int. Thermal Spray Conf.*, Kobe, Japan, 1995.
16. Borisov, Yu.S., Pereverzev, Yu.N., Vojnarovich, S.G. et al. (1999) Microplasma spraying of narrow strip coatings by microplasma spraying. *Avtomatich. Svarka*, **6**, 53–55.
17. Kalita, V.I. (2000) Physics and chemistry of formation of bioinert and bioactive surfaces on implants. *Fizika i Khimiya Obrab. Materialov*, **5**, 28–44.

MATHEMATICAL MODEL OF TECHNOLOGICAL ADAPTATION OF THE ROBOT TO THE GAP IN ARC WELDING

I.F. KORINETS and JI CHENG CHUNG
National Technical University of Ukraine «KPI», Kyiv, Ukraine

A deterministic-statistical model was developed of robot adaptation to the gap in consumable-electrode arc welding in a mixture of Ar + 25 % CO_2. It may be applied in development of the software of adaptive control systems of robots for MIG and TIG, as well as submerged-arc welding.

Key words: *arc welding, consumable electrode, protective mixture, robot, control system, mathematical model*

Advance of robotics is becoming the main direction of automation in welding fabrication [1]. For instance, in Germany almost half of all the industrial robots are used in welding [2]. They were initially applied for capacitor-type spot welding, robotisation of which was simpler in engineering terms, compared to arc welding [3, 4]. With the advance of robotic means, arc welding robots began to be applied (more than 90 % of them perform MAG welding and about 5 % MIG welding).

Wide application of robotic arc welding is restrained by random deviations from the line of blank joining, as well as the size of the gap between them and shape of edge preparation. The need to solve this problem led to development of adaptive control systems of robots, capable of automatically adjusting to environmental changes [5]. Problem of spatial adaptation of the robot, i.e. automatic following of the arc along a complex contour of the welded joint is practically solved [6]. More complex is the problem of technological adaptation of the robot, i.e. automatic correction of mode parameters during welding (for instance, at an irregular gap in a welded joint, due to insufficient accuracy of fit-up and deformation of edges during welding).

A promising means of technological adaptation are video sensor systems [1–5, 7]. However, video sensors, located on the torch in the immediate vicinity of the welding zone, are exposed to the impact of thermal and light radiation, electromagnetic noise, drops of molten metal and aerosol, this lowering their reliability [7]. At present, due to minituarisation of the hardware, its protection from the welding arc impact and reduction of the cost of technical means, the leading world manufacturers of robots have switched from laboratory testing of video sensors to their practical application. In case of technological adaptation of the robot, the information, coming from the video sensor (Figure 1), should be processed in real time and should provide correction of mode parameters during welding. This leads to higher requirements to the response of adaptive system of robot

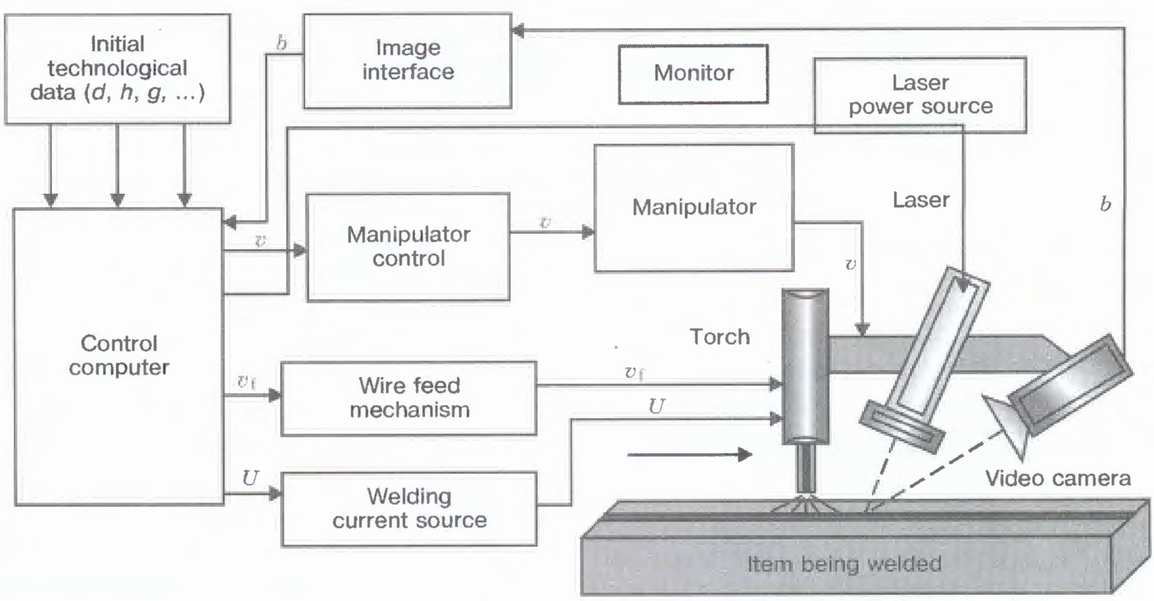

Figure 1. Block diagram of technological adaptation to the gap in robotic gas-shielded consumable-electrode arc welding

h = 3.0 mm, g = 1.5 mm, b = 0–2.0 mm

Mathematical model of welding mode adaptation to the gap

$$I = 104.954 \cdot 0.592^{b} \frac{h^{1.180}}{g^{0.620}} \qquad (1)$$

$$v = 17.865 \cdot 0.454^{b} \frac{h^{0.712}}{g^{1.659}} \qquad (2)$$

a

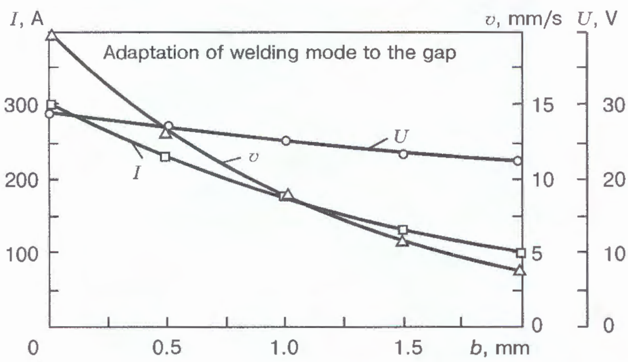

b

Control of the shape of a butt weld with a gap

$$h = 0.020 \cdot 1.284^{b} \frac{I^{1.094}}{v^{0.409}} \qquad (3)$$

$$e = 0.069^{b} \frac{I^{1.051}}{v^{0.324}} \qquad (4)$$

$$g = 1.062 \cdot 0.692^{b} \frac{I^{0.469}}{v^{0.778}} \qquad (5)$$

c

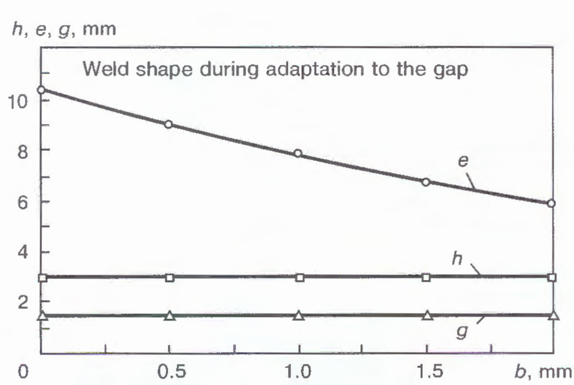

d

Criteria of weld shape quality

$h_{sh} = h \pm 0.1h$, $g_{sh} = g \pm 0.5$ mm,

$e_{min} \geq b_{max} + 4$ mm

e

Figure 2. Mathematical model of technological adaptation to the gap in consumable-electrode robotic arc welding in a mixture of Ar + 25 % CO_2

control and special requirements to development of its software.

The gap in the butt is known to have a significant influence on penetration depth and quality of weld formation. Therefore a priority task in arc welding is technological adaptation of the robot to the gap. This adaptation should be performed in real time.

In this connection, the objective of this work is construction of a mathematical model of technological adaptation of the robot to the size of the gap in a butt joint in consumable-electrode arc welding, which would be simple, and, therefore, would require minimal time for calculation and correction of the welding mode.

Method of deterministic-statistical modeling of weld shape in arc welding [8] was used to develop the mathematical model of weld shape in arc welding of square-butt joints with a variable gap [9]. In order to solve the problem of adaptation of arc welding mode to the gap first of all a mathematical model of weld shape (direct problem) was developed, allowing for the influence of the gap (expressions (3)–(5)). Experimental evaluation of the influence of the gap and welding mode parameters on weld shape in the case of consumable-electrode arc welding in a mixture of Ar + 25 % CO_2 demonstrated that the mathematical model of weld shape may have a sufficient level of adequacy, when allowing for just the two main parameters, namely welding current I and welding speed v. Solution of the system of equations (3) and (4) with respect to current and welding speed (inverse problem) yielded the simplest mathematical model of adaptation of the mode of arc welding to the gap (Figure 2, *a*, expressions (1) and (2)).

Use of the model is shown in Figures 1 and 2. Part of input information (d is the electrode wire diameter, h is the penetration depth, g is the height of weld convexity, etc.) is assigned by the operator during robot programming. During welding the video sensor system determines the gap width, which is sent to the computer, where the current parameters of the welding mode are calculated, namely welding current and speed (by expressions (1) and (2)). The other parameters of the welding mode (welding voltage U and electrode wire feed speed v_f) are the derivatives of earlier determined parameters and are also calculated in the computer. So, the rate of electrode wire feed can be determined by the formula derived in [10]:

$$v_f = 0.53 \frac{I}{d^2} + 0.7 \cdot 10^{-3} \frac{I^2}{d^3}. \qquad (6)$$

Optimal welding voltage may be calculated, depending on welding current, by the following formula:

$$U = 14 + 0.05I. \qquad (7)$$

Calculated current parameters of welding v, v_f and U are sent to the robot actuators for correction of the welding mode.

Analysis of the process of technological adaptation of the robot to the gap shows that with the increase of the gap, all the parameters of welding mode I, U and v decrease (Figure 2, *b*). Calculation of the dimensions of the weld by the initial model of weld shape (expressions (3)–(5)) shows that during the adaptation process the weld width does not remain constant, but decreases with the increase of the gap, provided a constant depth of penetration and height of weld reinforcement are maintained (Figure 2, *d*).

Under the conditions of arc welding of low-carbon and low-alloyed steels, in which the thermal cycle of welding does not result in any significant change of properties in the HAZ metal, the correspondence of the actual produced dimensions and shape of the weld to the requirements of the standard may be the criterion of quality of technological adaptation (Figure 2, *e*).

CONCLUSIONS

1. Deterministic-statistical model was developed of technological adaptation to the gap in robotic consumable-electrode arc welding, which features simplicity (the two main parameters of the welding mode are taken into account). Model application allows improvement of the response of the adaptive control system of the robot.

2. During adaptation to the gap, the welding current and speed and weld width, respectively, decrease with the increase of the gap in the butt, provided the specified penetration depth and height of weld reinforcement remain constant.

3. Method of simulation of technological adaptation to the gap may be applied in development of the software and hardware of the adaptive system of robot control in other processes of arc welding of steels and non-ferrous metals and alloys, namely submerged-arc, inert gases consumable and non-consumable electrode welding.

1. Timchenko, V.A., Bernadsky, V.N. (1997) State-of-the-art and tendencies of development of robotisation of welding manufacturing. *Avtomatich. Svarka*, **3**, 23–27.
2. Cloos, K.-E., Dilthey, U. (1991) Application of robotic technological work stations for arc welding. *Ibid.*, **7**, 55–59.
3. Timchenko, V.A., Sukhomlin, A.A. (1988) *Robotisation of welding manufacturing*. Kyiv: Tekhnika.
4. (1988) *Welding robots*. Ed. by G. Gerden. Moscow: Mashinostroenie.
5. Morozov, B.I., Stankevich, L.A., Yurevich, E.I. (1987) *Robot control systems*. Leningrad: LPI.
6. Timchenko, V.A., Nechev, G. (1982) State-of-the-art and tendencies of development of welding robots. *Avtomatich. Svarka*, **7**, 45–57.
7. Bortnyakov, Yu.L., Ustinov, N.G. (1990) Development of adaptation path of robot control system for arc welding. *Svarochn. Proizvodstvo*, **10**, 34–36.
8. Korinets, I.F., Ji Cheng Chung (2001) Deterministic-statistical model of weld shape in arc welding. *The Paton Welding J.*, **10**, 39–44.
9. Korinets, I.F., Ji Cheng Chung (2002) Effect of gap on sizes of butt weld in consumable electrode arc welding in Ar + 25 % CO_2 mixture. *The Paton Welding J.*, **8**, 15–17.
10. Korinets, I.F. (1995) Mathematical model of electrode wire melting in arc welding. *Avtomatich. Svarka*, **10**, 39–43.

PECULIARITIES OF PHASE FORMATION IN PRESSURE WELDING OF DISSIMILAR METALS UNDER CONDITIONS OF HIGH-RATE DEFORMING

L.I. MARKASHOVA, V.V. ARSENYUK, G.M. GRIGORENKO and **E.N. BERDNIKOVA**
The E.O. Paton Electric Welding Institute, NASU, Kyiv, Ukraine

Results of investigations into peculiarities of the processes of mass transfer and phase formation in joints of dissimilar metals characterized by a limited mutual solubility (Cu + Al, Ti + stainless steel, St.3 + Al, etc.) are given. The joints were made by pressure welding using high-rate methods of deforming.

Key words: *pressure welding, explosion welding, dissimilar joints, rate of deforming, dislocations, segregation, phase formations, stoichiometric composition, structural parameters, yield strength, hardening, mechanical properties*

Formation of brittle phases, and also fusible eutectics is associated usually with a reduction in mechanical properties of dissimilar metal joints made by a pressure welding [1–8], especially those joints of metals which have a limited mutual solubility. Taking into account the negative effect of the above-mentioned phases on the properties of the welded joints, different methods, blocking the formation and growth of these phase formations, are widely used. One of the most widely-spread methods of this blocking is the use of interlayers of metals forming unlimited solid solutions with metals being welded. Owing to this, the tendency of formation of intermetallic layers in the transition zone is reduced greatly.

Other technological solutions are investigated to prevent the formation and growth of brittle phases. For example, technological conditions are selected so that the temperature of welding could not exceed $T_m/2$ of the most fusible material, and the welding time could not exceed the incubation period of their formation [2, 4]. Authors of the above-described works outline that the formation of hard brittle in-

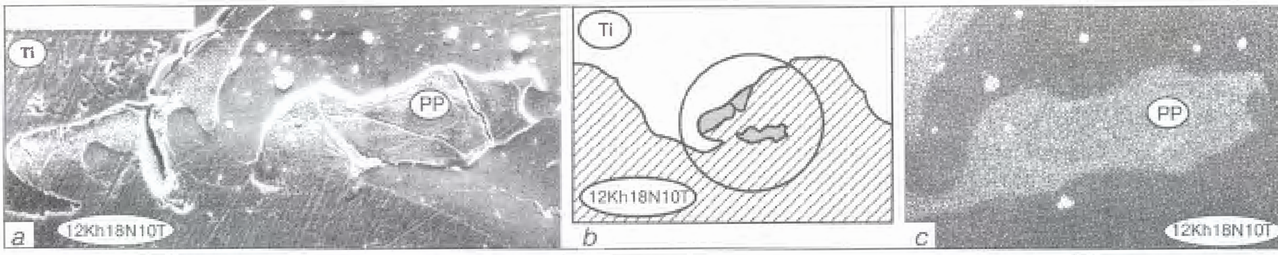

Figure 1. Structure in the zone of 12Kh18N10T + VT1-0 joint made by explosion welding: *a* — structure parts (×163); *b* — scheme of wave formation zone (×655); *c* — nature of titanium distribution (characteristic radiation) (×655)

terlayers can also provoke the appearance of the fusible phases. The latter is due to the fact that during formation of carbides the blocking of heterodiffusion is occurred, thus leading to a local increase in temperature and appearance of liquid phases [2].

In some cases the decrease in intensity of formation of brittle phases is noted with increase in rates of deforming in welding [8–10]. This stimulates the search for new technologies of welding using high-rate methods of deforming.

Complexity and variety of physical-chemical processes proceeding under the action of welding thermodeformational loads require the more complete information about the peculiarities of formation of the transition zone structure of dissimilar joints and processes associated with the formation of phases unfavorable for the joint quality. A more clear understanding of interrelation between the nature of phase formation and mechanical properties of joints is also necessary. Some of the results of investigations in this aspect are presented in this work.

Commercial titanium VT1-0, steel 3 (wt.%: 0.14–0.22C; 0.3–0.6Mn; Fe — balance), corrosion-resistant steel 12Kh18N10T (wt.%: 0.12C; 17.0–19.0Cr; 0.8Si; 1.0–2.0Mn; 9.0–11.0Ni; up to 0.02S; up to 0.035P), commercial aluminium alloy AD1, copper M-O and M-1 were selected as metals to be joined. The dissimilar metals were joined by explosion and friction welding. The examinations were performed using a system of methods including optical, analytical scanning and transmission electron microscopy in units SEM-515 («Philips») and JEM-200 CX (JEOL). Specially-developed methods of thinning in preparation of thin foils made it possible to carry out direct investigations of processes proceeding directly along the zone of interaction of materials being welded [11].

Results of experiment. Figure 1, *a*, *b* shows the specifics of phase formation directly in the zone of contact of titanium–steel 12Kh18N10T joint made by the explosion welding. The general nature of titanium and iron distribution in the transition zone and also local changes in their concentrations in the region of formation of phases and vortices of waves, which are manifested themselves in examination using the method of a scanning electron microscopy in a characteristic radiation, are shown Figure 1, *c*.

As is seen from the Figure, the distribution of elements and structural-phase state of the metal in the welding area is not uniform. Thus, in some zones from wave depression to crest a rather uniform variation in concentration of chemical elements is observed during transition from titanium to steel. Near the vortex zone a laminar nature of titanium and iron distribution is observed (see Figure 1, *c*). This is a result of a directed movement of flows of masses of one of the joining metal (titanium) inside the volumes of another metal (steel 12Kh18N10T) in the field of effective stresses. The quantitative analysis of distribution of chemical elements showed the uniform change in their concentration and also the presence of zones with a constant level of content of these elements that proves the formation of phases of a definite stoichiometric composition in this region.

As to the structures, forming in the zones of fusion and localized, as rule, in areas of vortecies of waves, then these zones in optical examinations are manifested as clusters of fine-grain structures (see Figure 1, *a* and *b*). Results of more detailed transmission microscopy examinations showed that the mentioned fine-grain structures represent formations of an eutectic type which have a form of dispersed grains γ-Fe of a globular form fringed with interlayers of a solid solution of titanium and iron.

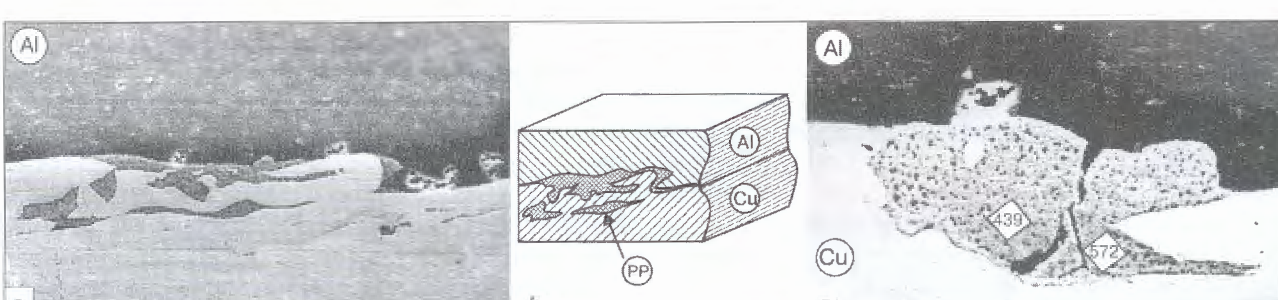

Figure 2. Zone of copper–aluminium alloy joint made by explosion welding: *a*, *b* — appearance (×356) and scheme of contact zone, respectively; *c* — fragment of contact zone with a forming phase of $CuAl_2$ type (×680)

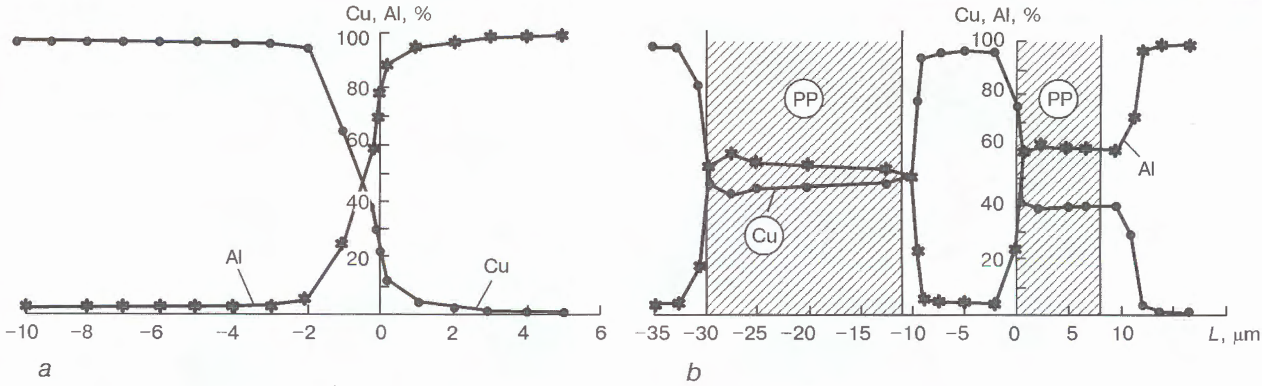

Figure 3. Change in content of main elements in the zone of copper–aluminium joint made by explosion welding (*a*) and in local areas of forming phases (*b*); *L* — distance from interface

The structure in the area of eutectic is typical of the presence of the chaotically disoriented grains with signs of proceeding of recrystallization and polygonization processes having a minimum density of dislocations. With transition to the parent metal (steel 12Kh18N10T) in the zone of mating with steel a formation of a complex stress-strain structure is observed. The latter is characterized by the presence of dense dislocation clusters, elements of twinning and also microvolumes of steel with clear features of turns and rotations.

Thus, it was established that a rigid stressed state is realized at the boundaries of the mating zones of fusible eutectics with the parent metal (with steel in the given case), which is manifested in the form of a local increase in density of dislocations, twinning and turns of metal volumes. As a rule, the formation of cracks is observed in the mentioned zones that is clearly shown in Figure 1, *a*.

In copper–aluminium alloy joints made by explosion welding, in the zone of a contact interaction at the distance approximately 100–150 μm from the interface (Figure 2, *a*, *b*) the regions of solid solutions of a variable concentration (Figure 3, *a*) and forming phase structures of a different morphology and degree of dispersity (Figure 2, *a*–*c*) are observed the same as in joints of steel 12Kh18N10T + titanium. These phase formations are differed greatly in microhardness (*HV* 572 to 205) and stoichiometric composition (Figure 4). In phase precipitations (PP) with the highest hardness the cracks (Figures 2, *c*; 3, *b* and 4) are very clearly observed. As a rule, at some distance from the surface of contact the sizes of region of forming phases, their microhardness and susceptibility to brittle fracture are decreased.

The similar situation of processes of formation of phases is observed also in the St.3 + Al joints made by explosion welding. The formation of complex zones consisting of regions of variable concentration and phase formations of different type is also occurred directly in the zone of contact.

Using comprehensive transmission electron microscopy examinations of the welding transition zone the peculiarities of formation of phase structures through its depth were revealed. In some areas the ultradispersed phases of about 0.03–0.10 μm, clusters of segregations and also compact intermetallic formations of an extended form, which are compactly arranged within the separate grains are revealed in internal volumes of aluminium grains (Figure 5). Moreover, in the zone of segregation clusters and ultradispersed phases the abrupt gradients of dislocation density are not observed, while at the same time the formation of sufficiently large non-equiaxial phases of an extended form is accompanied by the appearance of local very dense clusters of dislocations.

In friction welding it is possible to prevent the formation of intermetallic layers oriented along the plane of contact of surfaces being joined by using a local and short-time heating and method of external loading. However, under different welding conditions (conditions of conventional and inertia welding) great differences in formation of intermetallic phases in transition zone are revealed (Figure 6). It should be noted that if the conditions of the conventional welding (judging from abrupt decrease in density of dislocations and coarsening of structure) correspond to the conditions of hot deformation, then the conditions of inertia welding at which the peak temperatures in the butt are short-time, correspond mostly to the conditions of thermal deformation. Respectively, at hot deformation directly in the zone of contact the structure recrystallization is typical. It is most important that in crack initiation the growth of phase formations occurs mainly along the sub- and intergrain boundaries. This leads to the formation of extended phases of a line type, their arrangement along the intergrain boundaries has, sometimes, a twinning nature (see Figure 6, *a*).

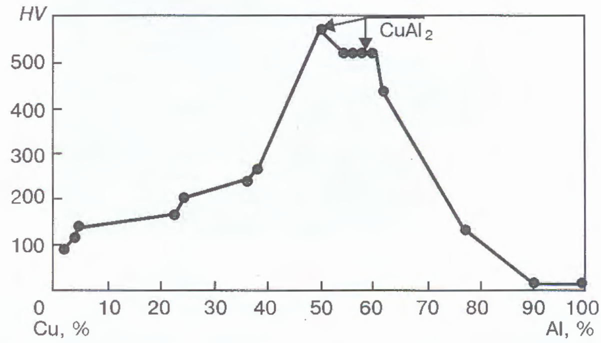

Figure 4. Dependence of microhardness *HV* of phase formations on content of copper and aluminium in them

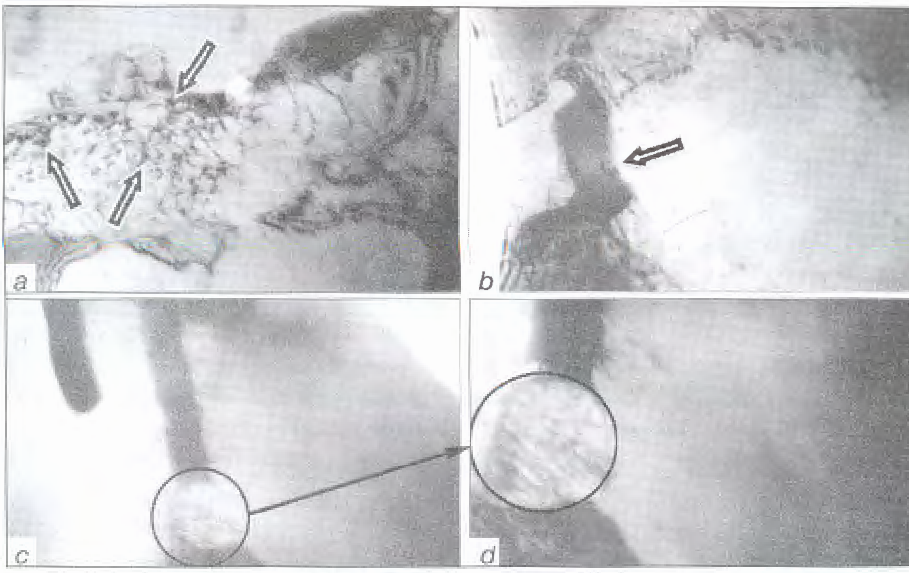

Figure 5. Formation of segregation clusters and dispersed phases (*a*) (×30000), and also non-equiaxial long phase formations ((*b*) (×37000), (*c*) (×20000), (*d*) (×30000)) in the zone of contact of St.3 + Al joint made by explosion welding

Under welding conditions corresponding to the thermal deformation conditions (inertia welding), the nature of structure and phase formation in the contact area is greatly changed. In the structure, the processes of polygonization in the volumes of grains deformed are clearly prevailed, that is accompanied by refining of structural elements preserving the increased density of dislocations. However, a principal feature of the mentioned welding condition is the change in nature of the phase formation and distribution of growing new phases. In grains of aluminium (more soft material among two materials being welded) the formation of ultradispersed particles of new phases of $d_p \approx \approx 0.1$ μm and smaller is occurred at dense and uniform their distribution inside the volumes of grains (see Figure 6, *b*). This proves that aluminium directly in the zone of contact represents quite a new structure, i.e. quasi-composite structure. For the given type of joints, probably, the presence of such structure in the zone of contact from the side of more ductile metal from the pair of metal being joined, should contribute to the levelling of an abrupt gradient of mechanical properties, observed usually along the area of welding.

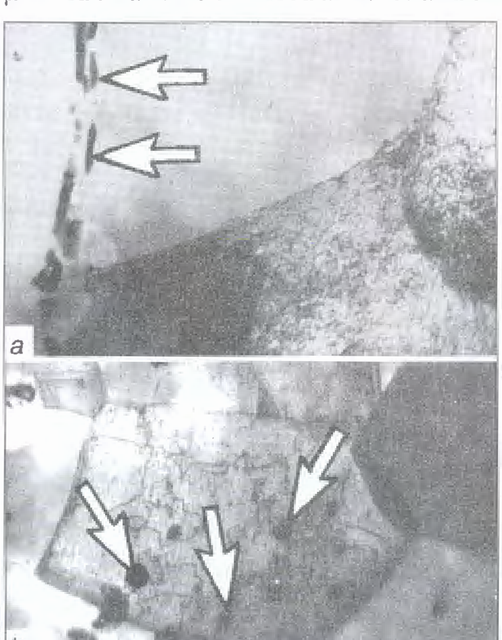

Figure 6. Change in nature of phase formation in St.3 + Al joints depending on friction welding conditions: *a* — grain boundary distribution of phases under conditions of hot deformation in case of conventional welding; *b* — intravolumetric distribution of phases at a thermal deformation in case of inertia welding (arrows show the forming intermetallic phases) (×20000)

Analyzing the revealed specifics of formation of different structures which are unfavorable for the quality of welded dissimilar joints, it is possible to emphasize the following. Formation of eutectics, connected with the formation of fusion zones in the region of waves vortex, is manifested at the parameters of waves above the optimum values. In narrow local zone of transition from fusion zone to the parent metal of size ≈ 10–15 μm the change in relaxation processes and the presence of abrupt gradients of internal stresses are observed. As in the conditions of high temperatures the dislocation mechanisms of relaxation realized by recrystallization, polygonization, are prevailed, then with transition to the parent metal the rotational mechanisms of relaxation, twinning (as a random case of a rotational mechanism), and also material turns of larger microvolumes of the parent metal are observed. And, finally, the most rigid mechanism of release of internal stresses at which the relaxation of internal stresses occurs by crack formation is realized in the parent metal where structural elements are not subjected so much to the effect of high temperatures [12].

To prevent, probably, the occurrence of unfavorable, from the point of view properties, structures, the control of the upper energy level of external effect is necessary in selection of welding conditions, eliminating an abrupt change in temperatures and, respectively, mechanisms of relaxation of the internal stresses.

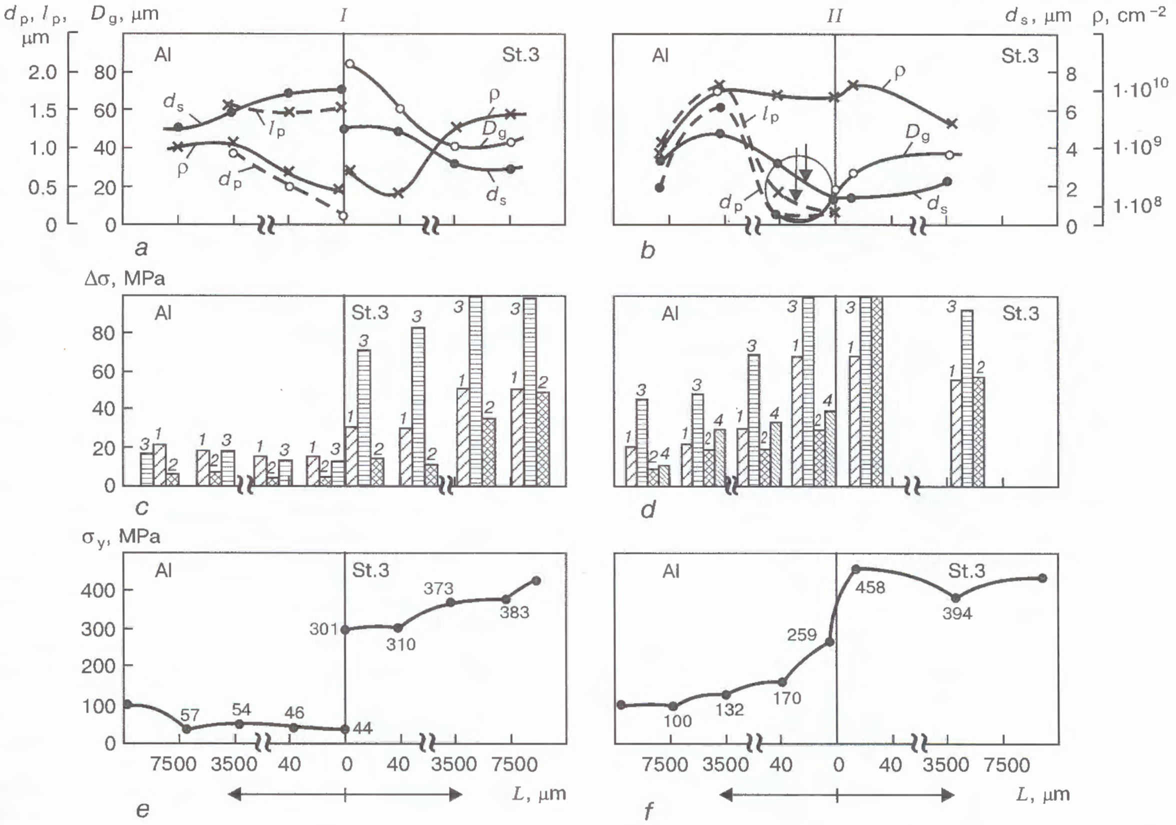

Figure 7. Structure and properties of St.3 + Al joints made by friction welding under conditions of hot (*I* — conventional welding) and thermal deformation (*II* — inertia welding): *a, b* — change in main structural parameters along the zone of welding; *c, d* — contribution of separate structural parameters to hardening of different zones of the joint; *e, f* — total hardening stipulated by the structure of welded joint metal; *1–4* — for designation see the text

As to the unfavorable structures of another type, to which brittle phases are referred, then the formation of intermetallic phases at high-rate methods of welding occurs not only in the region of contact of surfaces being welded, but also in a rather wide transition zone. Its length is about 100–150 μm. Moreover, the separate phase formations are characterized by a stoichiometric composition, hardness, sizes, nature of their distribution. As is seen, the conditions of high-rate methods of deforming in welding contributes to refining and distribution of forming intermetallic phases over the sufficiently wide transition zone of welding. In addition, the phases located closer to the interface are characterized by a high hardness and brittleness.

It was also found that the mentioned phases depending on their distribution and morphological characteristics can influence greatly the metal properties in the zone of welding.

Definite quantitative estimates of variation of yield strength depending on all the structural and phase parameters (chemical composition, sizes of grain and subgrain, density of dislocations, size, morphology and distribution of phase formations, etc.) confirm this assumption [13–22]. Figure 7 shows changes in structure and properties in St.3 + Al joints made by the friction welding for the conditions of conventional and inertia welding.

Figure 7, *a*, *b* shows changes in structural parameters: sizes of grain D_g, subgrain d_s, density of dislocations ρ, sizes of particles d_p and distance between them l_p. Figure 7, *c*, *d* reflects contribution of the above-mentioned structural and phase parameters to the hardening of different zones of the joint directly at the contact surface (here, $\Delta\sigma_s$, $\Delta\sigma_g$, $\Delta\sigma_d$, $\Delta\sigma_p$ — subgrain, grain boundary, dislocation, dispersion due to PP particles, respectively). Total (integral) hardening, stipulated by the structure of welded joint metal, is shown in Figure 7, *e*, *f*. The more detailed calculations are given in [23].

It should be noted, that on steel side of the joints made under the conditions of a thermal deformation (inertia welding) the decrease in strength is not observed. The hardening of the weld zone is provided by increase in density of dislocations ρ ≅ 21 %, refining of structure and substructure (their total contribution is about 35 %) and pearlite component.

In this case, on side of aluminium directly in the zone of contact a great increase in the yield strength σ_y is observed. The main contribution to the hardening (relative to the level of strength of the parent metal) is given by refining of grain and subgrain structure, respectively: 105 MPa (95.5 %) and 70 MPa (63.6 %), formation of dispersed phases — 40 MPa (36.4 %), and also the increase in density of dislocation — 30 MPa (27.3 %). The total hardening in this, as a rule, weakened zone of the joint is σ_y ≅ 260 MPa, that amounts to 227–236 % of aluminium strength in initial state.

Thus, as is seen from comparison of results of structural examinations and quantitative estimates under welding conditions providing formation of dispersed new phases, uniformly distributed over the transition zone, a smooth change in mechanical properties in dissimilar joints is observed with a transition from a more strong to a less strong metal that is reached due to a sufficient hardening of the joint on the aluminium side. This effect is attained by the fact that aluminium during completion of the welding cycle represents an almost new material by its structural-phase state which differs greatly from its initial state. The structure of this new material (aluminium, saturated with dispersed particles of phase precipitations) is similar to the structure of composite that is confirmed by its higher strength characteristics.

CONCLUSIONS

1. The use of high-rate methods of pressure welding of dissimilar metals leads to a considerable (≈ 100–150 μm) widening of area of phase formation over the transition zone of welding. The forming new phases of an intermetallic, carbide type are characterized by the degree of dispersity, stoichiometric composition and hardness.

2. Nature of phase formation depends greatly on the temperature field of welding deformation. Conditions of hot deformation initiate mainly the grain boundary nature of phase formation in the area of welding on the side of a less strong material and contribute to a significant enlargement of phases growing along the sub- and intergrain boundaries. In case of a thermal deformation the new brittle phases are formed, which are more dispersed in sizes at a comparatively uniform their distribution in internal volumes of grains. This contributes to the formation of structure of type of composites in softer materials being welded and makes it possible to level an abrupt gradient of properties, which is usually manifested in the zone of welding dissimilar metals.

1. Einbinder, S.B., Glude, R.K., Loginova, A.Ya. et al. (1964) Principles of theory of pressure welding. *Avtomatich. Svarka*, **5**, 21–27.
2. Gelman, A.S. (1970) *Principles of pressure welding*. Moscow: Mashinostroenie.
3. Kochergin, A.K., Shestakov, A.I. (1968) Some peculiarities of welded joint formation and calculation of pressure welding parameters. In: *Welding*, Issue 2.
4. Shron, R.Z., Zelezin, V.N. (1978) *Heat treatment and properties of welded joints*. Leningrad: Mashinostroenie.
5. Bakshi, O.A. (1977) *Theory and practice of welding manufacturing*. Sverdlovsk.
6. Hokamoto, K., Izuma, T., Andoh, T. et al. (1993) Parameters of explosion welding and strength of joint in cladding stainless steel with different aluminium alloys using an intermediate stainless steel plate. *J. JWS*, **1**, 16–21.
7. Ito, Y., Shindo, T., Saito, M. et al. (1998) Characteristics of behaviour of diffusion in the transition zone of a copper-aluminium joint during friction welding. *Transact. of Jap. Soc. Mech. Eng. A*, **618**, 494–499.
8. Abe, A. (1997) Numerical study of the mechanism of wary interface generation in explosive welding. *JSME Int. J. B*, **3**, 395–401.
9. Trykov, Yu.P., Arisova, V.N., Volobuev, S.A. et al. (1997) Structure and properties of titanium-steel composite made by explosion welding. *Svarochn. Proizvodstvo*, **8**, 8–11.
10. Markashova, L.I., Sabokar, V.K., Zamkov, V.N. et al. (1995) Structure-phase transformations in contact zone during pressure welding of titanium with copper. *Avtomatich. Svarka*, **12**, 8–13.
11. Darovsky, Yu.F., Markashova, L.I., Abramov, N.P. et al. (1985) Method of preparation for electron microscopic examinations. *Ibid.*, **12**, 60.
12. Panin, V.E., Likhachev, V.A., Grinyaev, Yu.V. (1985) *Structural levels of deformation of solids*. Novosibirsk: Nauka.
13. Suzuki, H. (1967) About yield strength of polycristalline metals and alloys. In: *Structure and mechanical properties of metals*. Moscow: Metallurgiya.
14. Ashby, M.F. (1972) On Orowan stress. In: *Physics of strength and plasticity*. Moscow: Metallurgiya.
15. Goldshtejn, M.I., Litvinov, V.S., Bronfin, B.M. (1986) *Physics of metals of high-strength alloys*. Moscow: Metallurgiya.
16. Konrad, G. (1973) Strain hardening model used to describe the influence of grain size on metal flow stress. In: *Superfine grains in metals*. Moscow: Metallurgiya.
17. Armstrong, R.V. (1973) Strength properties of superfine grain metals. *Ibid*.
18. Petch, N.J. (1953) The cleavage strength of polycristalline. *Iron and Steel Inst.*, **1**, 25–28.
19. Orowan, E. (1954) *Dislocation in metals*. New York: AIME.
20. Ashby, M.F. (1983) Mechanisms of deformation and fracture. *Adv. Appl. Mech.*, **23**, 118–177.
21. Kelly, A., Nicholson, R. (1966) *Dispersion hardening*. Moscow: Metallurgiya.
22. Ebelling, R., Ashby, M.F. (1966) Yielding and flow of two phase copper alloys. *Phil. Mag.*, **7**, 805–809.
23. Markashova, L.I., Grigorenko, G.M., Arsenyuk, V.V. et al. (1998) On interaction between structure and properties of steel-aluminium joints made by friction welding. *Avtomatich. Svarka*, **8**, 7–14.

SLIME OF WATER-CONDITIONING UNITS OF THERMAL POWER ENGINEERING AS RAW MATERIAL FOR ELECTRODE COATINGS

P.P. LAZEBNOV and **N.N. PULINA**
Zaporizhya National Technical University, Zaporizhya, Ukraine

The paper demonstrates the advantages of thermal power plant slime over marble, which is traditionally applied as gas-slag-forming component of welding consumables. Electrochemical investigations and gravimetric corrosion testing demonstrated the high quality of deposited Cr–Ni metal and the possibility of applying slime in electrode manufacture.

Key words: *thermal power plant slime, deposited metal, metallographic and electrochemical investigations, petrographic analysis, non-metallic inclusions, welding slags, corrosion, mechanical properties*

For almost a century now marble has been used in the world practice in welding consumables (electrodes, fluxes, flux-cored wires, etc.) as the main gas-slag-forming component. Its share reaches 50–57 % in the charge of electrode coatings of various types. Up to 28 % $CaCO_3$ are also added to all the fluxes for welding nickel, copper and their alloys. Tens of thousand of tons of this mineral are annually imported into Ukraine for the needs of industry. In this connection, studying thermal power plant slimes for their application in welding consumables is very urgent.

This paper describes the results of pioneer research as proof of validity of using the slime of water-conditioning units (WCU) of thermal power engineering as a gas-slag-forming component in welding metallurgy.

In thermal power engineering water, after deep cleaning by the method of chemical desalination in WCU, is used in TPP and NPP for technological purposes. Initial treatment — in-coming water pretreatment to remove weighted substances, organic contamination, bicarbonates and silicic acid — is performed by coagulation with subsequent precipitation and filtering in lightening filters of VTI-630I, VTI-1000I grades, etc. In this case, the problem of recycling solid wastes, in particular WCU slime remains to be very urgent. Up to 6.5 thous. ton of valuable secondary raw materials are annually dumped at each TPP («Dneproenergo» system). Provision of slime reservoirs involves additional cost. Industrial utilization of slime for production of construction materials, purification of power plant waste water and reclaiming of lime is being now introduced in the national economy [1–3]. A greater part of this product, however, still does not find application.

Slime of Pridneprovsk HPS has been studied, which has the following weight fraction of components, %: CaO — 43.0–45.0; SiO_2 — 10.4–11.0; MgO — 2.6–2.8; FeO — 2.5–2.7; Al_2O_3 — 1.6–1.7; K_2O — 0.66–0.73; Na_2O — ≤ 0.12; CaO_3 — balance. Compared to marble (GOST 4416–73), used in welding fabrication ($CaCO_3 \geq 97$ %; $SiO_2 \leq 0.7$ %; $MgO \leq$ ≤ 1.0 %), slime advantages are obvious. Analyzed slime is a multicomponent system of $CaCO_3$–CaO–SiO_2–MgO–FeO–Al_2O_3 type, consisting of basic (CaO, MgO, FeO), acid (SiO_2) and amphoteric (Al_2O_3) oxides, being favourable for thermodynamics and metallurgy of welding. Presence of alkali element oxides (potassium, sodium) promotes a stable arcing, higher coefficients of melting and deposition of filler materials, and further promotes desulphurization and refining of welds [4–6].

Petrographic study of marble and slime provided the following information. Refined marble designed for welding electrodes is a grayish powder, containing dust-like particles of ≤ 1 μm size and coarser (10–95 μm) ones of mostly fragment shape. Most of the particles have indices of refraction n_g = 1.658 and n_p = 1.486, corresponding to the composition of pure calcite ($CaCO_3$). Some of them have the granular or streaky microstructure, characteristic of marble. Thus, crushed rock consists of calcite and marble particles of different size and shape.

Already in the initial condition the slime is a powder-like component of brown colour with particle size of ≤ 60 μm of a constant mineralogical composition. Its base is dolomite Ca(Mg, Fe)O·CO_2; impurities are represented by iron hydrooxide $Fe_2O_3 \cdot H_2O$ of brownish-reddish colour, giving the slime a similar colouring, sodium $Na_2O \cdot SiO_2$ and potassium $K_2O \cdot SiO_2$ silicates, as well as complex (non-stoichiometric) oxides and calcite $CaCO_3$. Slime is marble analog in the first approximation, but differs from it by a stable granulometric, mineralogical and chemical compositions.

Experimental part of the work included manufacture of electrodes of fluoride-calcium type, which were used for welding plates of 600×100×10 mm size of 12Kh18N10T (C — ≤ 0.12; Cr — 17.0–19.0; Si — ≤ 0.8; Mn — 1.0–2.0; Ni — 9.0–11.0; S — up to 0.02; P — up to 0.035 wt.%) steel and for multi-layer deposition into a mould. In this case, marble and slime

Table 1. Composition of deposited metal

No. of sample series	Weight ratio of marble and slime in electrode coating, %	Weight fraction of elements, %								
		C	Si	Mn	Cr	Ni	Nb	S	P	$[O_2]$
1	54:0	0.09	0.69	1.20	18.20	9.60	0.54	0.025	0.029	0.035
2	40:14	0.09	0.72	1.26	18.30	9.58	0.52	0.018	0.028	0.033
3	30:24	0.08	0.67	1.25	18.33	9.62	0.47	0.017	0.026	0.032
4	20:34	0.10	0.70	1.30	18.30	9.60	0.49	0.016	0.026	0.030
5	10:44	0.09	0.75	1.29	18.60	9.55	0.53	0.015	0.019	0.028
6	0:54	0.08	0.76	1.35	18.58	9.62	0.52	0.016	0.020	0.024

content in the coating charge was varied in the proportion of 54:0, 40:14, 30:24, 20:34, 10:44, 0:54. Welding-technological properties of experimental electrodes were the same as those of the standard ones. Produced welded joints and deposited metal were used to make samples for metallographic, metallophysical and electrochemical investigations, and corrosion and mechanical testing.

Metallographic investigations of the sections demonstrated a high quality of welds, favourable orientation of the crystallites and absence of defects (pores, cracks, etc.). In samples of all the series (Table 1) the deposited metal practically has the same composition. It should be noted, however, that, compared to samples of series No.1, in the deposited metal of 08Kh19N10B type of series No.6 the coefficients of desulphurization and refining for sulphur, phosphorus and oxygen are equal to 36 and 31.4 %, respectively (compared to samples of series No.1, deposited with standard electrodes). At the same time, transition of silicon, manganese and chromium into the weld pool was somewhat increased. These indices are proof of the refining effect of slime, as impurities concentration was reduced by one third, compared to that of the standard.

In samples of No.1 series (see Table 1) the metal has a characteristic austenitic-ferritic structure (Figure 1, *a*). When marble–slime ratio in the coatings (Figure 1, *b*) was varied and at complete substitution of $CaCO_3$ no significant changes were found in the structure, although the crystallite size and amount of δ-ferrite decreased in the metal of welds of No.6 series (Figure 1, *c*). Contrarily, when the nature of nonmetallic inclusions (NMI) was studied, differences in the morphology, phase composition and degree of contamination of the welds of series No.1 and 6 were found. In the metal of samples, deposited by electrodes with 54 % $CaCO_3$ in the coating, inclusions are characterized by a predominantly angular, more rarely sharp-angled shape (Figure 2, *a–c*). NMI size is equal to 3–5, individual ones being 10–13 μm. The first, as a rule, are single-phase, amorphous, and are characterized by variable indices of refraction, pointing to unstable chemical composition. Larger formations have a grain structure, characteristic of marble. Their optical properties, similar to those of the fine ones, do not always correspond to the stoichiometric composition of $CaCO_3$. Pores are observed on the surface of coarse NMI – traces of the gaseous phase (CO_2) or new growth – phases, resulting from interaction of marble particles with the alloying elements of welds (Figure 2, *b*).

X-ray microanalysis demonstrated the presence of calcium and silicon in the composition of the inclusions, and of chromium and manganese in some of them, which is indicative of marble interaction with the metal. This factor is noted also in studying the locally isolated particles, extracted in a carbon copy, in UEMV-100K electron microscope. It is established that fine particles of $CaCO_3$ undergo a complete, and coarser particles a partial transformation, thus forming the film and rounded (globular) forms, respectively. New film growth is spread over the metal grain boundaries, it is amorphous (glass-like) and does not correspond to the stoichiometric composition. These excess phases impair the metal quality and promote corrosion attack.

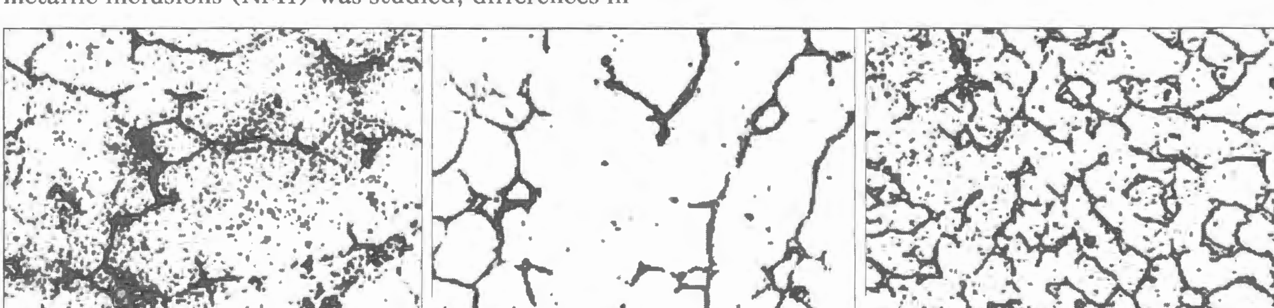

Figure 1. Microstructure of metal of 08Kh18N10B type with different ratio of marble and slime in the coatings: *a* – 54:0; *b* – 20:34; *c* – 0:54 (×500)

Sulphides are quite often found in the composition of the film and globular NMI, which sometimes precipitate on the surface of marble particles with formation of oxysulphides. Thus, the deposited metal of the standard electrode is strongly contaminated by fine and dispersed inclusions, which have an unfavourable film and sharp-angled forms. Mineralogical phases in the welds, made using electrodes with the weight fraction of slime of 54 % in the coating (Figure 2, *d–f*) have a predominantly round shape and noticeably smaller dimensions (1–1.5, individual ones – 3–5 µm). A reduction of the overall amount of NMI is observed, as marble is substituted by slime. In addition, the content of film inclusions markedly decreases, and no inclusions are found in the metal of the samples of series No.4 and 5. No interaction was established between slime particles and metal, which is confirmed by the data of X-ray microanalysis; sulphides are practically absent. It should be noted that intensive interaction of slime and marble particles results in formation of new $Na_2O{\cdot}CaO{\cdot}SiO_2$ silicates and $Na_2O{\cdot}Al_2O_3{\cdot}4SiO_2$ alumosilicates, as well as phases of a nonstoichiometric composition of an isometric, and not film form, as in the case of marble. In the metal of samples of No.5 series, added to sodium silicates and alumosilicates are refractory Mg-containing $CaO{\cdot}2SiO_2$ and $2MgO{\cdot}SiO_2$ silicates, which in this case prevail [7]. Quantitative analysis of inclusions to GOST 1778–70 (Table 2) showed that the index of metal contamination in samples of series No.6 decreased by 22 %, compared to that for samples of series No.1. Size and amount of non-metallic phases decreased simultaneously (to 16 %), which promotes improvement of physical-chemical indices of welds [7, 8].

Petrographic methods allow determination of the composition, microstructure, phase formation, establishing the mechanisms of their transformation on the slag–metal interface. Welding slag, when using the standard electrode (54 % $CaCO_3$ in the coating) is a grayish-coloured crust. Surface, adjacent to the weld, is enamel-like, smooth, porous in places, and the outer surface is rough, of black colour. High rate of solidification in welding leads to formation of fine-crystalline slag with chemical and structural heterogeneity. It has a complex composition, no CaF_2 and $CaCO_3$ relics, is saturated with the metal phase and mineral new growth, which is due to physical-chemical processes of exchange, complexing, etc. Phase composition and microstructure of the slag (Figure 3) mostly are represented by two-component eutectics of disperse CaF_2 and long-prizm crystallites of oxyfluoride compound. Its crystals are colourless, anisotropic, have refraction indices $n_g = 1.60$ and $n_p = 1.59$. Presumably, this is a compound of the type of $p[2CaO{\cdot}Al_2O_3{\cdot}SiO_2]CaF_2$. Practically all the coating marble is present in the composition of the oxyfluoride phase in the form of CaO, and just a small part of the oxide is in calcium aluminate. Fluorite is present in a free state and in the compounds. In view of the gradient of slag solidification temperatures, in some zones these are coarse grains, dendrites, and in others – a disperse mixture with calcium oxyfluoride and entrapped metal cold shot. Structural heterogeneity is enhanced by the presence and nature of distribution of needle-like and X-shaped $CaO{\cdot}6Al_2O_3$ crystals (Figure 3, *a, b, d, e*). Also found are cubic-shaped $5CaO{\cdot}3Al_2O_3$ compounds, which form intergrowth with $CaO{\cdot}6Al_2O_3$ (Figure 3, *a, d*) and individual clusters of octahedral crystals (Figure 3, *b*). Dispersed entrapped metal cold shot is distributed through the entire volume of slag (Figure 3, *f*), containing traces of iron, chromium and nickel.

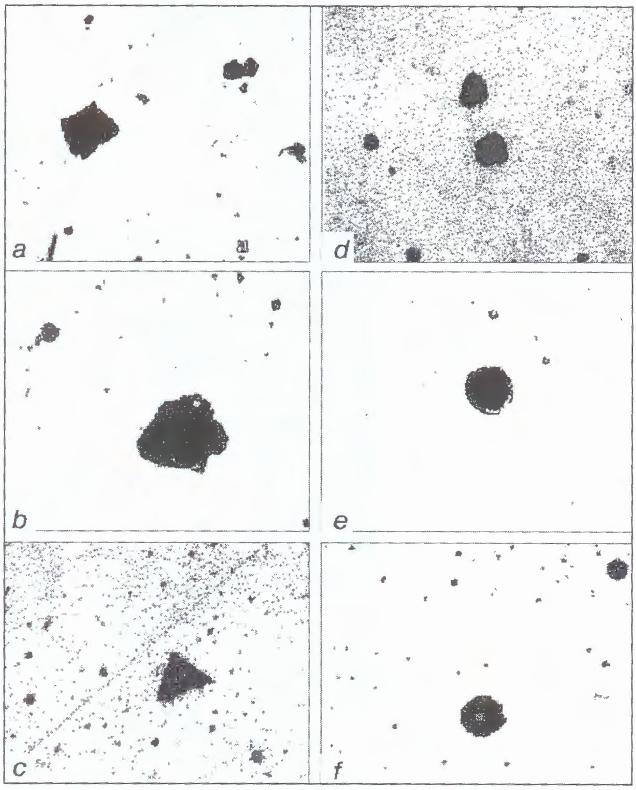

Figure 2. Microstructure of NMI in the deposited metal of 08Kh19N10B type: *a–c* – 54 % $CaCO_3$; *d–f* – 54 % slime in electrode coating (×1000)

Based on the obtained results and preceding investigations of oxyfluoride alloys of CaF_2–Al_2O_3, CaF_2–Al, CaF_2–SiO_2 system [9, 10] the mechanisms

Table 2. Content of NMI in weld metal

No. of sample series	Content of NMI (J index)	Average size of oxide inclusions*, µm	Number of inclusions in a unit of volume $n{\cdot}10^6$, mm^{-3}
1	0.0219	1.496/10.7	4.178
2	0.0189	1.671/11.0	3.588
3	0.0174	1.488/11.0	3.799
4	0.0179	1.433/6.5	3.799
5	0.0180	1.579/7.0	2.488
6	0.0172	1.475/4.0	3.515

*Numerator gives the average and denominator the maximum size of inclusions, found during calculation.

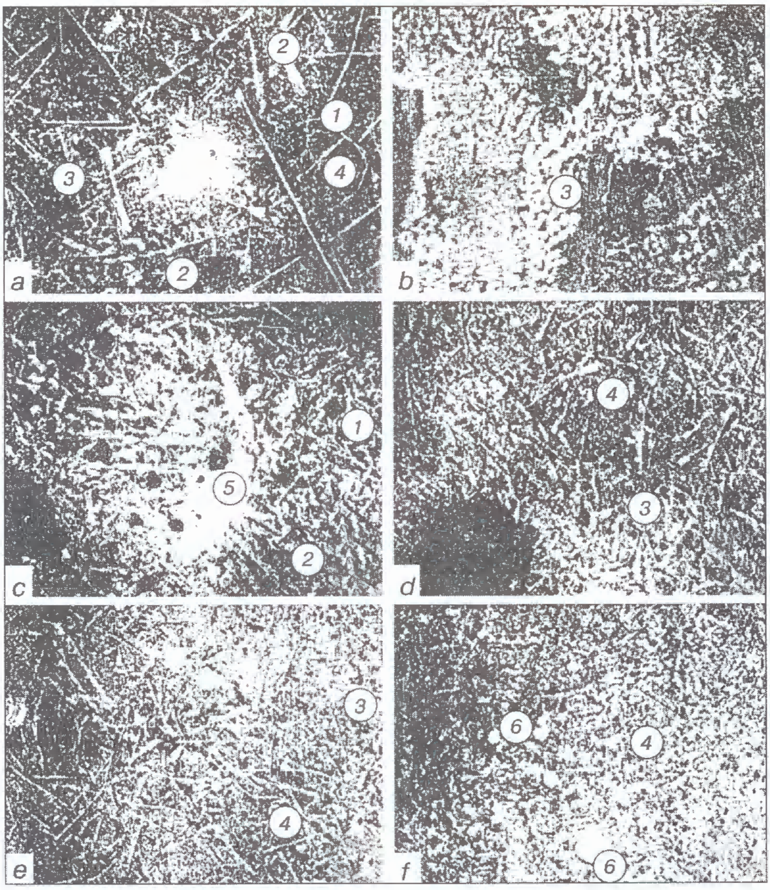

Figure 3. Microstructure of welding slag, when using electrodes of fluoride-calcium type: *a* — middle of slag crust; *b* — slag–metal interface; *c–e* — complex oxyfluorides; *f* — entrapped metal cold shot on slag–metal interface; *1* — fine dark CaF_2 grains; *2* — grey prisms of oxyfluorides; between *1* and *2* — eutectic mixture; *3* — white needles and X-shaped $CaO{\cdot}6Al_2O_3$ compounds with $5CaO{\cdot}3Al_2O_3$ prisms at the ends; *4* — eutectic CaF_2–$p[2CaO{\cdot}Al_2O_3{\cdot}SiO_2]CaF_2$; *5* — Al; *6* — entrapped metal cold shot (Fe, Cr) (×210)

of chemical and phase transformations in the slag may be presented as follows:

$$2Al + 4CaF_2 = 3Ca + CaF_2 + 2AlF_3; \quad (1)$$

$$Al + Ca = CaAl \text{ (intermetallic)}; \quad (2)$$

$$4Al_2O_3 + 4CaF_2 = 3CaO{\cdot}CaF_2{\cdot}3Al_2O_3 + 2AlF_3; \quad (3)$$

$$2AlF_3 + 3H_2O = Al_2O_3 + 6HF; \quad (4)$$

$$6Al_2O_3 + CaO = CaO{\cdot}6Al_2O_3; \quad (5)$$

$$mCaO{\cdot}nAl_2O_3 + CaF_2 \rightarrow p[CaO{\cdot}Al_2O_3]CaF_2. \quad (6)$$

Reaction of equation (5) proceeds up to complete binding of aluminium and calcium oxides into stable $CaO{\cdot}6Al_2O_3$ and $5CaO{\cdot}3Al_2O_3$ compounds. Behaviour of silicon is similar to that of aluminium — in this case oxidation to suboxides and formation of tetrafluorides takes place:

$$3CaF_2 + Si = 2Ca + CaF_2 + SiF_4; \quad (7)$$

$$2CaF_2 + SiO_2 = 2CaO + SiF_4; \quad (8)$$

$$SiF_4 + 2H_2O = SiO_2 + 4HF; \quad (9)$$

$$p[mCaO{\cdot}nSiO_2] + CaF_2 = p[mCaO{\cdot}nSiO_2]CaF_2. \quad (10)$$

Ternary oxyfluoride compounds interact with each other with formation of a quaternary $p[CaO{\cdot}Al_2O_3{\cdot}SiO_2]CaF_2$ complex. The data derived in an X-ray microanalysis system MS-46, confirm the presence of calcium, aluminium and silicon in the latter (no coefficients were determined at the oxides).

Studying a series of samples of slags, formed when using electrodes with slime-containing coatings, showed that during welding the slime was fully absorbed (no relics are observed). Phase composition and nature of slag microstructure are mostly the same as those of initial slag, produced after welding with a standard electrode (Figure 4). Notable is the fact that in the cases of application of secondary raw materials with a high content of aluminium oxide in all the variants (from 14 to 54 % slime) the calcium hexaaluminate is absent in the slags. In all probability, aluminium oxide interacts with calcium fluoride more intensively than aluminium proper, forming a gaseous compound:

$$3CaF_2 + Al_2O_3 = 3CaO + 2AlF_3. \quad (11)$$

Various impurities in the slime and oxides of magnesium, aluminium, manganese and iron form spinels of a complex composition (Mg, Al, ...)O·(Al, Mn, $FeO)_2O_3$ in it, the amount and size of which increase with the increase of the amount of studied component additives (Figure 4, *a*, *b*). When electrode coatings

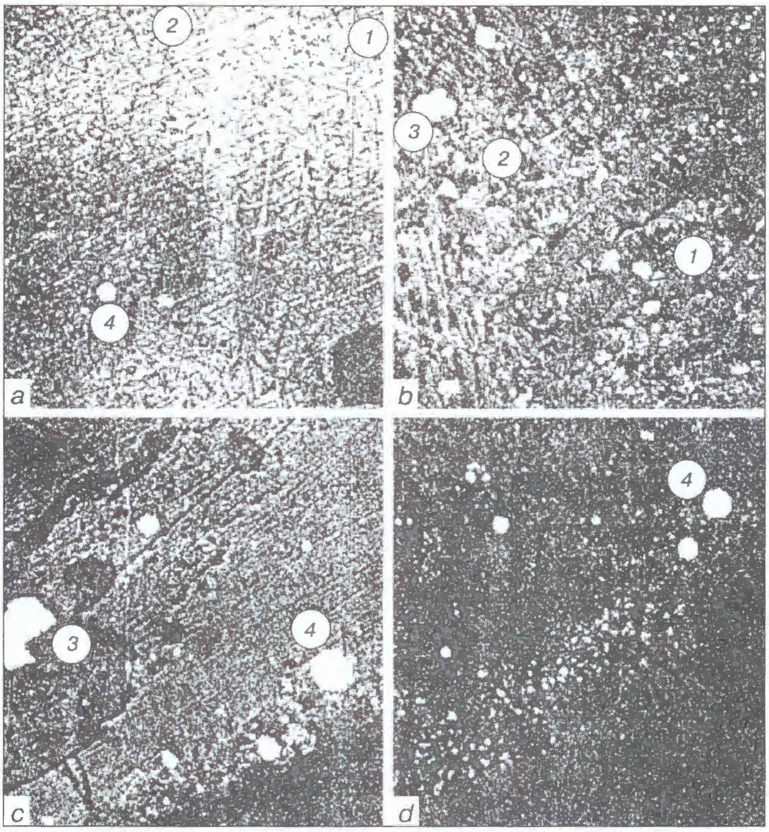

Figure 4. Microstructure of welding slag, using slime-containing electrodes (*a, c* — 44 %; *b, d* — 54 % slime): *1* — grey background — two-component eutectic of calcium oxyfluoride with CaF_2; *2* — darker inclusions and X-shaped dendrites — CaF_2; *3* — lighter-coloured (white) formations of a rectangular shape — spinel; *4* — round — entrapped metal cold shot; *c, d* — metal–slag interface zone; right lower angle — weld (×210)

with the weight fraction of slime of 14, 24 and 34 % are used, slags are formed of a similar composition and microstructure. In these cases, entrapped metal cold shot (5 μm) is spread over the volume of the slag crust. Further increase of slime additives to 44 and 54 % leads to an incomplete assimilation of metal compounds of electrode coatings; dispersed (3–5 μm) and individual coarse (≤ 80 μm) entrapped metal cold shot is located at slag–metal interface (Figure 4, *c, d*).

In order to determine the physical-chemical properties, and compare the role of marble and slime, a series of investigations of the deposited metal were conducted. The results of electrochemical investigations and evaluation of physical-mechanical properties are given in Figure 5 and Table 3. Anode potentiometric curves *1* and *2* of metals, deposited by a standard electrode and with addition of 14 % slime in the coating, are practically identical. They reflect the anode process of dissolution of steels of 18–10 type in solutions of sodium hydroxide and point to formation of passive oxide films based on iron and alloying elements. With the increase of the amount of slime (30, 40 %) the shape of anode curves changes essentially (samples of series No.3–5). Passivation region is significantly widened, and double peaks of active dissolution disappear. On samples with potentials of −(0.15–0.20) V anode current density rises, which is

Table 3. Corrosion-electrochemical characteristics of deposited metal and welded joints

No. of sample series	Corrosion potentials (30 % NaOH, 140 °C)			ICC resistance		Losses at testing in the solution, $g/(m^2 \cdot h)$		
	E_{cor}, V	$E_{p.f}$, mV	$E_{p.r}$, mV	E^{ICC}_{cor}, V	AM method (GOST 6032–89)	65 % HNO_3 (t_b)	40 % NaOH (150 °C)	5 % HCl (t_b)
1	−1.03	−26	+294	−0.23	High resistance	0.4507	0.9192	43.09
2	−0.93	−46	+214	−0.22	Low resistance	0.4912	0.9884	44.13
3	−0.96	−223	+247	−0.24	Same	0.5008	0.9750	46.28
4	−0.80	−174	+36	−0.27	»	0.5425	1.1597	46.60
5	−0.80	−10	+160	−0.34	High resistance	0.4229	0.8759	45.37
6	−0.92	−64	+284	−0.36	Same	0.4275	0.9037	42.85

Notes. 1. Number of samples in each series is 5. 2. Values E_{cor}, $E_{p.f}$, $E_{p.r}$, E^{ICC}_{cor} are potentials of steady-state corrosion, of formation and repassivation of pitting and ICC initiation, respectively. 3. Duration of testing was 144 h (24 h cycles) in 40 % NaOH and 65 % HNO_3; 48 h (24 h cycles) in 5 % HCl; 48 h (8 h cycles) by AM method.

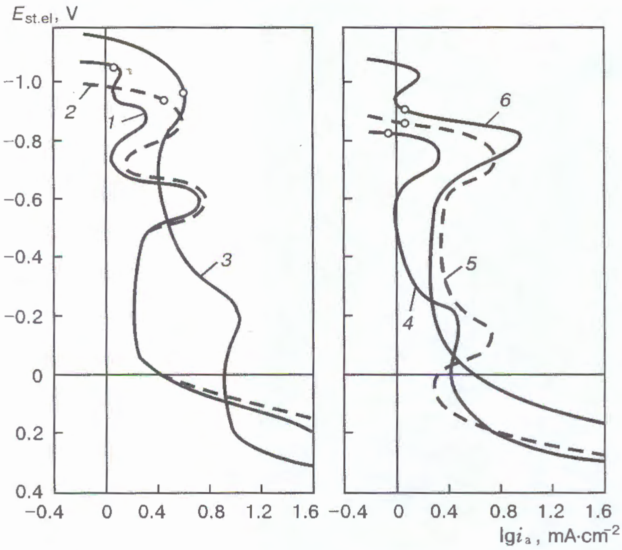

Figure 5. Anode potentiodynamic polarization curves of deposited metal (30 % NaOH, 140 °C, dE/dt = 1 mV/·s^{-1}); curve numbers correspond to the number of sample series (see Table 1)

due to manifestation of metal susceptibility to intercrystalline corrosion (ICC). The shape of the curve for samples of series No.6 (54 % slime in electrode coating) is the same as that of samples of series No.1. Increase of current density in the region of Fliade potential and of passive condition was noted, compared to the deposited metal in samples of series No.1. A common feature of the studied steels is their corrosion failure in the region of potentials of active dissolution of −(0.80–1.03) V. Data on gravimetric corrosion testing correlate with the results of electrochemical studies (Table 3). Corrosion-electrochemical properties of samples of series No.1 and 6, deposited with electrodes with marble and slime, are due to improved quality of metal, absence of film inclusions, morphology, nature of distribution of excess phases and improvement of thermodynamic stability of grain boundaries.

Samples of all the series were tested for ICC susceptibility by potentiostatic method in 10 % H_2SO_4 + 0.025 g/l KCNS solution. It is established that ICC of deposited metals is probable at the potential of about −0.75 V, and steels have a characteristic wide region of passive condition of −0.6–0.2 V, where no rejection loops of anode current were found. In addition, similar data were obtained in determination of ICC resistance by AM method (GOST 6032–89): all samples, except for series No.2–4, have satisfactory resistance.

Table 4. Physical-chemical properties of deposited metal

No. of sample series	*Weight ratio of marble and slime in electrode coating, %*	σ_t, *MPa*	$\sigma_{0.2}$, *MPa*	δ, %	*KCU, kJ/m²*
1	54:0	542/610	342	26	980/970
2	40:14	540/613	338	27	1050/990
3	30:24	543/610	348	26	1080/995
4	20:34	545/609	345	26	980/980
5	10:44	549/615	342	26	985/976
6	0:54	552/615	343	27	985/990

Note. Numerator gives the results of testing the deposited metal, and denominator — metal on fusion line.

Mechanical testing results illustrate that at partial or complete substitution of marble in electrode coatings, the indices of weld metal strength are on the same level, and ductile properties are somewhat improved (Table 4). Performed investigations and experimental results lead to the conclusion on the competitiveness of thermal plant slime against marble, which is the traditional gas-slag-forming ingredient of welding consumables.

1. Solodyannikov, V.V., Kostrikin, Yu.M., Tarasov, A.G. (1986) Industrial application of sludge mineral precipitates of waste waters from chemical water treatment facilities. *Energetik*, **6**, 7–8.
2. Kostrikin, Yu.M., Dik, E.P., Korbut, K.I. (1977) Possibilities of use of slime after lime pretreatment. *Ibid.*, **1**, 20–22.
3. Smoryadov, B.A., Gorev, N.F., Potekhin, V.Yu. (1982) Use of clearing agent slime from chemical water treatment for removing mineral oil from waste water. *Elektrich. Stantsii*, **8**, 25–27.
4. Leskov, N.I. (1970) *Electric welding arc*. Moscow: Mashinostroenie.
5. Lazebnov, P.P., Aleksandrov, A.G., Ershov, A.V. (1988) Influence of caesium on metallurgical processes in arc welding of chrome-nickel steels. *Avtomatich. Svarka*, **1**, 32–35.
6. Lazebnov, P.P. (1998) Improvement of physical-chemical properties of chrome-nickel deposited metal by modification. *Ibid.*, 10, 24-28.
7. Lazebnov, P.P., Pirozhkova, V.P., Byalik, G.A. (1993) Possibilities of application of slime in electrodes for chrome-nickel steels welding. *Ibid.*, **4**, 45–49.
8. Lazebnov, P.P., Smirnov, V.D., Shkolnikov, E.V. (1992) Corrosion-electrochemical properties of chromium-nickel metal deposited by electrodes containing slime and marble. *Svarochn. Proizvodstvo*, **8**, 31–33.
9. Litvinova, T.I., Pirozhkova, V.P., Petrov, A.K. (1972) *Petrography of non-metallic inclusions*. Moscow: Metallurgiya.
10. Podgaetsky, V.V., Kuzmenko, V.G. (1988) *Welding slags*. Kyiv: Naukova Dumka.

Our concepts of heat source distribution, heat exchange and hydrodynamic phenomena in the weld pool are only slightly developed so far. In this respect the article by G.I. Leskov and S.V. Pustovojt «About the problem of construction of a dynamic model of weld pool in electric arc welding», earlier published in our journal (The Paton Welding J., 2001, No. 1, p. 11–15) is a step forward. Some postulates, assumed in this article, are disputed by S.V. Gulakov and B.I. Nosovsky, the authors of the paper, published below.

In view of the complexity of the problem and importance of correct understanding of the physical phenomena, occurring in the pool, the editorial board decided to complement publication of the article by S.V. Gulakov and B.I. Nosovsky by a reply to it, provided by G.I. Leskov and S.V. Pustovojt. Editorial board does not intend to continue publishing the discussion between the above authors in the journal, until new data are derived and studied, which are required to construct the physical model of weld pool.

At the same time, we hope that the published articles will attract the attention of researchers to this complex and important problem.

Editorial Board

ON CONSTRUCTION OF THE MODEL OF WELD POOL IN CONSUMABLE-ELECTRODE ARC WELDING

S.V. GULAKOV and **B.I. NOSOVSKY**
Priazovsky State Technical University, Mariupol, Ukraine

Analysis of statistical and dynamic modes of weld pool was conducted, revealing their contradictions and drawbacks. Calculated and experimental data are given, allowing evaluation of the conditions of weld pool formation in consumable-electrode arc welding.

Key words: *arc welding, weld pool, liquid interlayer, liquid metal flows*

Construction of models of weld pool formation is a highly urgent problem now. Use of such models in research and practical work allows a detailed study of the processes of formation of sound welded joints, forecasting their parameters and controlling them. It order to obtain valid results, however, it is necessary to thoroughly verify the correctness of these models.

In this connection, proceeding from the results of study [1], we believe it is necessary to express our opinion on the issue in question.

First let us analyse the known quasistatic axially symmetric model of weld pool. Its construction is based on the assumption of the energy source heat being transferred in-depth of the metal due to metal heat conductivity, the melting–solidification interface being a straight line, which coincides with a plane, passing through the electrode axis, and maximums of weld pool depth and width [2].

The validity of the assumption of spatial stability of liquid metal of the pool, which is schematically represented in Figure 1, and its condition of stability is described by equation (2) in [1], raises doubts. The latter may be true in the presence in the weld pool front part of three walls, containing the liquid metal to prevent spreading. Under actual conditions without it, the liquid metal will not rise to $h + h_p$ height, calculated from the above equality, but will spread behind the arc. Such a wall, supporting the liquid metal, may be created by the plasma flow of the arc, reflected from the pool bottom. In this case, however, corrections should be made in the above expression, as the energy of the plasma flow will be spent not only for ousting and raising the liquid metal into the crater tail part, but also for containing it near the rear wall of solidifying metal. In addition, as noted

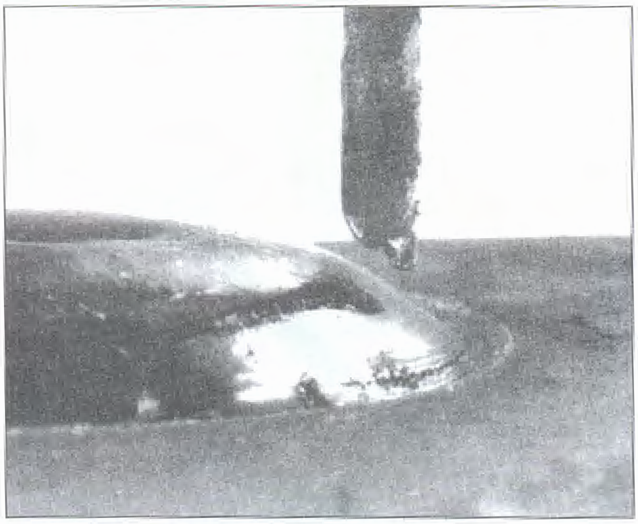

Figure 1. Location of electrode tip relative to weld pool

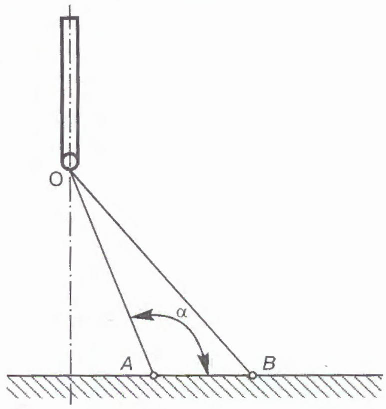

Figure 2. Schematic of calculation of arc position (for explanations see the text)

in [1], this flow should direct the liquid metal not only to the tail part of weld pool crater, but to other sides as well, also to the front of the arc.

In consumable-electrode arc welding, a flow of liquid electrode metal comes to the weld pool, in addition to plasma flow. The considered schematic does not allow for the work of this flow in formation of the pool crater in the arcing zone (current density, by the data, given in the work being discussed, is by five orders of magnitude higher than in arc plasma).

Problems also arise, which are related to melting of the crater front wall by arc column radiation. By the data of [3], the energy released in arc column, in SAW with fused flux is equal to just 15–20 % of the total energy, evolving in the arc. Effectiveness of light radiation in heating of the ambient medium is not high. Therefore, intensive heating of the crater front wall and its melting at the speed of welding are hardly probable. This is confirmed by the data of [4], which indicates that even flux does not melt in the immediate vicinity of the arc column under the arc impact.

As regards the properties of the layer of liquid metal under the arc, which is a kind of thermal insulator, the following may be noted: liquid metal is mobile and at displacement is capable of transporting heat from one region into another at a speed, which is many times higher than that of heat transfer, due to heat conductivity. In order to evaluate the effectiveness of heat mass transfer in the weld pool through heat conductivity and liquid metal flows, the shape and size of the actual weld pool [5, 6] should be compared with the pool, where the parameters are calculated by the theory of heat conductivity.

The above facts do not permit considering the quasistatic model of weld pool as being correct or applicable for analysis of the processes of weld formation.

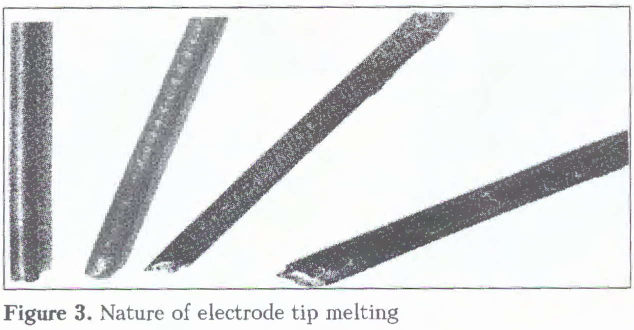

Figure 3. Nature of electrode tip melting

Authors of [1], proceeding from investigation results of other authors, made an attempt, based on this scope of information, to construct a dynamic model of weld pool, using the theory of heat conductivity. No subsequent verification of this model on practical experiments was conducted (at least the paper does not have any information about it).

As regards the essence of the problem, we should, probably, dwell on the issues, which are the basic ones for construction of the dynamic model of weld pool: processes of melting of the crater front wall and the forces, causing the motion of liquid metal over it; presence of a liquid interlayer in the weld pool under the arc, its shape and dimensions; location of electrode axis relative to the formed weld pool; geometrical shape of weld pool in consumable-electrode arc welding; nature of electrode tip melting in arc welding; size and position of arc column, running under a layer of flux.

Study [7] gives the data and calculations, which indicate that electrode axis is not located above the maximum of weld pool penetration depth, but is in the immediate vicinity of its front edge (Figure 1). The above effect may be observed also in Figure 3 from [1]. A significant factor is that in the majority of cases the maximums of weld pool width and its depth do not coincide (are not in one plane) [5], while the shape of the boundary between the fusion zone and the solidification region differs from the straight line and mostly is either concave or convex [8, 9]. Now, considering that the pool depth often is not equal to half of its width (see, for instance, Figure 1 from [5]), this statement of the authors of [1] that «... a section of the latter by a plane of symmetry, formed by a moving electrode, is a curve of approximately the same radius of curvature R_c with the center at the tip of wire electrode ...», is incorrect.

Authors of [10, etc.], who experimentally determined the thickness of liquid interlayer, assumed that the high-temperature tantalum insert is only melted by the arc, and not by the liquid metal. In reality in SAW the tantalum and even tungsten inserts dissolve in the liquid metal of weld pool. As a result, the thickness of liquid interlayer, measured by the method, mentioned in [10], turned out to be much smaller than the actual value [7]. In study [7] also the length of arc column is calculated, using the data of [3] on energy distribution in the welding arc. In keeping with them, the length of the arc, running under a layer of fused flux at mode parameters, given in the paper, is about 2 mm. As follows from [1], distance R_c (see Figure 2) should be by an order of magnitude greater. Otherwise, the above schematic is incorrect.

In order to evaluate the shape and size of the cavern (gas cavity, formed by the force impact of the arc) in liquid metal under the arc, the following experiment was conducted. During deposition of a bead on a plate in the modes, indicated in [7], weld metal splashing was performed by a procedure, described in [11] and the volume of splashed metal was determined by weighing the materials, participating in the deposition before the experiment and after splashing. Then, taking plasticine in the amount, equal to the volume of splashed metal, it was placed into the weld pool cavity, formed after liquid metal splashing. However, the volume of plasticine was so much greater, that it was impossible to obtain a cavern of the shape and size, given in [1, 10], while ensuring the formation of a thin interlayer in the region of maximal penetration depth. In this connection a model of weld pool filling with liquid metal, shown in Figure 1, was proposed in [7].

As the electrode during arc welding practically is at the front edge of weld pool, current distribution will correspond to the data of [12]. As stated by the authors of [1], spatial position of the arc, running under a layer of flux from a vertical or inclined electrode, can hardly be determined by X-ray filming. Arc plasma and gas in the space near the arc do not differ as to image contrast or density, and are indistinguishable in the radiogram.

The nature of melting of electrode tip with a bevel of its front part, which is assumed for plotting the dynamic model, also raises doubts. Examples of it are radiograms, given in [13], where electrode tip bevel has an opposite direction.

Authors of [1] suggested a procedure of calculation of power density distribution in the arc in the crater by the shape of its front wall, and Figure 4 gives the calculation procedure. From this Figure and from expression (4) it does not at all follow that the arc cannot run vertically. In keeping with the above Figure the angle of arc inclination α to surface being welded will be minimal at the horizontal position of the arc (arc runs to the front edge), and not at its vertical position, as stated by the authors of [1]. This completely crosses out all the further reasoning about the adequacy of the suggested model. Figure 2 raises the following question: what is line r, originating from point A, shown in it? Why angle α is measured exactly relative to it ? In what region of the electrode does it end and why?

We proposed the following procedure to determine the spatial position of the arc. In keeping with this procedure, discrete displacement of the electrode to a specified distance c is performed, amplitude of arc voltage increment ΔU_a at the moment of displacement and arc voltage U_a before displacement are measured, and subsequent mathematical processing of measurement results is performed. The essence of the procedure is illustrated in Figure 2, where sections $0A$ and $0B$ conditionally denote the axes of symmetry of arc column before electrode displacement relative to the item and at the first moment after displacement. Knowing the arc length before and after displacement (schematic shows item displacement relative to the electrode to distance $AB = c$), as well as this displacement c, it is possible to determine from three sides of $A0B$ triangle the angle of inclination α of the arc to the surface being welded.

Arc length before and after displacement may be found from the following expressions:

$$L_{a(0A)} = \frac{U_a - (U_{an} + U_c)}{E_a}; \qquad (1)$$

$$L_{a(0B)} = \frac{U_a + \Delta U_a - (U_{an} + U_c)}{E_a}, \qquad (2)$$

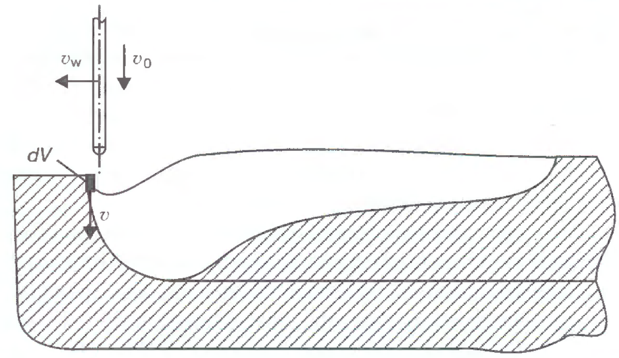

Figure 4. Shape of weld pool in the longitudinal section (for explanations see the text)

where U_a is the arc voltage, V; U_{an}, U_c is the near-electrode voltage drop on the anode and cathode, respectively, V; ΔU_a is the voltage increment on the arc at displacement of the electrode or item for distance c; E_a is the gradient of voltage drop in arc column, V/mm (given in publications, for instance, in [3]).

Then,

$$\alpha = \arccos \frac{[U_a - (U_{an} + U_c)]^2 + E_a^2 c^2 - [U_a + \Delta U_a - (U_{an} + U_c)]}{2cE_a[U_a - (U_{an} + U_c)]}. \qquad (3)$$

Considering that $U_a - (U_{an} + U_c) = U_{col}$, (here U_{col} is the voltage drop in arc column), equation (3) may be simplified:

$$\alpha = \arccos \frac{U_{col}^2 - (U_{col} - \Delta U_a)^2 + E_a c^2}{2cU_{col}E_a}. \qquad (4)$$

Increment of arc voltage at the moment of discrete displacement of the electrode relative to the item was determined using a cathode-ray oscillograph: a differentiating link was connected at its input, which isolated just the alternating component of arc voltage, namely amplitude of this voltage increment.

Measurements showed that in the studied range of values of welding parameters (U_a = 27–40 V, I_a = = 400–800 A, v_w = 0.3–1.5 cm/s) and at the angle of electrode inclination to the processed surface of 30 to 90° the arc practically did not deviate from the normal to this surface. This is confirmed by the nature of electrode tip melting (see Figure 3), which proceeded in parallel to this surface at the change of the angle of inclination of electrode axis.

The results of investigations, performed by the authors and the above materials indicate that the nature of formation of the front wall of weld pool crater differs from those described earlier both by the static and dynamic model, presented in [1].

If the weld pool shape, distribution of liquid metal in it and electrode orientation relative to it are presented as a schematic, shown in Figure 4, the process of the pool formation may proceed as follows.

An elementary metal volume dV during time dt, having been imparted a certain stock of kinetic energy, as well as energy in the form of heat, transferred to the metal volume, starts moving in the liquid metal flow at velocity v along the front wall of the crater, performing the work on its melting and overcoming the medium resistance. In this case, displacement of the pool front wall in the direction of the vector of welding speed (its transition from the solid into the liquid condition) proceeds not only due to its melting, but also due to dissolution [7] and dilution. As the stock of energy is spent, the intensity of melting of the front wall decreases, and the process of weld pool metal solidification and weld formation starts in the pool lower point (along its axis).

Thus, the energy, applied to the weld pool head part will be transported to that side, where the liquid metal flows, formed by external forces, are directed. Energy evolved in the arc and transferred to base metal, may be regarded as concentrated in the arc active spot (cathode at reverse polarity), located in the weld pool head part on its surface near the front edge. Then this energy (mainly, potential, thermal and kinetic in the form of the high-speed flow of the medium) is transported to different points of the pool volume, predominantly by liquid metal flows. Flows of the plasma arc and liquid electrode metal (in the form of drops at drop transfer or a jet at spray transfer) are active in formation of the liquid metal flows, in addition to electromagnetic or other forces, acting directly on the liquid metal of the pool. Direction of flows and their nature during formation of the weld pool in arc welding are described in [6]. These data are indicative of the consumable electrode metal participating in formation and intensification of flows in the weld pool, the metal moving under the impact of gravity forces, and kinetic energy of the moving electrode, electromagnetic and other forces.

In the gravity field the metal jet or drop, which separated from the electrode, will move with acceleration in the arc gap and by the moment of entering the pool, it will acquire a certain velocity

$$v = v_0 + \sqrt{2gh} + \frac{1}{m}\int F(t)dt, \qquad (5)$$

where v_0 is the electrode feed rate; g is the acceleration in the gravity field; h is the arc length; m is the drop weight; $F(t)$ is the law of distribution of electromagnetic, gas-dynamic and other forces along the arc, acting on the drop or electrode metal jet; t is the current time of flight of the drop in the arc gap.

It should be noted that at equal welding currents, the electrode feed rate increases with the decrease of its diameter. Therefore, the initial speed of the drop or jet of electrode metal in the weld pool will also be increased.

On the other hand, it is known that decrease of electrode diameter at a constant value of current leads to increase of penetration depth [7].

Electrode diameter, in its turn, has a considerable influence on the nature of electrode metal transfer into the pool, which determines the conditions of its interaction with the pool surface, and, therefore, also its role in the formation of flows in it.

At globular transfer, the drop, having a large area of contact with the pool surface, should overcome the surface tension forces. In this case, its kinetic energy is spent for formation of surface oscillations. In case of spray transfer of electrode metal the surface of the jet contact with the pool is small. In this case the consumable metal of the electrode freely penetrates (flows into) the pool depth, thus creating in the pool a flow, which moves at a high speed, providing an intensive heat transfer to the pool bottom and increasing its depth.

The plasma flow of the arc, acting on the weld pool surface, cannot penetrate (in the majority of cases at sound weld formation) into the pool depth, because of the low density of plasma relative to that of liquid metal. It spreads over the pool surface, deforming it and creating surface flows in it. The ratio of intensities of these flows (axial in-depth and surface) determines the conditions of heat and mass transfer in the weld pool, and influences the main geometrical parameters and quality of welded joint formation, accordingly.

1. Leskov, G.I., Pustovojt, S.V. (2001) About the problem of construction of a dynamic model of weld pool in electric arc welding. *The Paton Welding J.*, **1**, 11–15.
2. Erokhin, A.A. (1973) *Fundamentals of fusion welding*. Moscow: Mashinostroenie.
3. Leskov, G.I. (1970) *Electric welding arc*. Moscow: Mashgiz.
4. Gulakov, S.V., Nosovsky, B.I., Tarasenko, I.V. et al. (2001) Investigation of the process of flux melting by the arc. *The Paton Welding J.*, **8**, 21–24.
5. Gulakov, S.V., Nosovsky, B.I. (1981) Features of weld pool formation. *Avtomatich. Svarka*, **11**, 32–35.
6. Gulakov, S.V., Nosovsky, B.I. (1982) Influence of heat transfer by a flow of liquid metal on weld shape. *Svarochn. Proizvodstvo*, **10**, 2–3.
7. Gulakov, S.V., Nosovsky, B.I. (1982) On heat transfer from the source to melting front through liquid metal of weld pool. *Ibid.*, **6**, 5–6.
8. Gulakov, S.V., Nosovsky, B.I., Kulyabina, I.S. et al. (1998) On interface of melting and solidification fronts in the weld pool. In: *Transact. of PSTU*, Issue 6.
9. Chernyshov, G.G., Markushevich, I.S., Nikolaenko, M.R. (1987) Influence of metal flows in the weld pool on formation of defects of weld shape in submerged-arc welding. *Svarochn. Proizvodstvo*, **10**, 41–42.
10. Razmyshlyaev, A.D., Leshchinsky, L.K., Nesterenko, K.A. (1975) Distribution of thickness of liquid metal interlayer along the weld pool crater. *Avtomatich. Svarka*, **12**, 62–63.
11. Gulakov, S.V., Nosovsky, B.I. (1980) Device for liquid metal removal from weld pool. *Ibid.*, **10**, 75.
12. Rajchuk, Yu.I. (1967) Current distribution across the plate in arc welding. *Ibid.*, **4**, 19–22.
13. Grebelnik, P.G. (1950) X-ray investigation of the process of automatic submerged-arc welding. *Ibid.*, **6**, 18–19.

Reply by G.I. Leskov and S.V. Pustovojt

The above paper is again setting forth the authors' concepts of the weld pool in welding with deep (10–13 mm) penetration, published in journal «Svarochnoe Proizvodstvo», No.6, 1982.

In Figure 4 the authors present is as being adjacent along the entire depth, to the front wall, which, in their opinion, during welding is melted, «dissolved and diluted» by liquid metal, heated by the arc in the pool front part.

Such a situation, simple for visual observation, photographing and X-raying, was not observed by a single researcher. The authors have hardly seen it, either. The above photo of pool surface (Figure 1) was obtained after extinguishing of surface arc, when even a shallow crater is noticeable.

Indeed, as shown by numerous experiments [1–3], with immersed arc the liquid pool is ousted to the solidifying end, active spot and column of the arc are completely or partially immersed into the crater and more effectively melt off the pool bottom and its front edge. These important features of the weld pool are given in all the monographs and manuals on arc welding.

However, the nature of forces, causing the appearance of the crater and ousting of liquid metal into the pool rear part, is still subject to discussion. There exist discrepancies also as to the form of energy, melting the front wall of the crater: whether it is radiation of arc column or thermal flow, surrounding the arc active spot. Physical phenomena, causing the molten metal motion from the crater front wall to the zone of a higher pressure in its lower part, or pool equilibrium in the dynamic mode, are still not considered.

Our article [4] is an attempt to analyze these phenomena. We proceeded from experimental data of various researchers and fundamental laws of physics, in particular of hydro- and gas dynamics.

Suggesting their «model» of the pool, the authors first analyzed the initial postulates and methods of this analysis. Critical remarks are always useful to improve our concepts of the barely studied phenomena, so we will consider them in greater detail.

1. Section of the melting front wall of the crater by the pool plane of symmetry, observed in deep penetration welding, is considered to be incorrect. We assumed it; based on the results of observation of this wall by many researchers after applying a shock to the pool.

2. The data, used in our analysis, on thickness of liquid interlayer on the front wall and bottom of the crater, taken by us from experimental work [5], are considered to be erroneous. To contradict them, the authors of the article staged their own experiment, holding a tantalum indicator (T_{melt} = 2996 °C) in liquid steel so as to discover its dissolution, not taken into account in [5].

The obtained result coincides with the data of [5] and is assumed by us in our analysis. No dissolution of the indicator was found. Its height turned out to be unchanged.

3. Experiment of the authors with filling of the splashed out pool with plasticine, which as though demonstrates the absence of a «cavern» in it, and confirms their «model», is not credible. Crater and gas cavity between the electrode and its front wall always exist, and welding technology envisages its welding up at the weld end. We hope that the authors will reject their doubts on the validity of radiographs in determination of the arc position, after considering them in [1]. The main value of these radiographs consists in proving the existence of a crater in SAW, as well as rejecting any «models», negating the fact.

4. Procedure, proposed by us, and results of calculation of arc power distribution over the crater front wall, based on experimental data on equal rates of melting of all the elements of the crater front wall, in the opinion of the authors, «cross out all the further reasoning of the adequacy of the proposed model».

We proved that the constant level of the above rates will be ensured, if time Δt of the arc erring spot dwelling on ds elements of the front wall is proportional to $\sin \alpha = ds/df$. Elementary parts ds and df of the front wall in its lower and upper parts are clearly defined in Figure 2. An attentive reader will see that in the crater lower part $df >> ds$, therefore $\sin \alpha$ and Δt are close to zero. Now in the upper part, $df \cong ds$, therefore values $\sin \alpha$ and Δt are maximal. This was exactly the basis to make the conclusion on the different time of the arc active spot dwelling in the front wall zones — maximal in the upper part and minimal in the lower part. This conclusion should not be «crossed out».

5. Evaluation of the forces and pressures, acting on the molten metal of the crater front wall and shifting it downwards, was performed on the basis of experimental data about 70 % of arc current flowing to this wall and proceeding from Ampere and Bio–Savare equations. Their integration, application in calculation of magnetic intensity and electromagnetic forces is universally known. Therefore, we did not think it necessary to explain that dl is the element of a conductor with current, r is the radius-vector, β is the angle between radius-vector and direction of current, etc. The paper gives the integration limits in Bio–Savare equation, accepted by us. Therefore, the authors' comments as to «what is line r, in what region is its end located, ...» are out of place in a scientific journal.

6. Assessment of crater depth has been performed, proceeding from the second Newton law, molecular-kinetic theory of gases, and experimental data on the velocity of plasma in the conic arc column of 100–500 m/s. Taking its value of 330 m/s, average temperature of $5\cdot10^3$ K, weld root radius of 3 mm and depth of 1 cm, change of the direction of plasma movement in the crater by $\pi/4$, calculation was used to find a force, acting on the crater bottom, sufficient for its deepening to the specified value.

Authors may clarify their doubts on the possibility of such a phenomenon by blowing at water through a tube. A hollow is caused by the change of the amount of motion of any jet, and not by the density of liquid or plasma. Conditions of dynamic equilibrium of the pool and its parts have been analyzed, based on the law of movement of ideal liquid and Bernoulli equation.

Thus, the model of the weld pool, suggested by S.V. Gulakov and B.I. Nosovksy, does not have any experimental confirmation. Critical remarks on the published dynamic model are minor, even though this is just the first attempt to plot such a model. Widening the scope and generalization of experiments is required to develop this model.

1. (1948) *Automatic submerged-arc welding*. Kyiv-Moscow: Mashgiz.
2. Rykalin, N.N. (1951) *Calculations of thermal processes in welding*. Moscow: Mashgiz.
3. (1974) *Technology of fusion welding of metals and alloys*. Ed. by B.E. Paton. Moscow: Mashgiz.
4. Leskov, G.I., Pustovojt, S.V. (2001) About the problem of construction of a dynamic model of weld pool in electric arc welding. *The Paton Welding J.*, **1**, 11–15.
5. Razmyshlyaev, A.D., Leshchinsky, L.K., Nesterenko, K.A. (1975) Distribution of thickness of liquid metal interlayer along the weld pool crater. *Avtomatich. Svarka*, **12**, 62–63.

UNIQUE WELDED STRUCTURES

FIELD WELDING OF LARGE-SIZE SPHERICAL ISOTHERMAL TANKS FOR STORAGE OF CRYOGENIC PRODUCTS

K.A. YUSHCHENKO[1], **G.G. MONKO**[1], **T.M. STARUSHCHENKO**[1], **B.O. BELORUSETS**[2] and **A.S. NAUMOV**[3]
[1]The E.O. Paton Electric Welding Institute, NASU, Kyiv, Ukraine
[2]Research and Production Association «Criogenmash», Balashikha, Russia
[3]«Kislorodmontazh», Moscow, Russia

Methods for assembly, erection and welding of large-size spherical isothermal tanks of cryogenic application were proposed and implemented. The methods provide a maximum reduction of the scope of assembly-welding operations. A higher efficiency of mechanised welding and labour productivity, as well as shortening of a construction period are achieved.

Key words: *isothermal tanks, cryogenic products, assembly, field welding, automatic welding, stable-austenitic steel, increased strength, Invar, pipelines*

Liquefied oxygen, nitrogen, hydrogen and helium are widely used as a rocket fuel in modern aerospace engineering. Gases in the liquefied state have a minimum volume. They are stored in special tanks of different shapes. Liquefied gases can be transported to large distances via pipelines or by vehicles. Special systems for storage of such gases are required to ensure operation of test grounds. The most reliable method for storing liquefied gases is to use large-size spherical isothermal tanks.

The E.O. Paton Electric Welding Institute in collaboration with the Research and Production Association «Kriogenmash» and other organisations of Minmontazhspetsstroj of the Russian Federation completed a package of works on construction of large-size spherical isothermal tanks with a capacity of 1400 m^3. The world practice of tank construction had no previous experience in construction of such tanks.

The Project of «Kriogenmash» provided for building of an isothermal system consisting of two concentric tank casings: internal, with a diameter of 14 m, made from high-alloy steel 12Kh18N10T or 03Kh20N16AG6 20–22 mm thick, and external, with a diameter of 16 m, made from steel 09G2S 24 mm thick.

Figure 1 shows the spherical isothermal tank with a capacity of 1400 m^3. The working pressure in the tank is $1\cdot10^3$ kPa. The internal and external casings of the tank rest on eight supporting columns. The internal casing columns pass through the holes in the external casing (jacket), are located inside its columns and fixed to the common foundation plate. Pressure between the casings and columns amounts to $5\cdot10^{-2}$ Pa.

The internal and external casings of the tank consist of 24 lobes made at an engineering plant by cold expanding using the equatorial-meridian location and spacing of blanks. The shape of the lobes and sizes of their edges prepared for field welding are shown in Figure 2.

Assembly of the internal casing of the spherical tank includes two basic operations, i.e. assembly of the lobes into blocks and then assembly of the blocks on the manipulator supporting ring. Assembly of the lobes into blocks is done in a special rig using assembly devices. To prevent distortions, stiffening pipes are welded to the finished blocks. The three-lobe blocks are assembled first (Figure 3), and then they are enlarged. The sequence of assembly of a spherical casing from blocks on the supporting ring and schematic of location of the assembly joints are shown in Figure 4. First the blocks are fixed to each other using the assembly devices and then joined by the root welds made by the manual-argon-arc method using filler wire over the entire weld length, the weld leg being not less than 6 mm.

Automatic welding of assembly welds on the internal casing of the tank is performed without backing over the root weld in the flat position at the upper point of the vessel, while welding of internal welds is done at the lower point inside the vessel being rotated on the manipulator.

The quality of assembly of the tank before welding on the manipulator is checked and recorded in the form of the process documents.

The controlled sizes of elements of the internal casing of the spherical tank (Figure 5) should be maintained at an accuracy ensuring the quality manufacture of the latter on site within the ultimate deviations as per Table 1. Control of quality of welded joints in the cryogenic tank provides for the following

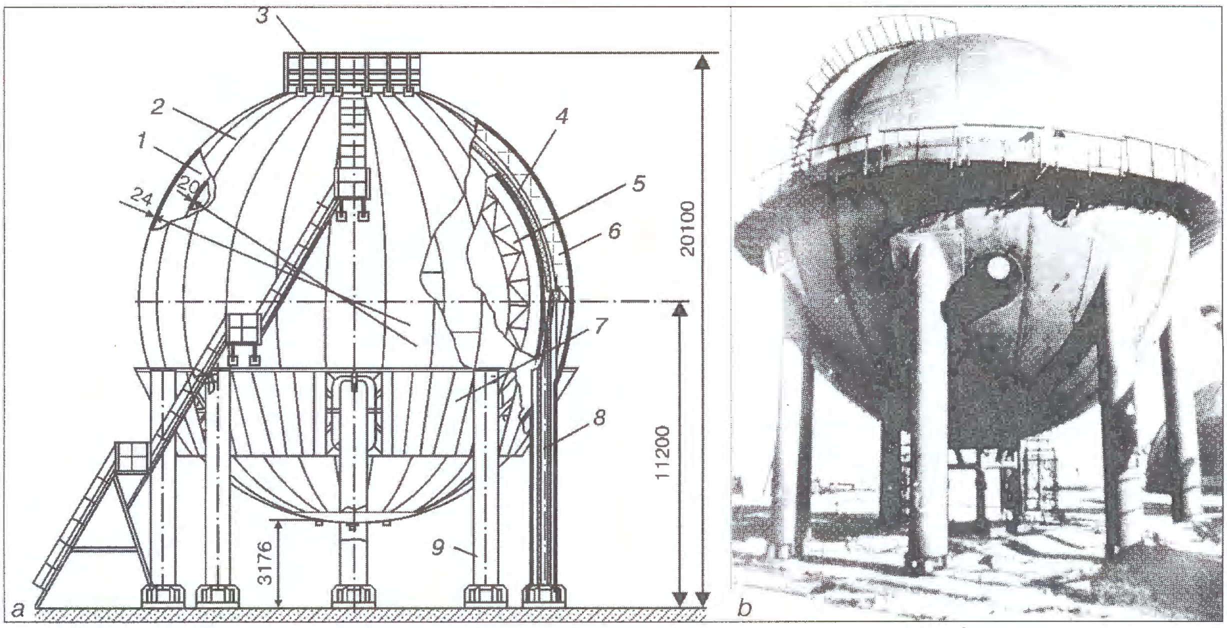

Figure 1. Schematic (*a*) and general view (*b*) of the spherical isothermal tank with a capacity of 1400 m^3: *1* — internal casing (vessel); *2* — external casing (jacket); *3* — circular platform; *4* — insulation; *5* — internal access ladder; *6* — rolling ladder in the casing spacing; *7* — supporting chord; *8, 9* — supporting columns of the vessel and jacket, respectively

Table 1. Permissible deviations in sizes of elements of the internal vessel in manufacture of the tank

Permissible deviations	*Measurement method*	*Ultimate deviation, mm*
Combined flat gradient of edges and surface curvature outwards and inwards on a length of not less than 500 mm (Figure 5, *a–c*)	Template not less than 1000 mm long	5
Local distortions in the form of bulges and dents (Figure 5, *d*)	Same	3 (total distortions should not exceed 5 mm)
Gradient of edges directly near the welds outside (Figure 5, *e*) and inside (Figure 5, *f*) the tank vessel	»	3
Buckles and displacement of lobe edges	Template and depth gauge	10 % of lobe thickness, but not more than 3 mm
Length of the circumference of a sphere measured along the equator and bands should not be more or less than the rated one by a sum of tolerance zones for the gaps on the equator, provided for by the project	Measuring tape of class 2	Same
Out-of-roundness in the equator section of the spherical tank	Same	Not more than 0.5 % of the diameter

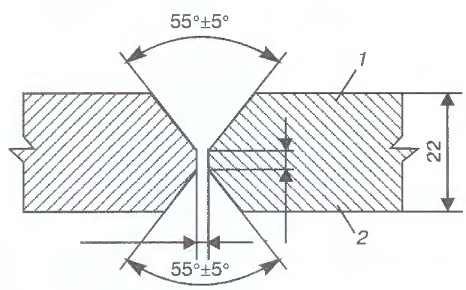

Figure 2. Groove preparation in lobes for welding using a manipulator: *1* — vacuum; *2* — manipulation environment

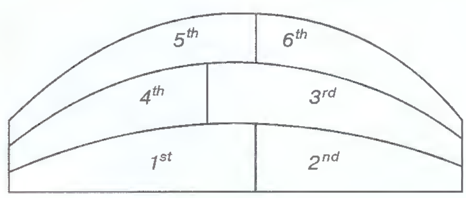

Figure 3. Schematic of assembly of a three-lobe block: *1st–6th* — lobes

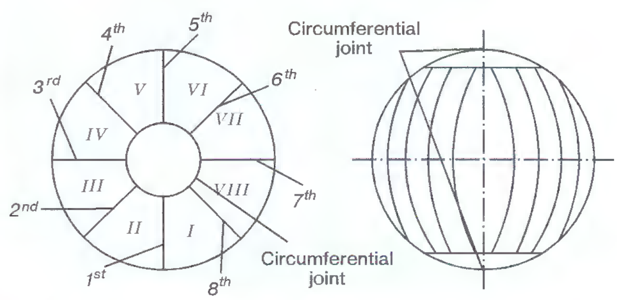

Figure 4. Schematic of assembly of blocks on a supporting ring: *I–VIII* — blocks; *1st–8th* — joints

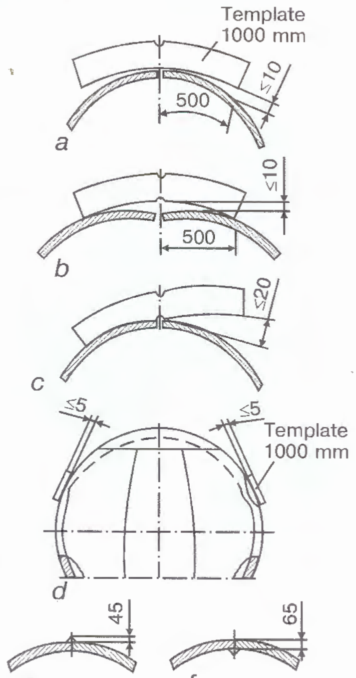

Figure 5. Controlled sizes of the cryogenic vessel: *a–f* — see explanations in Table 1

actions: external examination and measurements, X-ray or gamma inspection, vacuum tightness tests and laboratory tests. The list of the inspection methods and their scope are given in product specifications.

The rational flow diagram was developed in construction of a fleet of 24 1400 m^3 tanks: the external casing of the tank made from cold-resistant steel 03Kh20N16AG6 is assembled from individual lobes and fully welded by automatic SAW under the flux ANK-45 layer using the manipulator (Figure 6), welding of the process fixture in the flat position convenient for welding, 100 % X-ray inspection of all the welds and their repair, if necessary.

Table 2. Room- and low-temperature mechanical properties of the weld metal and welded joints of steel 03Kh20N16AG6 made by automatic submerged-arc welding

Test object	T_{test}, *K*	$\sigma_{0.2}$, *MPa*	σ_t, *MPa*	δ, *%*	ψ, *%*	*KCU*, *MJ/m*^{2}
Base metal	293	418	712	48.0	83.0	3.45
	77	810	1375	53.5	67.0	2.03
	20	1070	1590	35.0	–	2.15
	4.2	1230	1630	32.4	–	–
Weld metal	293	371	672/685	40.8	66.0	2.00
	77	703	1142/1160	43.5	44.5	1.21
	20	825	1370/1340	32.5	–	1.08
	4.2	975	1410/1450	27.0	–	–

Notes: 1. The values of σ_t of welded joints are given in the denominator. 2. In all the cases the bend angle was 180°.

Table 2 gives generalised data on properties of steel 03Kh20N16AG6 20 mm thick and its welded joints made by automatic SAW at test temperature T_{test} = 293–4.2 K. As follows from these data, this steel and its welded joints have increased strength properties and high values of ductility and impact toughness at a temperature of up to 4.2 K.

The internal casing of the tank 110 t in weight, fully welded, tested and prepared for erection, is transported from the workshop to the erection site by a hauler on a specially designed bed (Figure 7). Its external jacket of steel 09G2S is assembled on site from two hemispheres. Assembly and welding of the

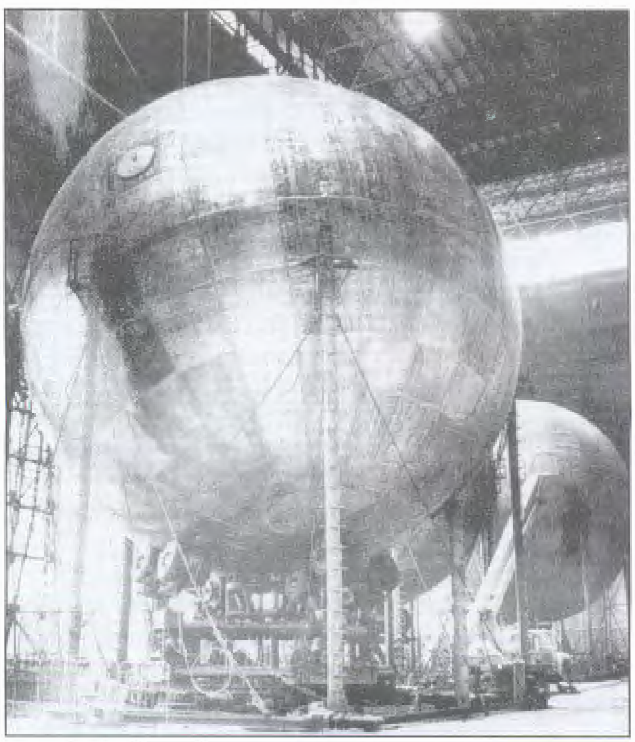

Figure 6. Automatic welding of the cryogenic vessel on a manipulator

Figure 7. Transportation of the internal casting of the tank 110 t in weight to the erection site

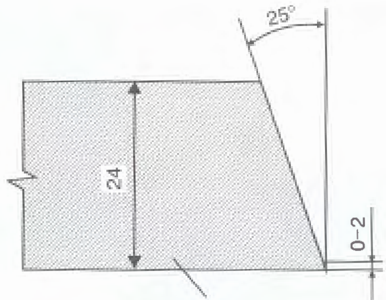

Figure 8. Groove preparation in lobes of the external casing

casing of the protective jacket are performed in the following sequence: groove preparation in lobes (Figure 8) at a manufacturing plant or under the field conditions using mechanical edge cutters and subsequent surface preparation, assembly of two hemispheres of the casing from the lobes on a special rig, geometry control, making of the root weld by the manual arc welding, the root weld on the groove side being 5–6 mm thick and reinforcement being 3–4 mm (Figure 9), welding of hemispheres with the automatic welding device A-1381M using a self-shielded flux-cored wire in different spatial positions in one pass, assembly, tack welding and welding of supporting columns of the jacket, and control of the tank geometry.

Therefore, erection, assembly and welding of the isothermal set are performed on the design reference mark (Figure 10) of three enlarged elements (the whole internal vessel and the external casing of two hemispheres) along the equatorial joint.

The sequence of erection is as follows: installation of the lower hemisphere of the jacket in the design position, erection and welding of the internal vessel supports, installation of the internal vessel in the design position and welding it to the internal supports, installation of the upper hemisphere of the protective jacket, welding of the equatorial joint on the protective jacket, inspection and evacuation.

The proposed methods for assembly, erection and welding of large-size spherical isothermal tanks with a capacity of 1400 m^3 were applied to advantage in construction of the «Buran» launching system at the Bajkonur ground, as well as other aerospace objects.

The PWI developed the technology for argon-arc welding of Invar 36NKh using filler wire 36NGMT (EP-803) for construction of cryogenic pipelines to

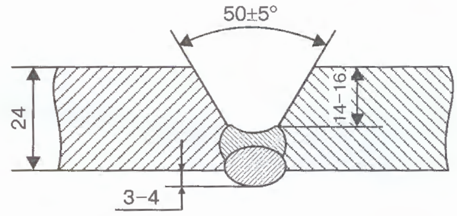

Figure 9. Appearance and parameters of groove preparation in the jacket lobes for automatic welding using the A-1381M device

be employed in the fuel systems. Mechanical properties of Invar and its welded joints are given in Table 3. Figure 11 shows an element of the cryogenic pipeline made from alloy 36NKh, and Figure 12 shows the cryogenic pipeline in the assembled form.

Welding of the cryogenic pipelines from Invar requires solution of a number of problems associated with hot cracking of the Invar welds. It was experimentally proved that susceptibility of the Invar weld metal to hot cracking was greatly affected by oxygen. Cracks in the Invar weld metal are formed along the

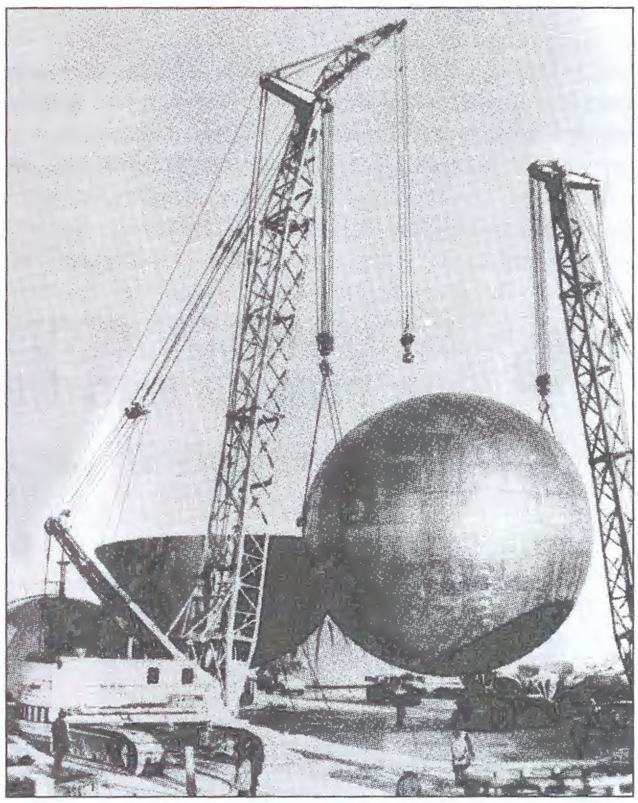

Figure 10. Erection, assembly and welding of the isothermal set

Table 3. Mechanical properties of Invar and its welded joints

Test object	T_{test}, *K*	$\sigma_{0.2}$, *MPa*	σ_t, *MPa*	δ, *%*	ψ, *%*	*KCU*, *MJ/m*^{2}
Base metal (steel 36NKh)	293	313	461	41.0	69.4	2.13
	77	607	802	40.0	72.8	1.76
	20	740	932	59.0	71.0	1.31
Welded joint (filler wire 36NGMT 1.2 mm in diameter)	293	320	471	32.3	62.0	2.65
	77	521	763	26.1	54.1	1.51
	20	624	892	23.1	48.2	0.84

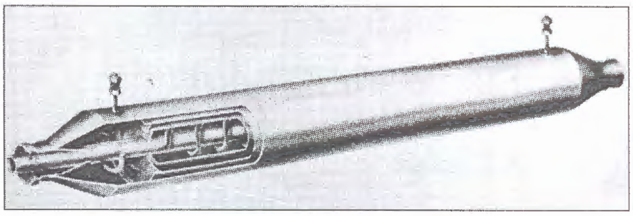

Figure 11. Element of the cryogenic Invar pipeline

secondary grain boundaries due to segregation of oxygen. It was suggested that the weld should be subjected to complex alloying with molybdenum, manganese and titanium to suppress diffusion of oxygen and combine it at the molten pool stage to form insoluble oxides. The new filler wire of the 36NGMT grade was developed and commercially applied for welding Invar.

The technology developed helped to solve the problem of construction of cryogenic pipelines from Invar alloy to be used as part of a fuel system.

CONCLUSIONS

1. The proposed technology for assembly, erection and welding of large-size spherical isothermal tanks provides a sibstantial decrease in the scope of assembly-welding operations under the field conditions, improvement in quality of mechanised welding and labour production, as well as shortening of the construction period.

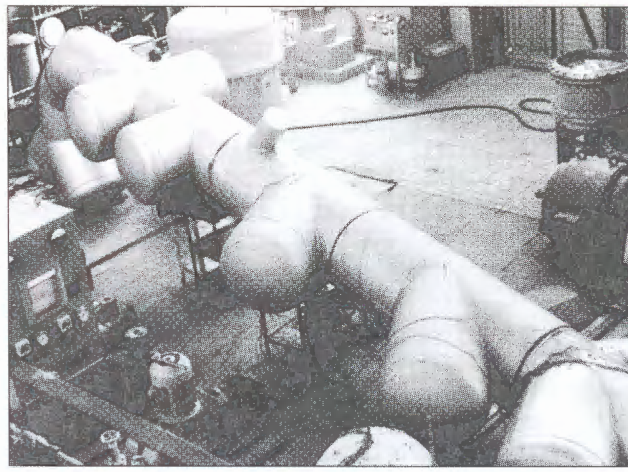

Figure 12. Cryogenic pipeline in the assembled form

2. The use of stable-austenitic increased-strength steel 03Kh20N16AG6 for construction of isothermal tanks for storage of cryogenic products made it possible to decrease metal consumption, simplify their design and manufacture technology, and employ them for the first time at an increased (up to $1 \cdot 10^3$ Pa) pressure.

A-TIG WELDING OF STRUCTURAL STEELS FOR POWER ENGINEERING APPLICATIONS

D.R. BAJIC[1], M.M. SAVITSKY[2], G.M. MELNICHUK[2] and A.F. LUPAN[2]
[1]Technical University, Podgorica, Montenegro
[2]The E.O. Paton Electric Welding Institute, NASU, Kyiv, Ukraine

Efficiency of application of tungsten-electrode inert-gas welding using activating fluxes (A-TIG) for low-alloy carbon and heat-resistant steels was studied. It is shown that increase in the penetrating power of the arc at decreased currents may initiate formation of structural components in the joints which increase strength and decrease ductility of metal. To avoid this effect on structural strength of the joints, it is advisable to subject them to tempering, including the local one, combined with self-pressing to provide a satisfactory geometry of the weld.

Key words: *argon-arc welding, activating flux, weld formation, self-pressing, structural steels, chemical composition, mechanical properties, metal structure*

As proved by studies performed at the E.O. Paton Electric Welding Institute in the field of metallurgy of welding high-strength steels and titanium alloys, activation of reduction-oxidation reactions occurring in the arc burning in the inert atmosphere by adding minor amounts of reactive elements leads to increase in the depth of penetration of metal welded and improvement in quality of welded joints [1]. The activation effect is used now to develop advanced technological processes for TIG and MIG welding [2]. In some countries, the USA and Japan in particular, these efforts have been included into the list of priority directions of development of welding [3, 4]. The PWI has accumulated a great experience in application of activators for many steel grades, i.e. from high-alloy to low-carbon rimming steels. The purpose of this study is to introduce readers to some new results on welding structural carbon low-alloy and heat-resistant steels.

The use of the activation effect in TIG welding of structural steels, as proved by our studies, provides a substantial improvement in operational and economic indicators of welding technologies (Table 1). Increase in the penetration depth on steel 5–16 mm thick leads to avoidance of groove preparation, de-

Table 1. Consumption of materials and time per running metre of the weld length in TIG and A-TIG welding of steels

Welding method	*Thickness of base metal, mm*	*Quantity of passes*	*Welding time, min*	*Consumption*		
				Wire, kg	*Argon, m^3*	*Power, kW·h*
TIG						
one-sided	5	3	26	0.28	0.26	1.10
	8	4	34	0.50	0.34	1.49
	10	5	40	0.64	0.43	1.95
two-sided	12	5	43	0.78	0.43	1.90
	14	7	60	0.81	0.60	2.60
	16	9	77	1.10	0.77	3.40
A-TIG						
one-sided	5	1	7	0.06	0.07	0.13
	8	1	15	0.08	0.15	0.63
	10	1	20	0.10	0.20	0.87
two-sided	12	2	24	–	0.24	0.88
	14	2	30	–	0.30	1.10
	16	2	40	–	0.40	1.53

crease in the number of passes and total welding time, as well as reduction of consumption of filler metal, shielding gas and power.

As far as the activating elements are concerned, their share in the total costs is insignificant due to low consumption. As experimentally proved, in the case of oxygen used as the activator, its amount consumed in welding related to the mass of molten metal is ≈ 0.02 %. This amount of oxygen can be produced from the base metal, e.g. in welding low-deoxidised steels. However, because of a short-time dwelling of molten metal in the liquid state and variable oxygen content of different heats of steel, it is very difficult to ensure its uniform feed to the inter-electrode gap, and intensification of its evolution from the in-depth layers of the weld pool may lead to porosity. Addition of oxygen from the shielding atmosphere yields more consistent results [5], although in this case ensuring a precise feed of oxygen and shielding of tungsten from oxidation may also present a problem.

An efficient method to introduce activators into the welding zone is to apply activating fluxes. The PWI developed a series of activating fluxes (finely dispersed mixtures of oxide and oxide-fluoride types for different steel grades) and methods for their application under different conditions [6], providing the desirable amount of the activators in the inter-electrode gap at a flux consumption of 1–2 g per running metre of the weld. A wide acceptance has been gained by the method of application of the flux in the form of a paste by using a reusable flux crayon filled up from special canisters (Figure 1). In this case the flux components participate in exchange reactions taking place on the surface of the weld pool, thus allowing the weld metal to be alloyed with minor elements and modified to improve its structure and properties. Data presented in Figure 2 are indicative of the fact that these operations are feasible and controllable, i.e. the amount of elements that transfer into the weld metal correspond to their amount in the flux.

This consumption of the flux hardly has any effect on the content of exhaust gases at the welding station location. As shown by estimation of evolution of the welding aerosol particulate matter (WAPM)*, during argon-arc welding of low-alloy steel of the 12Kh1MF grade at the ultimate current values (up to 300 A) using the oxide flux VS-2e, the amount of WAPM evolved per running metre of the weld is 0.274 g. Primarily, these are chromium (0.0179), manganese (0.0156), titanium (0.0139), silicon (0.0175) and iron (0.1625) oxides. With the argon flow rate of 0.2 m^3 per running metre of the weld the total amount of aerosols is not in excess of 0.1 wt.%, i.e. the use of

Figure 1. Canisters for storage and application of an activating flux

* The authors are grateful to O.G. Levchenko and his associates for the estimation they performed.

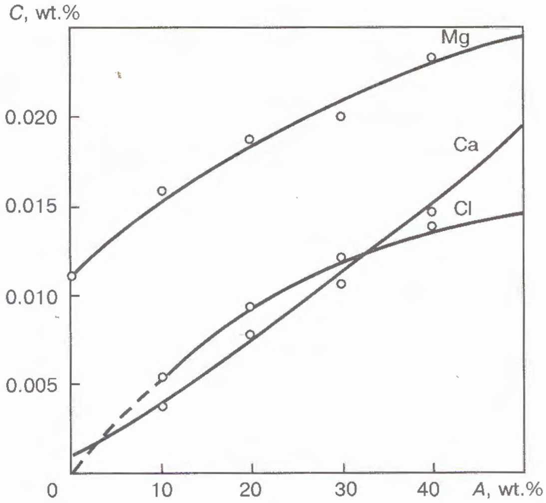

Figure 2. Dependence of the mass fraction of elements in weld metal, *C*, upon their content of the activating flux, *A*

A-TIG welding requires no extra means for protection of attending personnel, as this process can be performed under the same conditions as TIG welding. No specialised welding equipment is required either, as the arc ignition and burning conditions are determined primarily by a shielding gas, and the activators act on the local zones of the inter-electrode gap.

Distinctive feature of A-TIG welding is formation of narrow welds with deep penetration of the base metal, requiring no groove preparation. The form factor of such welds with the U-shaped penetration is ≤ 1 (Figure 3, *a*). They have structure consisting of finely dispersed disoriented crystalline grains, which provides high resistance of metal to formation of solidification cracks [2].

Omitting debates with supporters of the experimentally non-confirmed Heiple's assumption of the primary effect on penetration of steel by surface tension of molten metal, we just note that the above feature has a strong impact on the combination of operational and service properties of welded joints. On the one hand, it favours decrease in the level of welding stresses and, therefore, residual strains they cause. As shown by measurements of the latter, in A-TIG welding of flat butt joints the longitudinal and transverse strains are approximately 2 times lower than in TIG welding, the angular strains being close to zero. These results correlate with data obtained from testing welded joints to crack resistance: resistance of the A-TIG welded joints to hot and cold cracking is higher than that of the TIG welded joints [2].

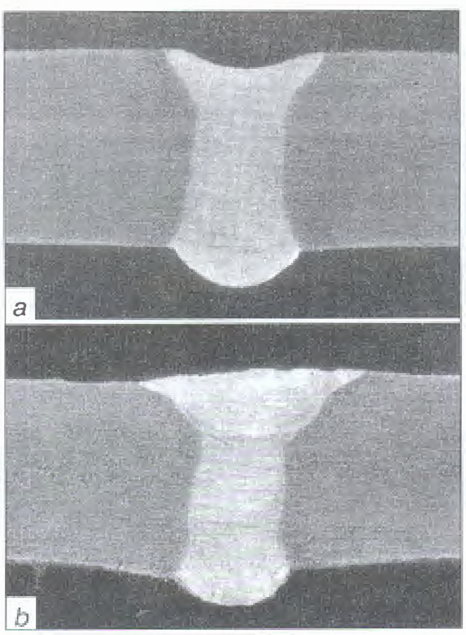

Figure 3. A-TIG weld made using no filler wire without (*a*) and with (*b*) self-pressing

On the other hand, welds with deep penetration, formed from the base metal without a filler wire having as a rule a decreased carbon content, are characterised by an increased hardenability, which is additionally enhanced by the fact that A-TIG welding is performed at a lower heat input, and the rate of cooling of the welded joints grows. The latter promotes a more intensive formation of quenching structures in the weld and HAZ metal, which increase its strength and decrease ductility and toughness. As follows from Table 2, this trend is clearly seen in the joints on low-alloy steels in testing specimens subjected to no postweld heat treatment. High tempering leads to elimination of differences in properties caused by welding within the limits of a given chemical composition of steel, including impact toughness at negative temperatures. As shown by the results of [6], this effect can be achieved not only through furnace heat treatment, but also through the local one using the welding arc combined with making a decorative layer to improve geometric sizes of the weld (Figure 3, *b*). As far as the effect of variations in chemical compositions characteristic of each steel grade is concerned, it will always show up in scatter of mechanical properties. However, unlike joints made by other arc welding methods, in our case variations in values of mechanical properties occur simultaneously for the base and weld metals, all the more so that they are very close in chemical composition and properties.

The similar trend is seen also for steels made in compliance with the standards of Ukraine, the only difference being that they contain 2–3 times more impurities (S, P, O_2 and N_2). The latter circumstance leads to increase in scatter of the impact toughness test results. For example, in welding steel 20 without postweld tempering the value of impact toughness KCV^{+20} was 54.1–39.7 J/cm^2 for the base metal and 36.3–29.3 J/cm^2 for the weld metal. Welded joints in steels 12Kh1MF and 10KhSND exhibited somewhat better values of impact toughness. However, the general trend to decrease in impact toughness of the cast weld metal immediately after cooling from the welding heating was also fixed in these cases, unless postweld tempering was used. This was caused by the increased rates of cooling of the A-TIG welded joints and formation of less ductile structural components as a result of the increased heating concentration. Tempering led to stabilisation of mechanical

Table 2. Chemical composition and mechanical properties of metal of different zones of a welded joint

Welded joint zone	*Content of elements, wt.%*									
	C	*Si*	*Mn*	*Cr*	*Ni*	*Mo*	*S*	*P*	O_2	N_2
BM	0.18	0.33	1.52	0.05	0.02	< 0.005	0.013	0.015	0.0021	0.0061
Weld	0.16	0.31	1.50	0.07	0.02	< 0.005	0.012	0.015	0.0025	0.0051
BM	0.11	0.23	0.80	0.23	0.05	0.01	0.015	0.017	0.0020	0.0086
Weld	0.09	0.21	0.81	0.27	0.05	0.01	0.013	0.017	0.0023	0.0078
BM	0.17	0.25	0.32	1.31	2.82	0.35	0.002	0.010	0.0018	0.0080
Weld	0.16	0.22	0.30	1.35	2.81	0.33	0.002	0.010	0.0023	0.0071

Table 2 (cont.)

Welded joint zone	*Mechanical properties*					
				KCV, J/cm², at T, °C		
	σ_t, *MPa*	σ_y, *MPa*	δ, *%*	*+20*	*–20*	*–20*
				No tempering		*Tempering at 650 °C*
BM	508.0	385.0	26.3	64.7	27.3	30.5
Weld	567.1	437.0	20.6	39.8	17.7	31.9
BM	459.7	360.1	29.1	71.1	32.3	34.0
Weld	485.8	375.6	22.9	41.5	23.2	35.3
BM	868.6	598.4	27.1	73.4	36.7	37.6
Weld	779.3	670.1	19.0	30.1	18.2	37.0

Note. Here BM stands for base metal.

properties of the A-TIG welded joints at a level of properties of the base metal, thus providing equal strength of metal in all the zones of the welded joint.

The effect by postweld local tempering on mechanical properties of joints in pipes of steels 20 (measuring 8×160 mm), 10KhSND (6×120 mm) and 12Kh1MF (6×76 mm) used in power engineering is shown in Table 3. In the first case welding of the main layer of the weld was performed at a current of 200 A, while in the second and third cases welding was performed at 150 A. To produce a decorative layer of the weld (Figure 3) by the method of self-pressing and tempering of the previous layer and HAZ metal, the welding speed was varied so that the optimal combination of the rates of heat transfer and growth of thermal stresses was provided in the welded joint during a period of development of plastic flow of the metal.

Data of Table 3 and Figure 3 show that self-pressing has a positive effect on shape and quality of the weld, and can be used for practical purposes. In addition, it provides improvement in the weld structure. The cast dendritic structure formed during welding the first (main) layer of the weld becomes less pronounced (smeared) after self-pressing (Figure 4). Austenite grain in the HAZ metal hardly changes. As to the secondary structure of the weld metal, after welding it can be identified as a mixture of globular bainite (HV_{50} 300–330) and martensite (HV_{50} 400–410) in the main layer of the weld in steels 10KhSND and 12Kh1MF. The overheated region of the HAZ metal has a lower amount of the martensite lamellae, and the metal structure is composed mostly of bainite (HV_{50} 270–350). After self-pressing the weld and HAZ metal structure becomes more dispersed. Micro-

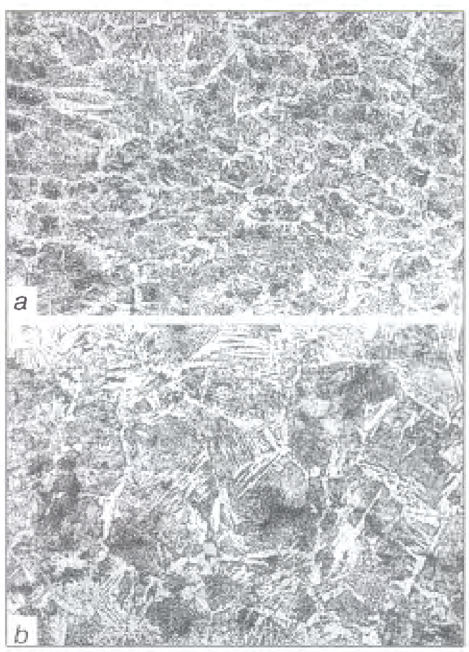

Figure 4. Microstructure of weld (*a*) and HAZ (*b*) metal in welding using self-pressing (×200) (reduced by 4/5)

Table 3. Mechanical properties of welded joints in steels 20, 12Kh1MF and 10KhSND made by A-TIG welding and self-pressing

Steel grade	*Welded joint zone*	*Test temperature, °C*	σ_t, *MPa*	σ_y, *MPa*	δ, *%*	ψ, *%*	*Impact toughness, J/cm²*		
							With self-pressing		*Without self-pressing*
							KCU	*KCV*	*KCV*
10KhSND	BM	20	736.0	589.4	21.3	66.6	166.3	72.4	72.0
	Weld		751.2	674.3	20.0	55.6	159.1	71.1	23.1
12Kh1MF	BM	20	523.9	328.7	23.1	67.3	117.1	67.4	67.4
	Weld		567.1	368.1	26.7	64.1	121.3	69.9	32.6
St.20	BM	20	440.7	356.1	24.1	65.0	116.7	70.0	69.7
	Weld		499.3	374.4	22.6	71.6	118.1	78.0	29.1
	BM	100	495.4	268.3	18.2	62.0	N/D		
	Weld	200	547.8	263.5	17.3	58.6			
	BM	250	531.7	256.4	16.2	51.4			
	Weld	350	526.2	232.1	18.0	53.3			

hardness of its components hardly changes, only the scatter of its values decreases.

Remelting of metal in argon has always had a positive effect in terms of ensuring the desirable combination of strength, ductility and toughness properties of welded joints. In this respect the use of the activating flux has no contraindications. According to the results of measurements made using the «Quantimet-720» microscope, coarser and chain-stretched sulphides and oxides present in the base metal are refined and acquire a globular shape in the A-TIG welds. Whereas the volume fraction of sulphides in the base metal was ≈ 0.01 % and that of oxides was 0.004–0.008 %, the amount of sulphides found in the weld metal was 0.0075 % and that of oxides was 0.0073 %.

Therefore, the application of A-TIG welding combined with self-pressing for carbon, manganese and low-alloy steels used in power engineering will provide an improvement in quality of welded joints by avoiding such complicated and expensive operations as groove preparation, volumetric furnace tempering, as well as the use of special filler wires.

1. (1974) *Technology for fusion welding of metals and alloys*. Ed. by B.E. Paton. Moscow: Mashinostroenie.
2. Savitsky, M.M., Kushnirenko, B.M., Olejnik, O.I. (1999) Peculiarities of tungsten-electrode welding with activators (A-TIG process). *Avtomatich. Svarka*, **12**, 20–28.
3. Gordon, J.R. (1995) Perspectives on welding research and development in the USA. *Weld. Rev. Int.*, **9**, 95–108.
4. (2001) Welding and joining technologies in the 21st century. *J. JWS*, **3**, 6–18.
5. Savitsky, M.M., Lupan, A.F., Melnichuk, G.M. et al. (2000) Methods for application of activators in TIG welding of steels. *The Paton Welding J.*, **3**, 52–53.
6. Savitsky, M.M., Kulik, V.M., Bursky, G.V. (2000) Peculiarities of arc treatment of quenching steels without melting. *Ibid.*, **5**, 30–35.

NARROW-GAP ARC WELDING OF TITANIUM ALLOYS (REVIEW)

V.Yu. BELOUS
The E.O. Paton Electric Welding Institute, NASU, Kyiv, Ukraine

Experience of practical application of narrow-gap welding of structures of titanium and its alloys has been analyzed. The advantages of the above-mentioned method of welding are shown. Prospects of application of magnetic methods of welding arc control are outlined.

Key words: *argon-arc welding, narrow-gap arc welding, narrow groove, titanium, titanium alloys*

High chemical activity of titanium as regards to atmospheric gases causes great difficulties at its hot treatment and, first of all, in welding. The noticeable absorption of oxygen by titanium is starting even at 500 °C temperature and that of nitrogen — at 600 °C, the titanium interaction with moisture and hydrogen dissolution in it occur even at lower temperatures [1, 2]. In turn, with increase in content of these impurities in titanium its strength characteristics are improved and ductility is decreased. It is known that each 0.05 wt.% of oxygen in titanium increases its ultimate strength approximately by 60 MPa. With increase in amount of oxygen in titanium its impact strength is reduced, especially at 0.1–0.3 wt.%. Nitrogen hardens titanium to a greater extent than oxygen and deteriorates its ductile properties. Hydrogen reduces significantly the impact strength of titanium, contributes to its embrittlement, causes a spontaneous failure of structures [3] and is one of the major causes of pores formation in welds.

Negative effect of gas impurities on properties of welded joints of titanium alloys is greater than on the properties of the alloys themselves. Besides the total reduction of ductility of metal of welds and HAZ, the impurities of oxygen and nitrogen promote developing of structural and chemical inhomogeneity that is an additional cause of a drastic reduction in performance of titanium alloy welded joints [4].

Thus, in welding of titanium alloy products it is necessary, first of all, to provide a safe protection of not only the welding pool, but also of the cooling weld metal and HAZ regions, which are heated in the process of welding above 350–450 °C, to provide the content of impurities of gases in weld metal and in HAZ equal to that in the parent metal.

The necessity in creation of a reliable protection of welding zone from the contact with air (with allowance for a low heat conductivity and relatively high heat content typical of titanium) defines greatly the parameters of welding titanium alloys, in particular it limits the welding current and narrows the interval of acceptable welding speeds [5]. Peculiarities of polymorphous transformation in titanium also influence greatly the selection of the welding conditions.

As is follows from [2], the polymorphous transformation in titanium has a martensitic nature and in cooling from β-region the microstructure of weld metal and near-weld regions of HAZ represents martensite-like precipitations in the form of needles or plates. Depending on the cooling rates, i.e. welding conditions, and degree of alloy alloying, the shape and sizes of these precipitations may change from large-plate α-phase to fine-acicular α′-phase. High serviceability is typical usually of welded joints having a fine-acicular structure of weld metal and near-weld region of HAZ.

Size of grain also influences greatly the mechanical properties of welded joints, however, it is not possible to control it in HAZ metal by selection of appropriate welding conditions [6]. It possible only to decrease the HAZ width and, consequently, the length of metal region with a coarse grain. Therefore, with increase in metal thickness in welding of titanium alloys it becomes more difficult to provide safe protection of welding zone and definite structural state of weld metal and HAZ.

At present the narrow-gap arc multilayer welding is more promising for thick metal joining [7]. As compared with welding using a conventional edge grooving, this method decreases the amount of deposited metal, reduces the labour intensity of welding jobs and heat input into the metal welded. This is very important for welding titanium alloys as the cost of titanium wire several times increases the cost of semi-finished products.

Narrow-gap welding of titanium and titanium alloys can be realized both with a non-consumable and consumable electrode. In [8] the experience of application of mechanized double-sided narrow-gap consumable electrode welding of titanium alloys is described. Thickness of metal of butt joints of VT5 alloy is 36–130 mm. Due to high electrical resistance of titanium the consumable electrode stickout did not exceed 35 mm in use of power source PSG-500 with a rigid characteristic and 60 mm in use of a modified power source. Therefore, the welding of joints of more than 60 mm thickness was performed from both sides. Preliminary, beads were deposited on the edge middle

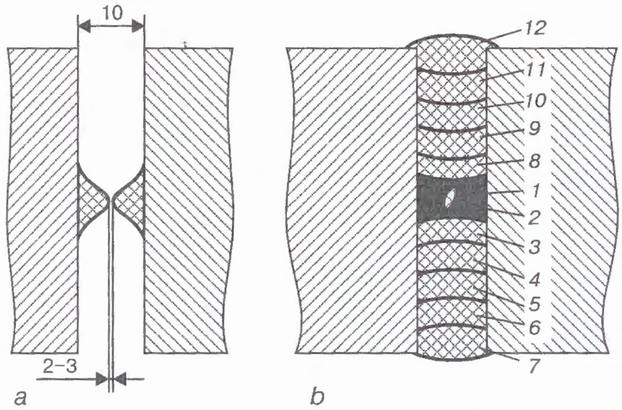

Figure 1. Scheme of joint with deposits, assembled for welding (*a*) and sequence of passes (*b*), indicated by figures

using a manual argon-arc tungsten electrode welding with a filler wire of VT1-00s alloy. Prepared pieces were assembled with a 2–3 mm gap (Figure 1, *a*) that made it possible to avoid additional mechanical treatment of edges of sheets welded to create the edge blunting. Root pass was also made by the manual argon-arc welding with tungsten electrode, while filling passes were made by a mechanized consumable electrode argon arc welding.

To prevent the possible short-circuits of current-carrying tip with product edges, special fasteners were mounted on the rear side of a gas protection attachment. Wire VT1-00s of 1.6 or 2 mm diameter was used as a filler material. In spite of the fact that in this case the ultimate strength of weld metal (400–430 MPa) is lower than that of the parent metal (750–850 MPa), the equal strength of welded joint was attained due to effect of a contact strengthening of joints with a soft layer [9].

It should be noted that as compared with a manual argon arc tungsten electrode welding, the narrow-gap welding could decrease significantly the number of passes (from 60–70 to 16–18 in welding of 100 mm thick plates). The main drawback of this method of welding is a high spattering of filler metal that deteriorates the gas protection of welding zone and can cause the process violation. In addition, the short-circuits between the current-carrying tip and product edges are possible.

The feasibility of realization of the effect of a contact strengthening in joints of titanium alloys, being narrow-gap welded, was used in [10]. The aim of investigations was to reduce the cost of welded joints. For this purpose, the use of filler wire with a smaller alloying and a lower strength than the parent metal, simplifying of edge preparation for welding and reduction in geometric sizes of weld and HAZ were envisaged. In particular, 25 mm thick butt joints of Ti–6Al–4V alloy were welded. Wire of 1.6 mm diameter, made from commercial titanium, was used as a filler wire. Welding was performed with a non-consumable electrode in flat position. The 6.5 mm thick remained backing of the same alloy was used. Welding of butt samples with a different width of the gap (19, 11 and 6.5 mm) was tested. Welding current was 300–340 A, welding speed 2.5–3.2 mm/s, arc voltage 14.5–18 V.

Results of investigations showed that with a decrease in a groove width the strength of welded joint is increased (Table). This is due not only to the increase in share of parent metal in the weld metal, but also to the formation of a complex stressed state in the zone of a plastic deformation promoting the contact strengthening.

The manual argon arc narrow-gap tungsten electrode welding is used for manufacture of power elements of chemical equipment from alloy VT1-0 (flanges, rings, high-pressure covers) where short welds on thick metal are required [11]. In this case a scheme of edge preparation, shown in Figure 1, *a*, is used. Welding is performed in the following sequence. Firstly, a root face created by a preliminary deposition is welded (from both sides) and then a gap is filled by a successive layout of beads on each other (Figure 1, *b*). Welding is made in argon with tungsten electrode of VL grade using a filler wire VT1-00s. Welding current was 380–400 A, arc voltage 10–12 V.

Some peculiarities of welding technique should be outlined (Figure 2).The electrode axis should be in a vertical plane normal to the weld axis. Transverse oscillations of the electrode are not used. Filler wires are fed into the arc zone at 5–10° angle without longitudinal displacements. In case of welding into a relatively narrow and deep groove, providing the above-mentioned conditions, the reliable protection of the metal being deposited is ensured without use of tips. A shield-reflector put on the torch nozzle is only used.

In welding of external layers the conventional tips with an additional argon feeding are used. Welded joints made by this technology possess sufficiently high values of mechanical and corrosion properties. According to data of [12] this technology was successfully used for welding an acetalator casing representing a 3000 mm diameter vessel made from sheet alloy AT3.

The major problem arising in narrow-gap welding is the guarantee of reliability of weld metal fusion with the groove walls. To prevent the possible defects a number of technological procedures was suggested, in particular welding at high current, making of welds with a layout of beads, forced oscillation of electrode and arc [13].

Properties of welded joints depending on weld width and parent metal thickness

B_m	Bw/δ_{PM}	σ_y, *MPa*	σ_t, *MPa*	*Place of failure*
20.6	0.70	413	551	Weld
11.9	0.39	614	765	Same
7.9	0.30	689	930	Parent metal

Note. 1. Here B_m — weld width; δ_{PM} — thickness of parent metal. 2. σ_y of parent metal is 803, filler metal — 422 MPa, and σ_t of parent metal is 903, filler metal — 516 MPa.

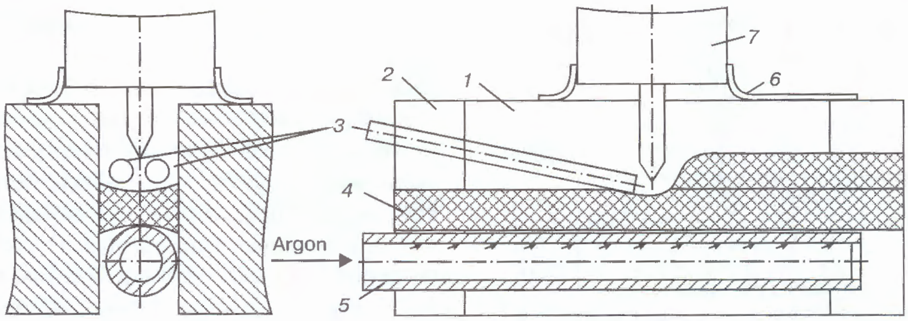

Figure 2. Scheme of manual non-consumable argon narrow-gap arc welding: *1* — part to be welded; *2* — run-out tabs; *3* — filler; *4* — deposited metal; *5* — device for blowing; *6* — shield-reflector; *7* — torch nozzle

To provide a reliable fusion of weld metal with vertical walls of a gap, a tungsten electrode of 4 mm diameter with 8–12 mm long working region, bent by 20–25°, was used in automatic argon arc welding of titanium [14]. At electrode rotation around its axis the welding arc is directed periodically to one, then to another wall of the gap (Figure 3, *a*), thus providing a uniform heating and melting. Stable edge penetration for a preset value was provided by adjusting amplitude of rotation (within 70–160°) and frequency of angular oscillations. Quality fusion of deposited metal with edges is proved by a typical formation of surface of each layer in the form of a concave meniscus. As the results of investigations showed the depth of penetration on titanium alloy VT6 was increased from 0.2–0.3 to 1.2–1.5 mm with a change in amplitude of rotation from 70 to 160°.

Metal protection from oxidation was provided by argon supply along the gap using a sprayer set at the weld beginning or moved in the gap behind the electrode. To prevent the air entering from the top and to protect tungsten the argon was supplied additionally through the water-cooled cover plates located over the gap.

The torch was designed for welding titanium of up to 100 mm thickness. The filler wire was fed to the head part of the pool. In welding short welds the rods of 3–5 mm diameter were put preliminary to the groove. Welding is made into U-shaped groove of 7–9 mm width (Figure 3, *b*).

At 230 A welding current and 5 m/h welding speed the height of the deposited bead for one pass is 2–3 mm. The welding torch design in this method of welding makes it possible to perform welding in different spatial positions.

Due to a small volume of weld pool the molten metal is maintained safely by the surface tension forces during the movement of welding head both downwards and upwards. The vertical welds are welded at the same conditions as the welds in the flat position. However in welding using this scheme a weak link is a bent electrode, as its working region is gradually failed and a multiple electrode sharpening with a bent tip is impossible.

In work [15] idea about use of tungsten electrode with a bent working part was realized in a two-electrode welding head. Welding (Figure 4) was realized simultaneously by two bent tungsten electrodes which are rotated around own axes at angular rates ω_1 and ω_2. Axes of electrodes and filler wire are located in a single plane coinciding with an axial plane of a butt narrow gap (Figure 4). Due to rotational movements of electrodes and their bent working regions both arcs perform transverse oscillations. Filler wire is fed into the narrow gap between two electrodes normal to the weld surface. Scheme of head control allows initially set values of arc current to be changed at front and rear electrodes, respectively, at the moment of a reverse of the longitudinal movement of the head. Most steady process of welding and stable weld formation

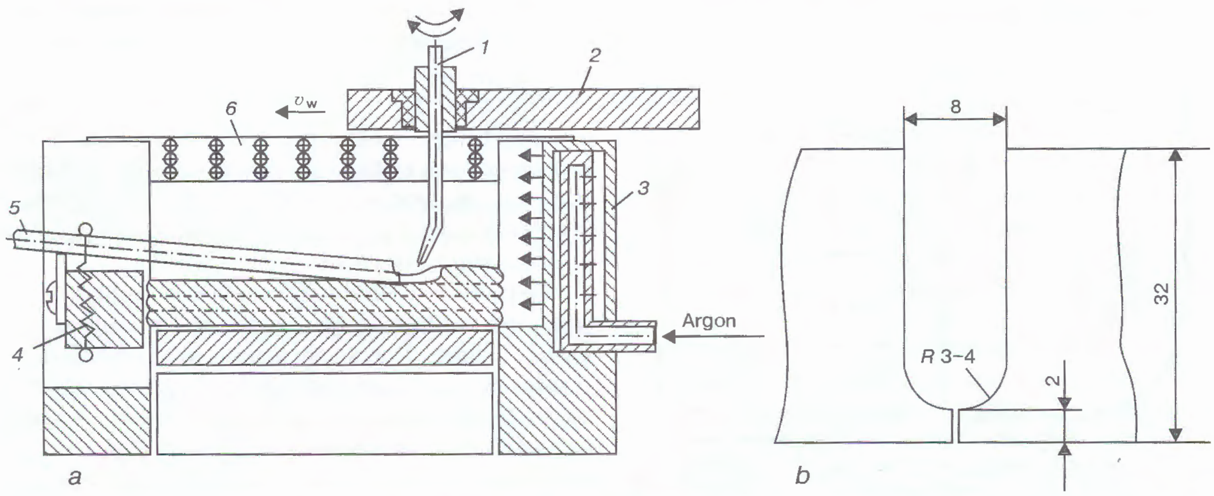

Figure 3. Scheme of process of narrow-gap argon arc welding with rotating bent tungsten electrode (*a*): *1* — tungsten electrode; *2* — movable gate; *3* — sprayer; *4* — clamping device; *5* — rod; *6* — protective cover plates; and scheme of edge preparation (*b*)

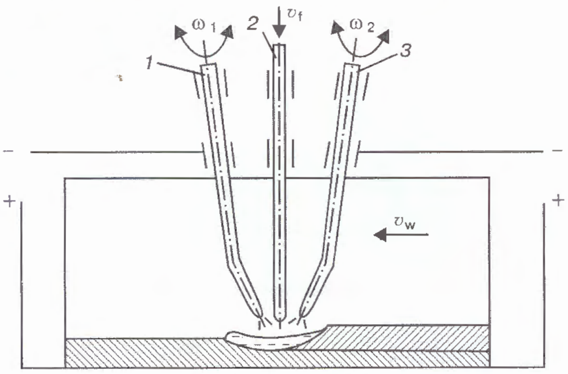

Figure 4. Technological diagram of the process of welding with non-consumable electrode: *1, 3* — bent tungsten electrodes; *2* — filler wire; ω_1, ω_2 — angular rates of rotation of front and rear tungsten electrodes, respectively; v_f — filler wire feed speed

were obtained in that case when the welding current at the front electrode was 100 A, and 200 A at the rear electrode. Penetration of the gap walls and depth of penetration of the metal of the previous layer were approximately similar and reached 0.3–0.6 mm.

In spite of evident advantages the suggested scheme of a twin-arc welding has the same drawback as the single-arc welding with a tungsten electrode having a bent working part. Therefore, to control the welding arc movement in a narrow gap the use of alternating magnetic field should be considered as most promising.

Narrow-gap tungsten electrode welding with a magnetically-impelled arc for titanium alloys was described in [16, 17]. Welding of 110 mm thick plates from alloys VT1-00 and AT3 was realized by a diagram, shown in Figure 5, with 5 mm diameter tungsten electrode using 4 mm diameter filler wire from alloy VT1-00s. Welding speed was 8 m/h, welding current 420 A, arc voltage 13 V. To generate control magnetic field, a special device (OI-119) was used, allowing the frequency of alternating magnetic field in the range of 1–80 Hz and level of magnetic induction to be changed.

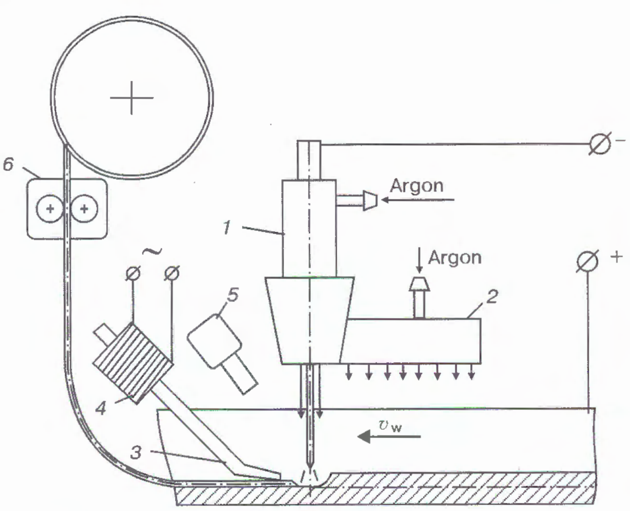

Figure 5. Scheme of automatic narrow-gap tungsten electrode magnetically-impelled arc: *1* — welding torch; *2* — shielding device; *3* — magnetic core; *4* — electromagnet; *5* — TV camera; 6 — mechanism of wire feeding

It was observed during experiments that the superposition of alternating magnetic field on the arc leads to the reduction in efficiency of the gas protection of the zone of welding and, as a consequence, to the deterioration of the welded joint quality. With increase in thickness of the metal being welded up to 100 mm the instability of the gas flow is so high that welding becomes impossible. To prevent this phenomenon a special welding head was designed, thus providing the stability of the gas flow in a gap during welding metal of up to 110 mm thickness. In this case a homogeneity of structure of weld metal and high level of mechanical properties of welded joints are observed.

The automatic argon arc narrow-gap welding of titanium alloys was performed with a consumable electrode on plates from 26–135 mm thick alloy VT6 [18]. Depending on their thickness single- or double-sided narrow-gap edge grooving of 9.5–10 mm width with 5 mm root face at a single-sided welding and 10 mm root face at double-sided welding were made (15–22 m/h welding speed, 3 mm diameter welding wire) using a current conductor inserted into a narrow gap without layout of beads in its width. After welding approximately of 10 m of weld it is necessary to clean the feeding channel from spatters and particles of a sticked metal. Protection of welding zone from air was provided by three chambers: front (for protection of edges heated by arc), middle (for protection of arc zone and weld pool) and rear (for protection of cooling weld at the length up to 350 mm).

Plates of up to 26 mm thickness were welded for one pass at 650–720 A current. Multipass welding at 450–480 A current was used for plates of more than 26 mm thickness. Filler wire feed speed in this case was 420–470 m/h in a single-pass welding and 220–230 m/h in a multipass welding. At optimum condition the deposition of bead of about 19 mm thickness at 10 mm groove thickness is provided. In spite of high efficiency of the process of welding this method has a serious drawback: a high spattering of the filler metal, that can cause the violation of the process, short-circuiting between the groove walls and current-carrying nozzle, deterioration of the gas protection of the welding zone.

The work [19] describes the technology of narrow-gap tungsten electrode arc welding used in manufacture of such critical structures as boilers of electric stations, apparatuses of deep water immersion and others. Welding was performed into U-shaped groove at 15° opening of edges.

To provide a reliable protection of weld pool, filler wire and cooling weld a triple gas shielding is provided. Three flows of argon are supplied independently into a welding torch: for protection of electrode, filler wire and cooling weld metal. A specifics in welding design consists in the fact that a shielding nozzle and a chuck with a tungsten electrode (3 mm diameter electrode and 20 mm stickout) are put into groove, and an auxiliary shielding device blowing the product surface with argon is arranged over the surface.

As the authors of [19] state, this technology makes it possible to weld parts of up to 400 mm thickness from both sides. Though the experience in welding titanium alloys is not informed, but it considers possible to use this method of welding for high-alloyed alloys, Inconel and titanium alloys.

Thus, the narrow-gap welding is considered to be an effective process for manufacture of titanium structures from elements of medium and large thickness and has the highest efficiency. However, the method of tungsten electrode welding having a relatively low efficiency, but high reliability, found the widest spreading. To produce the defect-free welded joints it is necessary to control the processes of edges melting and arc movement in the gap. Magnetic field is the most effective method of welding arc control. Therefore, the automatic non-consumable magnetically-impelled arc in combination with TV control system should be considered as the most challenging method of joining titanium and its alloys.

1. Tsvikker, U. (1979) *Titanium and its alloys*. Moscow: Metallurgiya.
2. Moroz, A.S., Chechulin, B.B., Dolin, I.V. et al. (1960) *Titanium and its alloys*. Leningrad: Sudpromgiz.
3. Guseva, E.A., Mordvintsev, L.A. (1991) *Cold cracks in welded joints of titanium alloys*. Moscow: Metallurgiya.
4. Sokiryansky, L.F., Gubanova, L.V., Latash, V.V. et al. (1969) Peculiarities of gas saturation of titanium alloys alloyed with α- and β-stabilisers. *Fizika Metallov i Metallovedenie*, **28**, 847–852.
5. Gurevich, S.M., Zamkov, V.N., Blashchuk, V.E. et al. (1986) *Metallurgy and technology of welding of titanium and its alloys*. Kyiv: Naukova Dumka.
6. Shorshorov, M.Kh. (1965) *Physical metallurgy of welding of steel and titanium alloys*. Moscow: Nauka.
7. Malin, V. (1987) Monograph on narrow-gap welding technology. In: *WRC Bulletin*.
8. Russo, V.L., Kudoyarov, B.V., Nikolaev, A.A. et al. (1971) Semiautomatic welding of titanium square butt joints of large thickness. *Svarochn. Proizvodstvo*, **10**, 20–22.
9. Bakshi, O.A., Shron, R.Z. (1962) Static tensile strength of welded joints with soft interlayer. *Ibid.*, **5**, 9–15.
10. Wells, M.E. (1992) Strengthening mechanisms on undermatched titanium welds. In: *Proc. of 7th World Titanium'92 Conf.*, San Diego, June 29–July 2, 1992.
11. Besedny, V.A., Shelenkov, G.M. (1970) Narrow-gap welding of large thickness titanium. *Khim. i Neft. Mashinostroenie*, **2**, 27.
12. Shelenkov, G.M., Blashchuk, V.E. (1974) Application of narrow-gap welding in manufacturing of chemical equipment from AT3 alloy. *Avtomatich. Svarka*, **9**, 50–53.
13. Katsuyoshi, H., Mitsuaki, H. (1999) Narrow-gap arc welding of titanium. *J. JWS*, **3**, 41–46.
14. Shtrikman, M.M., Grinin, V.S. (1971) Automatic narrow-gap welding of high-strength steels and titanium alloys. *Svarochn. Proizvodstvo*, **1**, 16–19.
15. Grinin, V.S., Shtrikman, M.M. (1982) High-efficient automatic narrow-gap welding. *Ibid.*, **7**, 21–23.
16. Prilutsky, V.P., Zamkov, V.N., Lapchenko, S.V. (1989) Technological and design particularities of narrow-gap welding of titanium. *Avtomatich. Svarka*, **3**, 71–73.
17. Paton, B.E., Zamkov, V.N., Prilutsky, V.P. (1996) Narrow-groove welding proves its worth in thick titanium. *Welding J.*, **5**, 37–41.
18. Shtrikman, M.M., Borodin, Yu.M., Ermakov, L.K. (1989) Automatic narrow-gap argon metal-arc welding of large thickness sub-assemblies. In: *Welding of non-ferrous metals*. Kyiv: Naukova Dumka.
19. Matsui, S., Nakayama, S., Sakurai, T. (1988) *Application of narrow gap GTA welding to various products*. Osaka: JWS.

HIGH-FREQUENCY POWER TRANSFORMERS FOR INDUCTION UNITS

A.S. PISMENNY, M.E. SHINLOV and **R.V. YUKHIMENKO**
The E.O. Paton Electric Welding Institute, NASU, Kyiv, Ukraine

Considered are high-frequency power transformers developed by the E.O. Paton Electric Welding Institute for low- and high-power specialised units. Their design peculiarities are described. Results of comparison of the high-frequency transformers under consideration and commercial-frequency transformers are given.

Key words: *heat treatment, high-frequency power transformers, induction units, design, magnetic circuit, windings*

Majority of high-frequency induction units of a technology application comprise power transformers to match electric parameters of a load (inductor with a part being heated) to parameters of a high-frequency current source.

The former Soviet Union (Stepanovan, Armenia) commercially produced for these purposes transformers of the TZ type (quenching transformer) with a power of 800 to 3200 kV·A and autotransformers of the ATS type with a power of 1500 kV·A, covering a current frequency range of 1 to 10 kHz. Those transformers and autotransformers had maximum possible unified designs. They included E-shaped magnetic circuits the external ends of which, together with nearby cooling tubes, were potted with an Al–Zn alloy to transfer heat from the circuit to the cooling system. Windings of the wafer type manufactured by a very complicated technology were used in the transformers.

The primary winding was a flat spiral consisting of several turns of the insulated copper tube.

The secondary winding was made by potting the primary winding and extra cooling tubes with aluminium. As a result, there was a permanent section (wafer) consisting of the primary winding fully enclosed by the secondary winding body. Advantages

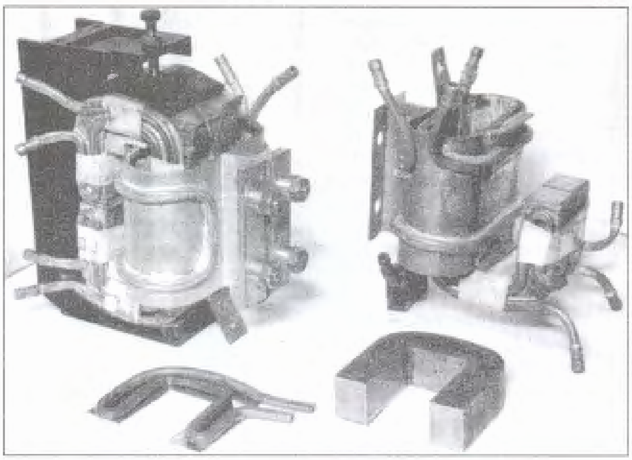

Figure 1. Low-power high-frequency welding transformer of the P-139 type

of this design of windings included the possibility to vary within wide ranges the transformation ratio and saving of copper. However, the efficiency of a transformer decreased because of increased losses in the secondary winding and output parts.

Versatility of the design was achieved due to a certain increase in weight and dimensions, compared with specialised transformers. Transformers and autotransformers manufactured by the Stepanovan factory met in the main the demand for them to complete electrothermic equipment. They were used in many cases even where power of the process equipment was much lower than 800 kV·A, as no transformers of a lower power were available (to be more exact, they were developed and manufactured, but only by specialised workshops).

At present the CIS countries have reduced production of some types of the electrothermic equipment. So, the manufacture of high-frequency transformers was almost stopped. This gave rise to a hot problem of replacement of the out-of-date machinery.

In addition, there exists a demand for low-power transformers (below 800 kV·A) both for specialised plants (such as welding machines with special weight and dimension requirements) and for other units, allowing for the up-to-date requirements, including reduction of costs and saving of electric power. The same applies to specialised high-power transformers, as they are more cost effective than the versatile ones.

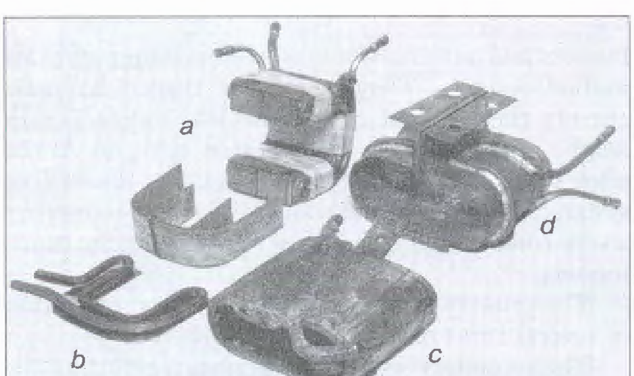

Figure 2. Main assemblies of the P-139 type transformer: *a* — U-shaped coiled sectioned magnetic circuit; *b* — radiator copper sheets with water cooling tubes welded to them; *c, d* — primary and secondary windings, respectively

Proceeding from the above-said, the PWI developed high-frequency transformers for low- and high-power specialised units.

The low-power high-frequency welding transformer of the P-139 UKhL4 type and its modifications P-144 and P-145 (Figure 1) have the following technical characteristics (for a specific modification):

Voltage, V	
primary	350
secondary	32
Current, A	
primary	490
secondary	5000
Load power, kV·A	160
Current frequency, Hz	2400
Transformation ratio*	11
Weight, kg	22
Overall dimensions (including a bracket), mm	
length	265
width	165
height	280

The transformer uses the U-shaped sheet (coil) sectional magnetic circuit (Figure 2, *a*). It has a simpler design and is more cost effective in manufacture, compared with a laminated core. In addition, it is more reliable than the laminated one, as it involves no pin coupling of the stack. The steel set after assembling is coupled by overwrapping it with a calico strip impregnated with a bakelite varnish, followed by heating for 3–4 h at a temperature of about 100 °C. Both sides of the steel strips prior to assembling the magnetic circuit are covered with insulators.

High losses in the transformer magnetic circuit make it necessary to use intensive cooling. Water-cooled screens consisting of copper radiator sheets with the cooling water tubes brazed to them are employed for this purpose (Figure 2, *b*).

The radiator sheets are made from the hot-rolled copper sheets characterised by high thermal conductivity, which allows the heat evolved in the magnetic circuit stacks to be transferred to a cooling water flowing via the tubes. Losses due to eddy currents flowing in the radiator sheets, even at their comparatively small thickness (1–2 mm), are not high under conventional conditions, as copper is a non-magnetic material.

The system for water cooling of the magnetic circuit is made so that it prevents formation of closed electric loops around the steel stacks, which otherwise could cause extra losses due to currents induced in these loops. To let water pass to the cooling systems of the magnetic circuit and windings, they are fitted with the required quantity of special copper, brass or steel tips (unions) with the rubber-cloth hoses directly put on to connect the cooling system tubes to each other and to feed water from a distribution device.

* The transformation ratio can be varied by replacing the primary winding, i.e. cylindrical copper tube spiral with the required quantity of turns.

Diameter of the unions can be varied over wide ranges, depending upon the cross section of the cooling system channel, and the wall thickness is varied accordingly. The union can be connected to the brass and steel cooling tubes through a threaded fastener, whereas to the copper tubes it is connected by brazing.

The use of intensive water cooling of the magnetic circuit makes it possible to operate with induction which is intolerable with any other cooling method, e.g. air or oil cooling. In the case of water cooling the cross section of the core and overall sizes of the magnetic circuit, as well as diameter of the windings arranged coaxially to the core, their length, active resistance and losses in them are decreased.

To arrange the radiator sheets, one should proceed from the fact that they have to bear as close thermal loads as possible. They should not be large in number, as each sheet with the tubes brazed to it, while taking part of the usable area of the core, decreases the duty factor of its cross section, thus leading to increase in radial sizes of the windings.

The transformer has a cylindrical system of windings with direct cooling. In the majority of cases it also has the secondary winding having one or, more rarely, two turns. The primary winding consists of 10–30 turns.

The primary winding (Figure 2, *c*) is made in the form of a single-layer spiral. Increase in the number of layers adjoining each other causes a substantial growth of losses in copper conductors of the windings, because each next layer is in the magnetic field generated by the total current of all preceding layers.

As at high frequencies, because of the surface effect, the active section of the wire is located in metal layers adjoining its surface, the primary winding spiral is made from a hollow copper tube the channel of which is used for intensive water cooling.

The cross section of the tube should be of a rectangular configuration, as current in the primary winding turns flows along a lateral side of the tubes, and such a configuration provides an increased active section of the wire, compared with a round tube, the turns being of the same height. In addition, this improves cooling conditions of the winding.

The primary winding turns are isolated from each other using a varnished cloth which is wrapped around a tube in one or two overlapping layers. Terminals of the winding are usually oriented to a direction opposite to the terminal blocks, normal to the transformer axis.

The secondary winding (Figure 2, *d*), which has the form of an open cylindrical turn, is located coaxially to the primary winding, enclosing it on the outside. The secondary winding may be of different modifications, depending upon the type and service conditions of the transformer. It is advisable to make it from a coiled tough-pitch copper sheet 2–4 mm thick, having the form of a cylinder. For cooling, the rectangular copper tubes are brazed in a certain sequence on the outside of the cylinder.

To minimise the magnetic flux leakage, it is expedient to make the primary winding with height as close as possible to that of the secondary winding.

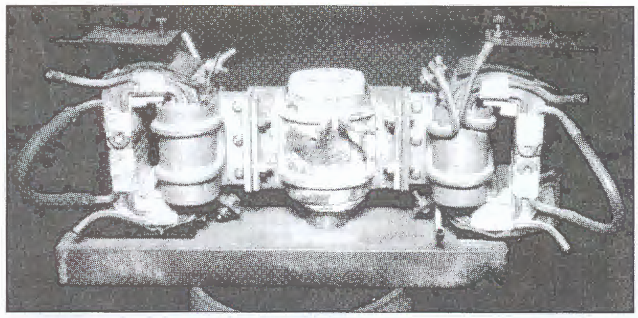

Figure 3. The use of a group of transformers of the P-139 type to supply power to the coreless induction furnace

Power of the transformer can be doubled by doubling the number of the core sections. This leads to a doubled width of the transformer.

Transformers can be used with the primary or secondary windings connected in groups. Figure 3 shows an example of using two transformers of the P-139 type to supply power to the coreless induction furnace, the secondary windings of the transformers being connected in this case in series.

Transformers of the P-139 type are applied in machines for induction butt braze-welding of pipes 114–325 mm in diameter (based on the flash butt welding machine K-584 M), those of the P-144 type are applied for joining pipes 57–114 mm in diameter and the P-145 type – for pipes 114–325 mm in diameter. Machines P-144 are commercially employed at the Tatarstan enterprises for joining oil pipes [1].

Another application of transformers of the P-139 type is as part of the unit for induction heat treatment of welded joints in pipes with a diameter of up to 426 mm.

The high-power high-frequency transformer of the OB-2030 type (Figure 4) has the following specifications:

Voltage, V	
primary	750
secondary (max)	300
Transformation ratio	15–2
Load power, kV·A	4000
Current frequency, Hz	2400
Weight, kg	355
Overall dimensions, mm	
length	665
width	620
height	515

Such transformers are used in special induction melting furnaces, machines for separation of pipes into measured lengths in lines for high-frequency welding of medium-diameter pipes, as well as other process units.

The transformers comprise a shell-type magnetic circuit, which is characterised by more favourable cooling conditions compared with the core-type one [2]. The steel set of the magnetic circuit for cooling is separated through thickness into several stacks, between which the copper radiator sheets with the cooling water tubes brazed to them are located.

Transformer has a disk system of windings characterised by a low leakage resistance and direct liquid

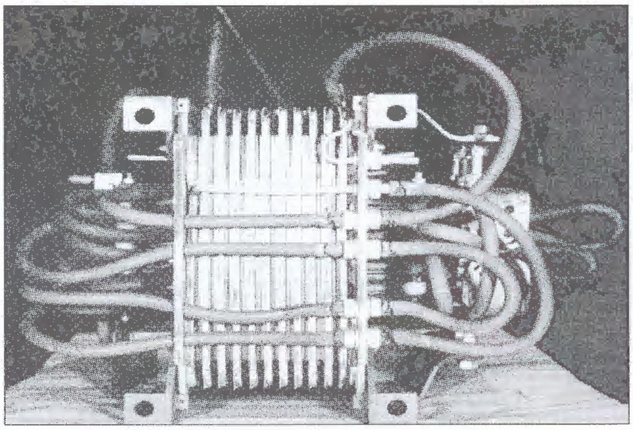

Figure 4. High-power (4000 kV·A) high-frequency transformer of the OB-2030 type

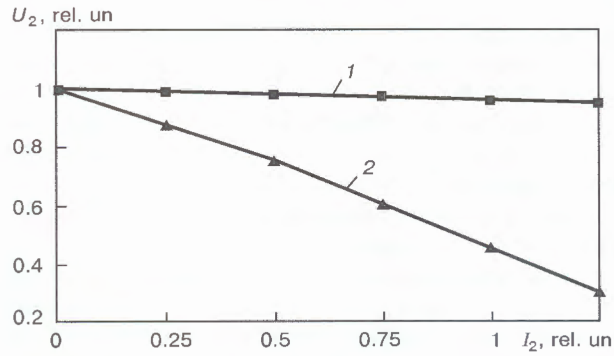

Figure 5. External characteristics of transformers of the P-139 UKhL4 (*1*) and TSS-400/0.5 (*2*) types

cooling of each of the winding sections. The transformation ratio can be varied over wide ranges by connecting the disks of the primary and secondary windings into appropriate groups.

Primary coils in these windings are a multi-turn flat spiral of an oval shape, made from a hollow copper tube. Such a tube has terminal blocks at its ends, used for connection to the circuit.

One-turn secondary disk coils are open disks made from copper sheets. Parts of the disk adjoining the cut have terminals at their ends, the terminals having the form of blocks or plates for joining the coils into a winding.

As each disk of the primary winding is placed between two disks of the secondary winding, leakage of the entire system is improved. The current is distributed not along one side of the tube, like in the single-layer cylindrical windings, but along both sides, which leads to a substantial increase in utilisation of copper. This is provided by a two-times increase in cross section of the wire, other conditions being equal. In addition, with this design it is possible to place windings of a comparatively small height with a large number of turns in the magnetic circuit window (4–15 in the primary winding and 1–2 in the secondary one).

Both high- and commercial-frequency transformers can be employed in some technological processes as power supplies.

It can be concluded by comparing the commercial-frequency power transformers with the high-frequency ones that in many cases the latter exhibit higher efficiency in application. For example, the useful power of a high-frequency welding transformer of the P-139 UKhL4 type is 2.55 kW per kilo of its weight, whereas that of the commercial-frequency transformer TSS-400/0.5 used for heating and supply of electric furnaces is 0.2 kW.

A high degree of compactness of the high-frequency transformers promotes their utilisation in remote units applied for heat treatment of parts.

To illustrate, consider design of the unit for induction heat treatment of pipes under field conditions (UIHT). In a working position the unit is located on a jib suspension of the hoisting mechanism of the system for heat treatment of pipes, connected via cables to the high-frequency current source and process control unit, as well as via hoses to the duct for forced liquid cooling of current-conducting parts of the inductor and transformer. UIHT consists of a rigid inductor with a static connector to ensure preset local heating of the weld zone (developed by the PWI), high-frequency transformers of the P-139 type (2 pcs), mechanism for drawing the inductor together and apart, mechanism for fixation of UIHT on a pipe and sensors of the heat treatment parameters.

The inductor is comprised of two symmetric semi-inductors, each having a removable induction turn, magnetic circuit stacks and current conductors. The inductor has such a design that it provides a uniform local heating of the welded joint on the entire perimeter of the pipe, fast installation in site of performance of heat treatment and dismantling, as well as the absence of the electric contact in the location of the semi-inductor connector, which offers a substantial improvement in performance and operational reliability of equipment. Design of the inductor provides for installation of sensors for the heat treatment parameters.

Specifications of the inductor

Maximum power, kW	160
Rated current frequency, Hz	2400
Pipe heating temperature, °C	any, within the specified HT conditions

Another very important parameter of the transformers is their external characteristic, i.e. dependence of secondary voltage U_2 of the transformer upon load current I_2, which determines in many respects the range of the effective utilisation of a required-frequency transformer in technological processes.

Appearance of the external characteristic (Figure 5) depends upon the character of transformer load ($\cos \varphi_2$). As seen from the Figure, the external characteristic of a high-frequency welding transformer is drooping with a high slope, which provides stable operation of the transformer when applied in electric arc technologies. This is achieved through increasing inductive resistance of the transformer and electric load circuits (in proportion to the current frequency).

1. Pismenny, A.S., Shinlov, M.E., Buzhenetsky, A.I. (1995) Application of induction braze-welding for joining oil pipes. *Avtomatich. Svarka*, **12**, 35–38.
2. Tir, L.L. (1961) *Transformers for induction heating devices of increased frequency*. Moscow-Leningrad: Gosenergoizdat.

DISTRIBUTION OF INDUCTION OF CONTROL LONGITUDINAL MAGNETIC FIELD IN WELDING T-JOINTS

S.M. SIDORENKO[1], **A.D. RAZMYSHLYAEV**[2] and **V.R. MAEVSKY**[3]
[1]Priazovsky State Technical University, Mariupol, Ukraine
[2]Company «Azovmash», Mariupol, Ukraine

In welding of T-joints from ferromagnetic steels a longitudinal component of control longitudinal magnetic field in the arc zone is 2–3 times lower than that in surfacing on flat surface. Optimum sizes of solenoid, generating a longitudinal magnetic field, are defined at which the required level of induction in the welding arc zone in ferromagnetic steel T-joint welding is provided.

Key words: *submerged-arc welding, ferromagnetic steels, T-joints, magnetic field, induction. solenoid, calculations, investigations*

In automatic SAW of T-joints of sheet structures from ferromagnetic steels the use of longitudinal magnetic fields (LMF) to control the formation (shape) of weld is problematic. This is connected with the fact that the magnetic power lines of LMF will be shunted by the sheets welded, and in the zone of welding arc (Figure 1, *a*, point 0) the longitudinal component of induction of field B_z will decrease as compared with surfacing on the flat plate (Figure 1, *b*).

To achieve maximum values B_z in the zone of mating sheets of T-joint (Figure 1, *a*, point 0) it is rational to decrease the outside diameter d_o of a ferromagnetic core of a solenoid which generates LMF. As to the design the inside diameter of a hole in this core providing passing a current-carrying nozzle and electrode wire (being often also of a ferromagnetic material of diameter d_e = 3–5 mm) should not be less than 12 mm. In further experiments and calculations the value d_o = = 12 mm, diameter of electrode wire d_e = 5 mm, distance from electrode end to point 0 (Figure 1, *a*) Δ = = 5 mm. Coil from a copper insulated 2 mm diameter wire with a number of turns w = 20 was arranged on the core. The alternating current of I = 42 A of 50 Hz frequency was passed in the coil.

The aim of the present work was to study the level of induction of LMF in the welding arc zone to find the feasibility of the LMF use for control of weld formation in T-joints from sheet structures made of ferromagnetic steels, and also to define the optimum sizes of solenoid elements as regards to welding of the above-mentioned joints.

The calculation investigations of components of induction were made using a procedure described in [1], and experimental investigations were made using a milliteslameter of F4356 type with a Hall sensor having a 4×4 mm measuring base. During investigations the sizes of core were varied: height H within 20–80 mm, outside diameter d_o within 20–50 mm, distance from solenoid edge to point 0 within 20–50 mm.

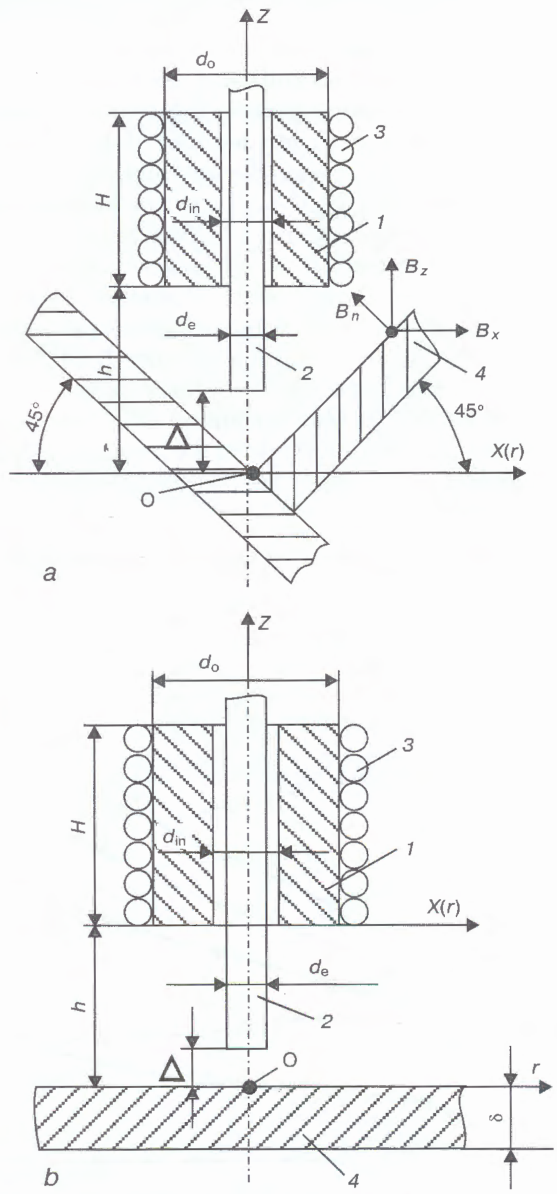

Figure 1. Scheme of welding T-joint (*a*) and surfacing (*b*) with use of LMF: *1* — core; *2* — electrode wire; *3* — coil turns; *4* — plate

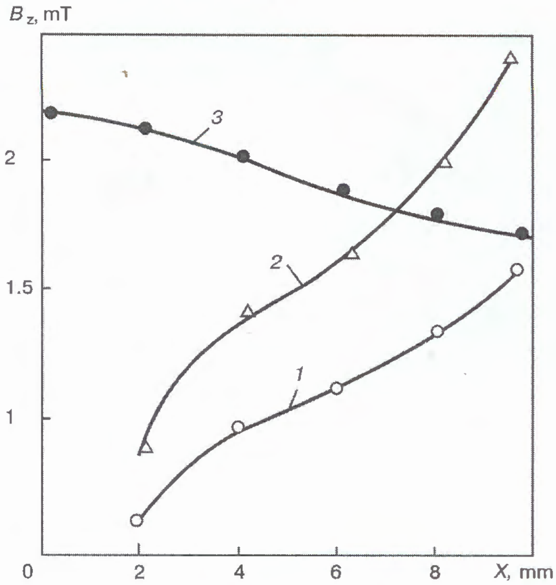

Figure 2. Distribution of induction of LMF along the axis $0X$ for T-joint (*1, 2*) and flat plate (*3*): *1, 3* — B_z; 2 — B_n

It should be noted that there is a good correlaton of experimental (points) and calculated (curves) data in Figures 2–4. With increase in values of coordinate X (it should be taken into account that values of coordinates Z are increased, respectively, by the same value; see Figure 1, *a*) the component of induction B_z is increased (Figure 2, curve *1*). Similarly, a normal component of induction B_n is increased (measurements were made along surface of plates (Figure 2, curve *2*). In this case the value of horizontal component of induction B_x is high (see Figure 1, *a*). In use of the flat plate from the same ferromagnetic steel (St.3 (killed) of 20 mm thickness) as a product, a component of induction B_z along $0X$ locating in plane of a diametrical section of the cylindrical solenoid is decreased (Figure 2, curve *3*). Horizontal (radial) component of induction B_x is negligible [2].

Significant differences in structure of LMF in these cases are caused by a high shunting of the magnetic field with near-by plates of T-joints to a ferromagnetic core of solenoid and weakening of induction B_z in the zone of an expected location of a welding arc (approximately at values $X \leq 4$ mm). It follows from Figure 2 that at $X = 4$ mm for T-joint $B_z =$ $= 1$ mT, while at location of this solenoid over the flat plate $B_z = 2$ mT, i.e. induction B_z is 2 times weakened. For region $X = 2$ mm the induction is much more weakened (3 times).

With increase of d_o the induction B_z is significantly increased (Figure 3). If to increase the height of solenoid H (at fixed ampere turns), then induction B_z in corresponding points (at equal values of coordinate X) is decreased significantly (Figure 4, curves *1–3*). With increase in parameter h and unchanged values of parameter H the induction B_z is also decreased in appropriate points (Figure 4, curves *4–6*). Thus, to increase the level of induction B_z in the arc zone in welding T-joints (from ferromagnetic steels) it is necessary to decrease the values of parameters H and h, and to increase the outside diameter d_o, however, within such ranges that coil turns were not short-circuited on the plate.

The following values should be considered, probably, optimum: $d_o = 30$ mm, $H = 20$–40 mm, $h =$ $= 30$ mm. If to take $H = 20$ mm, then it is necessary to have a double-layer variant of the solenoid coil for $w = 20$ (2 mm wire diameter).

In welding T-joints it is possible to attain (at equal magnetizing force of coil) the same level of induction B_z in the arc zone ($X = 2$–4 mm), which is observed in surfacing on the flat plate (Figure 3, curves *2, 3, 5*), in spite of a significant weakening of component of induction B_z of LMF only due to the selection of

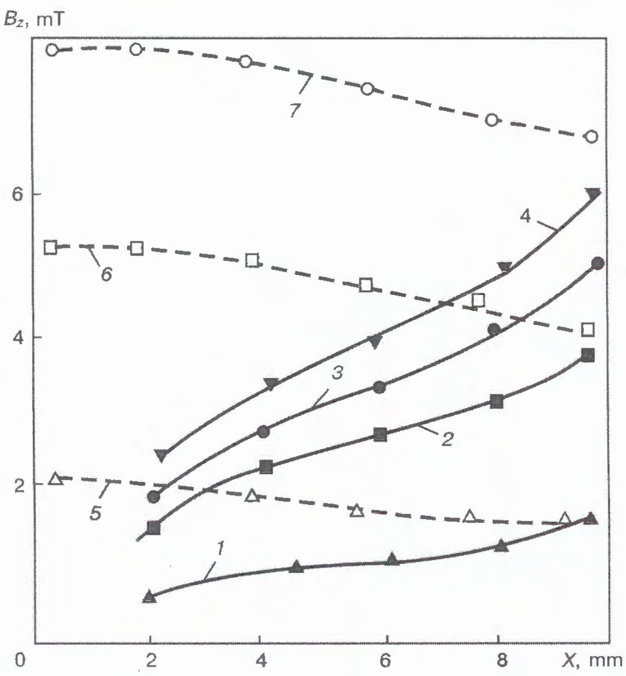

Figure 3. Distribution of component of induction B_z along the axis $0X$ at different values d_o ($H = h = 40$ mm): *1–4* — T-joint, $d_o =$ $= 20$, 30, 40, 50 mm; *5–7* — flat plate, $d_o = 20$, 30, 40 mm

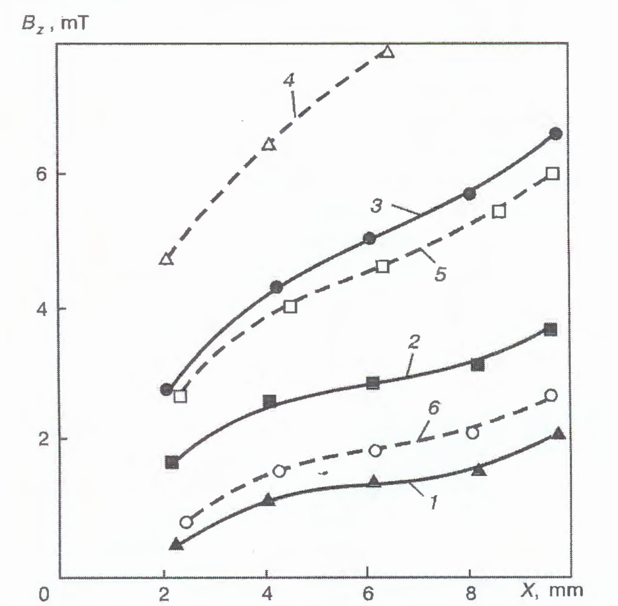

Figure 4. Distribution of component of induction B_z along the axis $0X$ ($d_o = 30$ mm): *1–3* — $h = 40$ mm, $H = 80$, 40, 20 mm; *4–6* — $H = 40$ mm, $h = 20$, 30, 50 mm

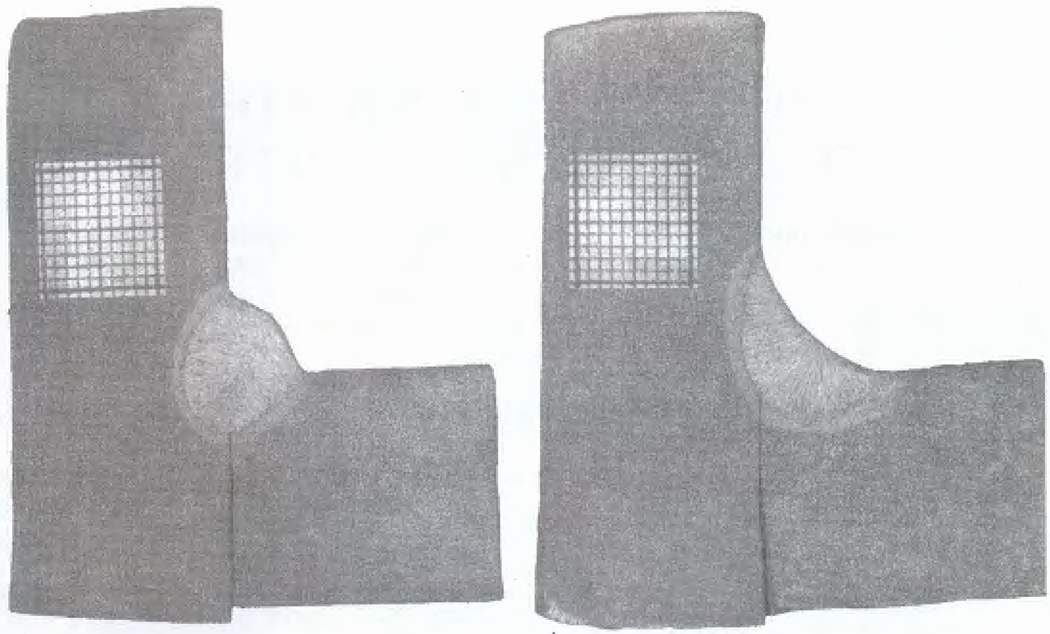

Figure 5. Macrosections of T-joints in welding without (a) and with (b) LMF effect (×1.5)

rational sizes of ferromagnetic core (and coil) of solenoid, such as d_o, H, h.

Welding of T-joints from steel 3 (killed) (wt.%: 0.14–0.22C; 0.3–0.6Mn; 0.12–0.3Si; ≤ 0.3Cr) was performed with 5 mm diameter wire Sv-12GS (wt.%: 0.12C; 0.8Mn; 0.4Si) under the flux AN-348A (wt.%: 41–44SiO_2; 34–38MnO; 5–7.5MgO; 4–5.5CaF_2) without and with effect of LMF of 50 Hz frequency. Welding of plates (20 mm thickness) was performed under the condition (I_w = 730–750 A, U_a = 27–29 V, v_w = 40 m/h), at which a convex weld is formed [3]. Solenoid of the following sizes was used: d_o = 40 mm, H = 50 mm (see Figure 1, a), magnetizing force of coil is 3000 ampere turns, electrode stickout h = = 40 mm. The measured longitudinal component of induction of LMF in plate under the electrode (in point 0 in Figure 1, a) is 50 mT.

In conventional welding the weld has a convex shape (Figure 5, a), while in welding with LMF effect it has a favourable concave shape (Figure 5, b) (from the point of view of decrease in coefficient of stress concentration) with a smooth transition of weld to the parent metal at the absense of undercuts.

Thus, it is possible to use LMF for control of the shape of T-joint welds. Further, it wiil be rational to study the interrelation of LMF parameters (induction, frequency of LMF) with a weld shape, its sizes in section and service characteristics of welded T-joints.

CONCLUSIONS

1. In welding of T-joints from ferromagnetic steels the longitudinal component of LMF in the arc zone is 2–3 times lower than that in surfacing on the flat surface.

2. With selection of optimum sizes of the solenoid in welding of T-joints it is posiible to attain the same level of LMF induction in the arc zone, as in surfacing on the flat plate at equal magnetizing force of the coil.

1. Razmyshlyaev, A.D., Maevsky, V.R., Sidorenko, S.M. (2001) Calculation of magnetic field induction of a solenoid with a ferromagnetic core for arc surfacing. *The Paton Welding J.*, **8**, 18–21.
2. Razmyshlyaev, A.D. (1996) Influence of magnetic field on sizes of penetration zone in submerged-arc surfacing. *Avtomatich. Svarka*, **8**, 25–26, 30.
3. Akulov, A.I., Belchuk, G.A., Demyantsevich, V.P. (1977) *Technology and equipment of fusion welding*. Moscow: Mashinostroenie.

VACUUM PERCUSSION WELDING OF ALUMINIUM TO COPPER

G.K. KHARCHENKO, Yu.V. FALCHENKO, V.V. ARSENYUK and **E.V. POLOVETSKY**
The E.O. Paton Electric Welding Institute, NASU, Kyiv, Ukraine

Features of mass transfer in vacuum percussion welding of aluminium to copper were studied. A process of joining without formation of intermetallics in the butt was developed.

Key words: *percussion welding, mass transfer, bimetal, intermetallic*

Bimetal joints of aluminium to copper have a high heat conductivity, electric conductivity, and are extensively used in different industries. Explosion welding (in view of a number of its features) is one of the most effective methods of producing Cu–Al transition pieces. Subsequent cold rolling, cutting out of flat or extrusion of complex-shaped composite transition pieces allows producing sound Cu–Al contacts for various purposes [1].

Bimetal overlap joints in the form of washers may be also made by diffusion bonding in vacuum, which greatly simplifies the technology of manufacturing Cu–Al contacts. During welding, however, a continuous interlayer of intermetallics is formed in the butt, having dielectric properties, which gives the bimetal contact a high electric resistance. In connection with the fact that the incubation period for intermetallic formation at the temperature of 500 °C, is not longer than several seconds [2], it may be stated that the traditional processes of diffusion bonding will not provide formation of a joint of aluminium to copper without an intermetallic interlayer.

It appears to be promising to apply for welding the above metals the process of vacuum percussion welding (VPW), during which the time of high-temperature deformation is equal to $\approx 10^{-2}$ s, i.e. much less than the incubation period of intermetallic formation. The authors established that VPW process is the most promising for joining dissimilar metals, having a limited mutual solubility and short duration of the incubation period of intermetallic formation. Examples of joining refractory metals to steel [3] were used to establish that in VPW at the stage of high-speed upsetting intensive diffusion processes proceed in the butt, which lead to formation of an extensive zone of bulk interaction in the form of solid solutions of the metals being welded without intermetallic formation.

The purpose of this work consisted in producing an overlap bimetal Cu–Al joint in the form of washers without intermetallic interlayer by VPW process. Copper M1 and commercial aluminium alloy AD1 in the form of billets of 30 mm diameter and 2 and 4 mm thickness were welded. Before welding the billets were degreased, and the abutted surfaces were scraped. Billets were welded in U-394M unit. VPW process parameters were as follows: welding temperature of 500 °C, impact energy of 2–3 kJ. Ring-shaped electron beam heaters were used for heating. The striker mass and speed of its displacement provided the required energy, consumed in formation of the welded joint. During preheating copper and aluminium samples were in a separated condition (the gap was 2–3 mm). Pulsed load eliminates the gap between the samples and shifts them into the cold forming matrix, where solid-phase welding proceeds with a simultaneous forming of a bimetal contact of the required configuration [4]. Deformation of copper and aluminium samples by thickness is 10 and 40 %, respectively, which is responsible for mechanical fracture of the oxide film in aluminium during welding. Metallographic examination and X-ray microanalysis of the welded joint showed the absence of intermetallics in the butt. Microhardness (10 g load) of copper, aluminium and the butt was 680, 350 and 400 MPa, respectively.

Features of mass transfer were studied in VPW of aluminium to copper. Before welding ^{63}Ni isotope was applied onto copper (coating thickness was 1–2 μm). It was established that ^{63}Ni moves into aluminium and copper for a distance of up to 50 μm. Mass transfer coefficient can be up to 10^{-2} cm^2/s, which once more confirms the earlier discovered phenomenon of anomalous acceleration of the diffusion processes in solid metal at highly intensive force impact [5].

Comparative testing of bimetal contacts, having an intermetallic layer in the butt or without it was conducted. To form an intermetallic layer 10–15 μm thick, the joints produced by VPW were further annealed at the temperature of 500 °C for 45 min. It is established that bimetal contacts, containing no intermetallics in the butt, have higher indices of heat- and electric conductivity.

1. Peev, A.P. (2001) *Development of technological processes of explosion welding of Cu–Al components of current-carrying sub-assemblies for power engineering and electrometallurgy plants*. Syn. of Thesis for Cand. of Techn. Sci. Degree. Volgograd: VGTU.
2. Trutnev, V.V., Yakushin, A.F., Yakushina, G.V. (1971) Kinetics of increase of intermediate phase in a Cu–Al joint. *Svarochn. Proizvodstvo*, **1**, 15–16.
3. Gurevich, S.M., Nerodenko, M.M., Kharchenko, G.K. et al. (1982) *Metallurgy and technology of welding of refractory metals and alloys on their base*. Kyiv: Naukova Dumka.
4. Arsenyuk, V., Ignatenko, A., Kharchenko, G. (1999) Vacuum percussion welding — a new method joining dissimilar metals. In: *Proc. of Symp. on Exploiting Solid State Joining*, Sept. 13–14, 1999, Cambridge. Abington: TWI, EWI.
5. Larikov, L.N., Falchenko, F.M., Mazanko, V.F. et al. (1975) Abnormal acceleration of diffusion under pulsed loading of metals. *Doklady AN Ukr. SSR*, Series A, **7**, 635–639.